

Ninevah University
College of Electronics Engineering
Electronic Department



Design and Implementation Multiband Rectenna for Ambient RF Energy Harvesting

Abdullah Mohammad Ajeel Hussein
A Thesis in
Electronic Engineering

Supervised by

Assist. Prof.
Dr Ahmed Mohammad Sabaawi

1445 AH

2023 AD

**Design and Implementation of Multiband Rectenna for
Ambient RF Energy Harvesting**

A Thesis Submitted by

Abdullah Mohammad Ajeel Hussein

To

The Council of the College of Electronics Engineering

Ninevah University

as a Partial Fulfillment of the Requirements

for the Degree of Master of Science

in

Electronic Engineering

Supervised by

Assist. Prof.

Dr Ahmed Mohammad Sabaawi

1445 AH

2023 AD

بِسْمِ اللَّهِ الرَّحْمَنِ الرَّحِيمِ

وَقُلْ إِعْمَلُوا فِى سَبِيلِ اللَّهِ عَمَلَكُمْ وَرَسُولُهُ وَالْمُؤْمِنُونَ وَسَتُرَدُّونَ
إِلَى عَالَمِ الْغَيْبِ وَ الشَّهَادَةِ فَيُنَبِّئُكُمْ بِمَا كُنْتُمْ تَعْمَلُونَ (١٠٥)

صَدَقَ اللَّهُ الْعَظِيمُ

سورة التوبة

ACKNOWLEDGEMENTS

In the name of God, and prayers and peace be upon the Messenger of God and his family and companions all until the Day of Judgment, Oh God, praise be to You as it should be for the majesty of Your countenance and the greatness of Your authority. Praise be to God who has enabled me to complete this work and helped me and guided me to be on the straight path.

The duty of loyalty invites me to extend my thanks and gratitude to everyone who extended a helping hand, and gave me guidance.

I am pleased to extend my sincere thanks and appreciation to my teacher and supervisor, Assist. Prof. Ahmed Mohammed Sabaawi, for the sound advice, correct guidance and abundant knowledge he gave me.

My thanks and gratitude to the President of the University of Ninevah and the Dean of the College of Electronics Engineering for their contribution to maintaining the continuity of the science and learning process.

My thanks and gratitude to the Head of the Department of Electronics Engineering and to all my professors in the College of Electronics Engineering who were a source of knowledge.

My thanks and gratitude go to the one who honored me with bearing his name and who spent the precious and precious things in order for me to reach a high academic degree, and today my father sees the fruit of what my he planted (may God have mercy on him) .

My thanks and gratitude to the light of my eyes, the light of my path, and the joy of my life, whose prayers and words were a shield and a fortress for me (my dear mother).

My thanks and gratitude to those who planted in me all the meanings of loyalty and sincerity and implanted in me all the motives of giving (my dear brothers Bassam and Saad).

My thanks and gratitude to my classmates who cooperated and worked with me by sharing knowledge and were the best for me during my hard times.

I ask God, the All-Knowing, to teach us what benefits us. And to benefit us with what he taught us. May our knowledge benefit others.

Supervisor's Certification

We certify that the dissertation entitled (**Design and Implementation Multiband Rectenna for Ambient RF Energy Harvesting**) was prepared by **Abdullah Mohammad Ajeel Hussein** under our supervision at the Department of Electronic Engineering, Ninevah University, as a partial requirement for the Master of Science Degree in Electronic Engineering.

Signature:

Name: Assist. Prof. Dr. Ahmad Mohammad Sabaawi

Date: /11/2023

Report of Linguistic Reviewer

I certify that the linguistic reviewing of this dissertation was carried out by me and it is accepted linguistically and in expression.

Signature:

Name: Aus Adel Abdulwahhab

Date: / 11/2023

Report of the Head of Department

I certify that this dissertation was carried out in the Department of Electronic Engineering. I nominate it to be forwarded to discussion.

Signature:

Name: Prof. Dr. Qais Thanon Najim Algwari

Date: /11 /2023

Report of the Head of Postgraduate Studies Committee

According to the recommendations presented by the supervisors of this dissertation and the linguistic reviewer, I nominate this dissertation to be forwarded to discussion.

Signature:

Name: Prof. Dr. Qais Thanon Najim Algwari

Date: / 11 /2023

Committee Certification

We the examining committee, certify that we have read this dissertation entitled (**Design and Implementation Multiband Rectenna for Ambient RF Energy Harvesting**) and have examined the postgraduate student (**Abdullah Mohammad Ajeel Hussein**) in its contents and that in our opinion; it meets the standards of a dissertation for the degree of Master of Science in Electronic Engineering.

Signature:

Name: Prof. Dr. Qais Thanon Algwari
Head of committee
Date: / 11/2023

Signature:

Name: Assist. Prof. Dr. Mohammed Sh. Ahmed
Member
Date: / 11 /2023

Signature:

Name: Assist. Prof. Dr. Mohamad A. Ahmed
Member
Date: / 11 /2023

Signature:

Name: Assist. Prof. Dr. Ahmed M. Sabaawi
Member and Supervisor
Date: / 11 /2023

The college council, in its meeting on / / 2023 , has decided to award the degree of Master of Science in Electronic Engineering to the candidate.

Signature:

Name: Prof. Khaled Khalil Muhammad
Dean of the College
Date: / /2023

Signature:

Name: Assist. Prof. Dr. Bilal Alaa Aldeen Jaber
Council registrar
Date: / /2023

Abstract

Rectifiers in this work are used based on voltage doubler technique and simulated by Advanced Design System (ADS) software. The designed rectifiers in this work exhibits an RF to DC conversion efficiency of around 45.22% at frequency band 2.4 GHz with an output DC voltage that reached 2.2 V. In addition, the achieved efficiency is around 29.89% at 3.6 GHz with an output DC voltage that reached 1 V and around 27% at 5 GHz with an output DC voltage that reached 1.7 V, which is sufficient to power up the most devices and/or charging the implanted battery. Moreover, several multi-band and wideband fractal slot antennas were designed, simulated and implemented in this research using CST studio software. Two antennas (Ultra Wide Band) UWB are designed at 2.4 GHz, 3.6 GHz and 5 GHz. Antennas are designed with a partial ground plane at the front side of the antennas and a Sub Miniature Version A (SMA) connector is attached to the input port of the antennas. This design makes it easy for the proposed antennas to be integrated with the rectifiers to form a compact rectenna for Wireless Power Transfer (WPT) system. The designed rectennas (rectifier and antenna) are fabricated using Print Circuit Board (PCB) technology. The performance of the fabricated prototypes is tested in the lab. The measured results are compared with the simulated ones and it is found that a good and acceptable agreement are achieved, which makes the rectifier and antenna designs valid. These experiments significantly confirmed the utility of the proposed rectennas in this work to produce sufficient amount of power for many devices and applications.

Acronyms

AC	Alternative Current
ADS	Advanced Design System
CC	Constant Current
CST	Computer Simulation Technology
ETSI	European Telecommunications Standards Institute
EIRP	Equivalent Isotropically Radiated Power
EM	Electromagnetic Wave
FCC	Federal Communications Commission
GPS	Global Positioning System
IMD	Implantable Medical Device
ISM	Industrial Scientific & Medical
MICS	Medical Implant Communication Service
RF	Radio Frequency
RX	Receiver
TX	Transmitter
UWB	Ultra-Wideband
WPT	Wireless Power Transfer
WMTS	Wireless Medical Telemetry Service

Abbreviations

Symbol	Explanation	Unit
ϵ_r	Dielectric permittivity	[Farad/ Meter]
G_{TX}	Gain of transmitting antennas	
G_{RX}	Gain of receiving antennas	
L_P	Path loss	[Decibel]
e_P	The polarization mismatch	
P_{RX}	Power received	[Watt]
P_{TX}	Power transmitted	[Watt]
ω	Rotational frequency	[radians/Second]
$ E $	Electric field intensity	[Volt/Meter]
dV	Differential volume element	
P_{in}	Input power	[Watt]
P_{rad}	Radiated power	[Watt]
Q_s	Serial Q Factor	
Q_p	Parallel Q Factor	
R_+	Load Resistance	[Ohm]
R_-	Source Resistance	[Ohm]
Z_{in}	Input Impedance	[Ohm]
X_C	Capacitive Reactance	[Ohm]
X_L	Inductive Reactance	[Ohm]

Equations

Equation	Chapter	Page
$P_{RX} = P_{TX} + G_{RX} + G_{TX} - L_P - e_p$	(2.1)	18
$\eta = P_{rad} / P_{in} \%$	(2.2)	20
$W_p = \frac{c}{2f_r \sqrt{(\epsilon_r + 1)/2}}$	(2.3)	23
$\epsilon_{reff} = \frac{\epsilon_r + 1}{2} + \frac{\epsilon_r - 1}{2} \left[1 + 12 \frac{h}{w} \right]^{-\frac{1}{2}}$	(2.4)	23
$L_{eff} = \frac{c}{2f_r \sqrt{\epsilon_{reff}}}$	(2.5)	23
$\Delta L = 0.412h \frac{(\epsilon_{reff} + 0.3) \left(\frac{w}{h} + 0.265 \right)}{(\epsilon_{reff} - 0.258) \left(\frac{w}{h} + 0.8 \right)}$	(2.6)	24
$L_p = L_{eff} - 2\Delta L$	(2.7)	24
$L_s = 6h + L_p$	(2.8)	24
$w_s = 6h + w_p$	(2.9)	24
$D = \frac{L}{\pi} \text{Cos}^{-1} \left(\sqrt{\frac{Z_{feed\ line}}{Z_{antenna}}} \right)$	(2.10)	24
$r = \frac{F}{1 + \frac{2h}{\pi F \epsilon_r} \left[\ln \left(\frac{\pi F}{2h} \right) + 1.7726 \right]^{\frac{1}{2}}}$	(2.11)	24
$F = \frac{(8.791 \times 10^9)}{(f_r \times \sqrt{\epsilon_r})}$	(2.12)	25
$r_{eff} = r \left[1 + \frac{2 \times h}{\pi \times r \times \epsilon_r} \left\{ \ln \left(\frac{\pi \times r}{2 \times h} \right) + 1.7726 \right\} \right]^{\frac{1}{2}}$	(2.13)	25
$R_j = \frac{8.33 \times 10^{-5} \times n \times T}{I_s}$	(3.1)	31
$Q_s = Q_p = \sqrt{\frac{R_+}{R_-} - 1}$	(3.2)	33

$$Q_s = \frac{X_s}{R-} \quad (3.3) \quad 33$$

$$Q_p = \frac{R+}{X_p} \quad (3.4) \quad 33$$

Contents

Subject	Page
CHAPTER ONE	1-11
INTRODUCTION AND LITERATURE REVIEW	
1.1 Radio Frequencies (RF)	1
1.2 Literature review	3
1.3 Aims of the thesis	9
1.4 Thesis Layout	10
CHAPTER TWO	12-26
THEORETICAL BACKGROUND	
2.1 Introduction	12
2.2 Wireless Power Transfer (WPT)	13
2.3 Rectifier Characteristics	15
2.4 Multi band Fractal Antenna	18
2.4.1 Difficulties and requirements for the design of an antenna	19
2.4.2 Typical Requirements of Antenna Systems	20
2.4.3 Antennas Parameters	22
2.4.4 Rectangular patch antenna with inset feeding	23
2.4.5 Circular patch antenna	25
CHAPTER THREE	26-67
DESIGN AND SIMULATION OF SINGLE-STAGE RECTIFIER CIRCUITS	
3.1 Matching Circuit Methods	27
3.2 Rectifier Circuit operating at 2.4 GHz with LC-Circuit Matching Method	37
3.3 Rectifier circuit operating at 3.6 GHz with LC-Circuit Matching Method	43
3.4 Rectifier circuit operating at 5 GHz with LC-Circuit Matching Method	47
3.5 Rectifier Circuit operating at 2.4 GHz with TL-Circuit Matching Method	50
3.6 Rectifier Circuit operating at 3.6 GHz with TL-Circuit Matching Method	55
3.7 Rectifier Circuit operating at 5 GHz with TL-Circuit Matching Method	59

3.8 Fabrication and experimental validation	63
CHAPTER FOUR Multiband and Wideband Antennas for Energy Harvesting Applications	67-104
4.1 Introduction	67
4.2 Antennas Design	67
4.2.1 Antenna 1 of Rectangular patch with inset feeding.	68
4.2.2 Antenna 2 of rectangular patch with inset feeding and slot.	75
4.2.3 Antenna 3 of rectangular patch with double slot.	78
4.2.4 Antenna 4 of rectangular patch with Sierpinski fractal slot.	80
4.2.5 Antenna 5 of Slotted UWB Circular Patch Antenna.	82
4.2.6 Antenna 6 of Hexagonal ring fractal antenna with slot	85
4.2.7 Antenna 7 of Circular ring fractal antenna with slot.	94
4.3 Fabrication and Experimental Validation.	101
CHAPTER FIVE CONCLUSIONS AND FUTURE WORKS	104-116
5.1 Conclusions	104
5.2 Future works	106
References	108

List of tables

No.	Subject	Page
3.1	DC Voltage output and (Vdc) and Efficiency (η) for different input power (Pin) at 2.4, 3.6 and 5 GHz.	39
4.1	Geometrical details of Antenna 1.	69-70
4.2	Geometrical details of Antenna 2.	75-76
4.3	Geometrical details of Antenna 3.	79
4.4	Geometrical details of Antenna 5.	83-84
4.5	Geometrical details of Antenna 6.	89
4.6	Geometrical details of Antenna 7.	97

List of Figures

No.	Subject	Page
1.1	Ambient RF energy source in urban area[15].	2
1.2	Schematic block diagram of RF energy harvesting[16].	3
2.1	Voltage doubler rectifier circuit diagram [49].	15
2.2	Voltage doubler output as sweep of input power compared with single diode rectifier [50].	16
2.3	Diagram of the rectification process using half-wave and full-wave rectification [53].	17
2.4	Diagram of a single diode rectifier showing the results of simulation [54].	17
3.1	Forward Current vs. Forward Voltage and Reverse Current vs. Reverse Voltage at Temperatures.	27
3.2	LC-Matching Methods.	28
3.3	Equivalent Circuit for LC-Circuit.	28
3.4	Simulated circuit that find Z_{in} at Frequency band 2.4 GHz.	29
3.5	Simulated value of Z_{in} .	29
3.6	Validity from Z_{in} value using Analysis.	30
3.7	Equivalent Circuit for Diode.	30
3.8	Analysis circuit.	31
3.9	Final Analysis Circuit after cancel the R_j .	32
3.10	Tools of Smith chart.	35
3.11	Window of the Smith chart in ADS.	36
3.12	Block diagram of Transmission Lines.	36
3.13	Window of the LineCalc to compute Width and Length.	37
3.14	Simulated Block diagram of Transmission Lines (TL) at 2.4 GHz.	37
3.15	Rectifier circuit operating at 2.4 GHz with LC-Circuit.	38
3.16	Simulated S_{11} of Rectifier circuit at 2.4 GHz with LC-Circuit.	39
3.17	V_{in} (V) of Rectifier Circuit at 2.4 GHz with LC-Circuit.	40

3.18	Vout (V) of Rectifier Circuit at 2.4 GHz with LC-Circuit.	40
3.19	Output current of Rectifier Circuit at 2.4 GHz with LC-Circuit.	41
3.20	Vout (V) versus Pin (dBm) of Rectifier Circuit at 2.4, 3.6 and 5 GHz with LC-Circuit.	42
3.21	Efficiency versus input power of Rectifier Circuit at 2.4, 3.6 and 5 GHz with LC-Circuit.	42
3.22	Rectifier circuit operating at 3.6 GHz with LC-Circuit.	43
3.23	Simulated S11 of Rectifier circuit at 3.6 GHz with LC-Circuit.	44
3.24	Vin (V) of rectifier circuit at 3.6 GHz with LC-Circuit.	44
3.25	Vout (V) of rectifier circuit at 3.6 GHz with LC-Circuit.	45
3.26	Output current of Rectifier Circuit at 3.6 GHz with LC-Circuit.	45
3.27	Vout (V) versus Pin (dBm) of Rectifier Circuit at 3.6 GHz with LC-Circuit.	46
3.28	Efficiency versus input power of rectifier at 3.6 GHz with LC-Circuit.	46
3.29	Rectifier circuit operating at 5 GHz with LC-Circuit.	47
3.30	Simulated S11 of Rectifier circuit at 5 GHz with LC-Circuit.	47
3.31	Vin (V) of rectifier circuit at 5 GHz with LC-Circuit.	48
3.32	Vout (V) of rectifier circuit at 5 GHz with LC-Circuit.	48
3.33	Output current of rectifier at 5 GHz with LC-Circuit.	49
3.34	Vout (V) versus Pin (dBm) of rectifier circuit at 5 GHz with LC-Circuit.	50
3.35	Efficiency versus input power of rectifier at 5 GHz with LC-Circuit.	50
3.36	Rectifier circuit operating at 2.4 GHz with TL-Circuit.	51
3.37	Simulated S11 of Rectifier circuit at 2.4 GHz with TL-Circuit.	51
3.38	Vin (V) of Rectifier Circuit at 2.4 GHz with TL-Circuit.	52
3.39	Vout (V) of Rectifier Circuit at 2.4 GHz with TL-Circuit.	53
3.40	Output current of Rectifier Circuit at 2.4 GHz with TL-Circuit.	53
3.41	Vout (V) versus Pin (dBm) of Rectifier Circuit at 2.4, 3.6 and 5 GHz with TL-Circuit.	54

3.42	Efficiency versus input power of Rectifier Circuit at 2.4, 3.6 and 5 GHz with TL-Circuit.	54
3.43	Rectifier circuit operating at 3.6 GHz with LC-Circuit.	55
3.44	Simulated S11 of Rectifier circuit at 3.6 GHz with TL-Circuit.	55
3.45	Vin (V) of rectifier circuit at 3.6 GHz with TL-Circuit.	56
3.46	Vout (V) of rectifier circuit at 3.6 GHz with TL-Circuit.	56
3.47	Output current of Rectifier Circuit at 3.6 GHz with TL-Circuit.	57
3.48	Vout (V) versus Pin (dBm) of Rectifier Circuit at 3.6 GHz with TL-Circuit.	58
3.49	Efficiency versus input power of rectifier at 3.6 GHz with TL-Circuit.	58
3.50	Rectifier circuit operating at 5 GHz with TL-Circuit.	59
3.51	Simulated S11 of Rectifier circuit at 5 GHz with TL-Circuit.	59
3.52	Vin (V) of rectifier circuit at 5 GHz with TL-Circuit.	60
3.53	Vout (V) of rectifier circuit at 5 GHz with TL-Circuit.	60
3.54	Output current of rectifier at 5 GHz with TL-Circuit.	61
3.55	Vout (V) versus Pin (dBm) of rectifier circuit at 5 GHz with TL-Circuit.	62
3.56	Efficiency versus input power of rectifier at 5 GHz with TL-Circuit.	62
3.57	Photo of fabrication of Rectifier circuit.	63
3.58	Photo of the front layer of Rectifier circuit.	63
3.59	Photo of the back layer of Rectifier circuit.	63
3.60	Measured S11 for Rectifier Circuit.	64
3.61	Photo show the measured Vdc (Vout) Versus Pin (dBm) for Rectifier Circuit.	65
3.62	Comparison between simulated and measured Vdc (Vout) versus Pin (dBm) at 3 k Ω .	66
3.63	Comparison between simulated and Measured efficiency versus Pin (dBm) at 3 k Ω .	66
4.1	Show the structures of Antenna 1.	69
4.2	Show the Antenna 1 of Rectangular patch with inset feeding without slot.	69
4.3	Simulated S11 versus Frequency for antenna 1.	70
4.4	Simulated 3D radiation pattern at 2.4 GHz for	71

	Antenna 1.	
4.5	Simulated 2D radiation pattern at 2.4 GHz for Antenna 1.	71
4.6	Simulated 3D radiation pattern at 3.6 GHz for Antenna 1.	72
4.7	Simulated 2D radiation pattern at 3.6 GHz for Antenna 1.	72
4.8	Simulated 3D radiation pattern at 4.5 GHz for Antenna 1.	73
4.9	Simulated 2D radiation pattern at 4.5 GHz for Antenna 1.	73
4.10	Simulated 3D radiation pattern at 4.7 GHz for Antenna 1.	74
4.11	Simulated 2D radiation pattern at 4.7 GHz for Antenna 1.	74
4.12	Antenna 2 Rectangular patch antenna with inset feeding.	75
4.13	Simulated S11 for Antenna 2 (rectangular patch antenna with inset feeding).	76
4.14	Simulated S11 for Antenna 2 by varying the Height the locate of front slot (H1).	77
4.15	Simulated S11 for Antenna 2 by varying the Height the locate of back slot (H2).	78
4.16	Antenna 3 (Rectangular patch with double slot) all dimension in mm.	79
4.17	Simulated S11 for Antenna 3 (Rectangular patch with double slot).	80
4.18	Triangle slot of Sierpinski.	81
4.19	Antenna 4 (Rectangular patch triangle slot antenna) all dimensions in mm.	81
4.20	Simulated S11 for Antenna 4.	82
4.21	Antenna 5 (An Ultra-Wide Band (UWB) Circular patch antenna) all dimensions in mm.	83
4.22	Simulated S11 for Antenna 5.	84
4.23	Simulated S11 for Antenna 4 by varying the distance between two slots (D).	85
4.24	Hexagonal patch without slot antenna.	86
4.25	Simulated S11 versus frequency for Hexagonal patch antenna.	87

4.26	Hexagonal ring patch antenna.	87
4.27	Simulated S11 versus frequency for Hexagonal ring patch antenna.	88
4.28	Hexagonal ring fractal antenna with slot with all dimensions in mm.	88
4.29	Simulated S11 for Antenna 6 (Hexagonal ring fractal antenna with slot).	90
4.30	Simulated 3D radiation pattern at 2.4 GHz for Antenna 6.	90
4.31	Simulated 2D radiation pattern at 2.4 GHz for Antenna 6.	91
4.32	Simulated 3D radiation pattern at 3.6 GHz for Antenna 6.	91
4.33	Simulated 2D radiation pattern at 3.6 GHz for Antenna 6.	92
4.34	Simulated 3D radiation pattern at 5 GHz for Antenna 6.	93
4.35	Simulated 2D radiation pattern at 5 GHz for Antenna 6.	93
4.36	Circular patch without slot antenna.	94
4.37	Simulated S11 versus frequency for Circular patch without slot antenna.	95
4.38	Circular ring patch without slot antenna.	96
4.39	Simulated S11 versus frequency for Circular ring patch without slot.	96
4.40	Circular ring fractal antenna with slot with all dimensions in mm.	97
4.41	Simulated S11 for Antenna 7 (Circular ring fractal antenna).	98
4.42	Simulated 3D radiation pattern at 2.4 GHz for Antenna 7.	98
4.43	Simulated 2D radiation pattern at 2.4 GHz for Antenna 7.	99
4.44	Simulated 3D radiation pattern at 3.6 GHz for Antenna 7.	99
4.45	Simulated 2D radiation pattern at 3.6 GHz for	100

	Antenna 7.	
4.46	Simulated 3D radiation pattern at 5 GHz for Antenna 7.	100
4.47	Simulated 2D radiation pattern at 5 GHz for Antenna 7.	101
4.48	Photographs of the fabricated hexagonal and circular fractal antennas.	102
4.49	Shows the experimental setup used to measure the S-parameters for the fabricated antenna.	102
4.50	Measured and simulated S11 for Antenna 6 (Hexagonal ring patch with slot antenna).	103
4.51	Measured and simulated S11 for Antenna 7 (Circular ring patch with slot antenna).	103

CHAPTER ONE

INTRODUCTION AND LITERATURE REVIEW

1.1 Radio Frequencies (RF):

RF energy harvesting technology is an innovative approach for converting ambient RF energy into electrical energy. Multi-band RF energy harvesting is a technique that enables the harvesting of energy from multiple frequency bands simultaneously. This technology has several advantages over single-band RF energy harvesting, including improved power density, wider frequency coverage, and the ability to harvest energy from multiple sources simultaneously. Multi-band RF energy harvesting has a wide range of potential applications, including the medical implants, smart homes, wireless sensor networks, and Internet of Things (IoT). In this work, a compact multiband rectenna operating for Bluetooth, Global System Mobile (GSM), WirelessLAN (WLAN), Wi-Fi MAX (Wi-MAX) and satellite communication band is proposed. In recent years, there is an enormous demand for portable wireless devices operating in L, C and S bands. Due to this increased demand for wireless equipment in all aspects of today's life, RF energy harvesting can be a fit and practical remedy for solving the problem of continues replacing of batteries in handheld and portable devices. The concept of RF energy harvesting developed during the 20th century and entails conversion of electromagnetic waves present in environment to direct current (DC) electricity [1]. Nowadays, there are a number of approaches for generating energy from environment "RF/microwave, signals, pressure, heat, light motion" or another source of energy like human body "finger strokes, body heat, foot strike" have been put forth [2] [3]. The envisioned antennas have the benefits of small antenna size, broad bandwidth and effective radiation efficiency. Various antenna

structures have lately been suggested in the literature for RF energy harvesting applications where set sources are found like, Universal Mobile Telecommunication System (UMTS), Global System Mobile (GSM), Long Term Evolution (LTE), WirelessLAN (WLAN), Bluetooth and 5G networks. Widely reported literature works with the goal of boosting systemic effectiveness and reducing complexity [4]-[7]. Dual band and wide band antennas were previously employed for energy harvesting applications due to their ability to harvest as much energy as possible from surrounding sources [8][9]. Most existing works either center around a particular station, for example, a TV slot [10]-[13], or utilize a multiband exhibit made out of various radio wires tuned to individual channels. While multi-band reaping increments the resulted DC power by consolidating the commitments from the individual circuits, such plans increment intricacy and cost of the framework [14].

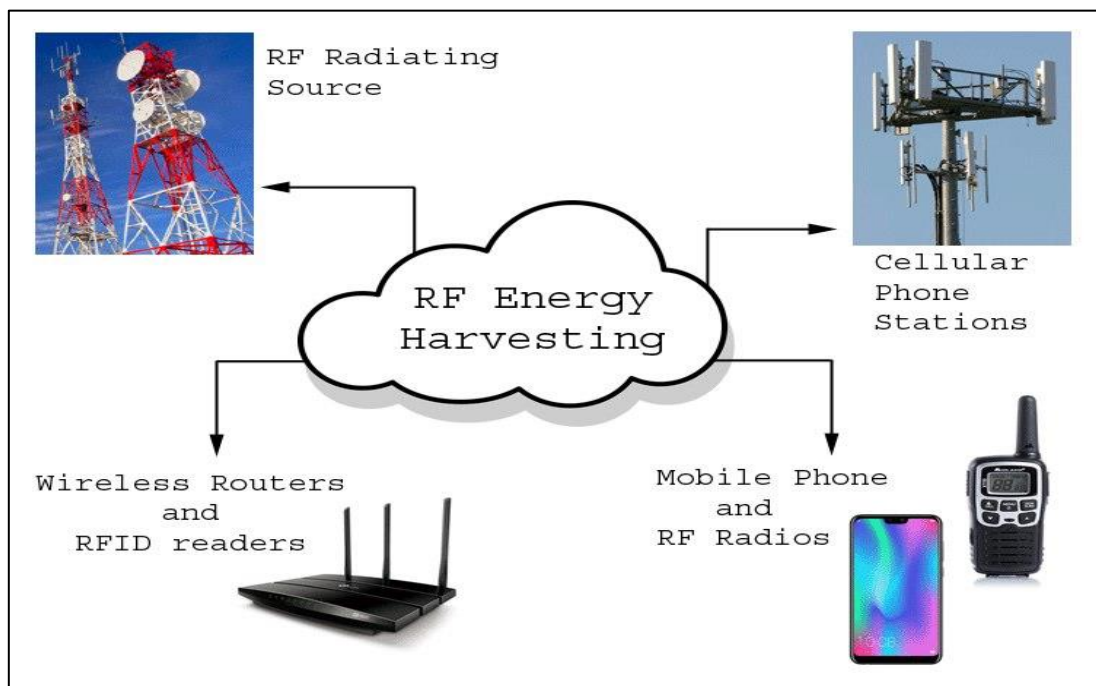


Fig.1.1: Ambient RF energy source in urban area [15]

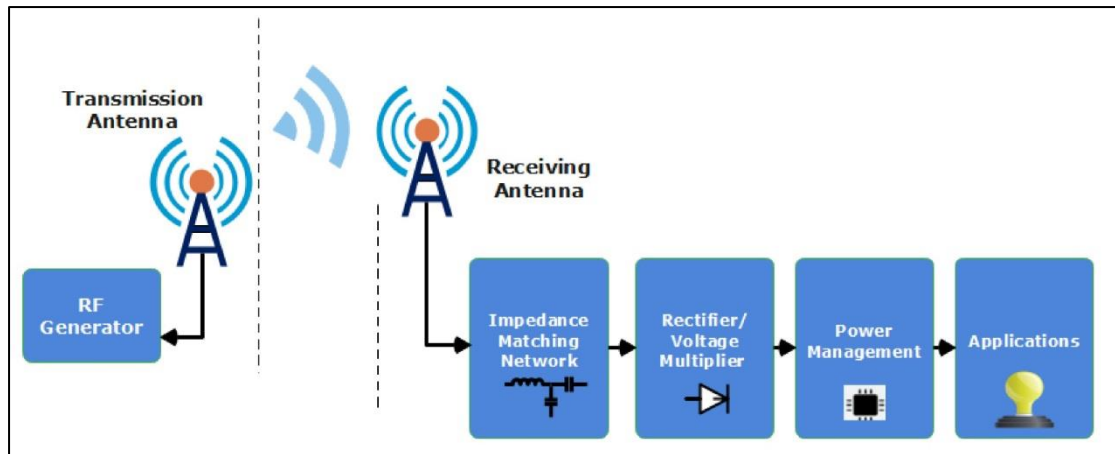


Fig.1.2: Schematic block diagram of RF energy harvesting [16].

1.2 Literature review

1- In (2004), Heikkinen and Kivikinen presented a paper on the design and fabrication of a rectenna for the circularly polarized 5.8 GHz band. The authors used a thin, flexible, and low-loss microwave laminate material to fabricate the rectenna. The design consisted of a circular patch antenna for receiving the electromagnetic waves and a rectifier circuit for converting the received signal into DC power. The authors reported that the use of a microwave laminate material allowed for a flexible and lightweight design, which is suitable for portable and wearable applications. The circular patch antenna was designed to have a circular polarization to match the polarization of the incoming signal. The rectifier circuit was designed using a Schottky diode and a low-pass filter to achieve high rectification efficiency [17].

2- In (2008), Yo et al. presented a paper on the design and analysis of a circularly polarized rectenna constructed on an FR-4 substrate. The rectenna consisted of a small circular patch antenna with two unbalanced slots and a rectifier circuit for converting the received signal into DC power. The authors reported that the use of unbalanced slots in the circular patch antenna allowed for circular polarization of the incoming

signal. The rectifier circuit was designed using a Schottky diode and a low-pass filter to achieve high rectification efficiency. The experimental results showed that the rectenna achieved a maximum rectification efficiency of 60% at a distance of 1.2 meters [18].

3- In (2010), Gao et al. presented a paper on the design and analysis of a rectenna with circularly polarized antennas for wireless power transmission and energy harvesting applications. The rectenna consisted of a circularly polarized patch antenna and a rectifier circuit based on a voltage doubler topology. The simulation results showed that the rectenna had a wide operating bandwidth of 3.1 GHz to 10.6 GHz with a peak gain of 6.2 dBi. The experimental results showed that the rectenna achieved a maximum rectification efficiency of 78% at a distance of 4 meters [19].

4- In (2012), Takhedmit et al. presented a paper on the design and analysis of a circularly polarized ring slot rectenna with a resonance frequency of 2.45 GHz. The authors reported that the circularly polarized ring slot antenna is suitable for wireless power transmission and energy harvesting applications due to its simple and compact design. The rectenna consisted of a circularly polarized ring slot antenna and a rectifier circuit based on a voltage doubler. The circularly polarized ring slot antenna was designed using a combination of a circular ring and a slot. The rectifier circuit was designed using two diodes and two capacitors to achieve high rectification efficiency. The results showed that the rectenna achieved a maximum rectification efficiency of 71% [20].

5- In (2013), Masotti et al. presented a paper on the design and analysis of a tetra-band annular ring patch rectenna for wireless power transfer and

energy harvesting applications. The authors reported that the design of such a rectenna is challenging due to the need to achieve high efficiency over multiple frequency bands. To address this challenge, the authors suggested the use of a genetic algorithm to optimize the design parameters of the rectenna. The rectenna consisted of an annular ring patch antenna and a rectifier circuit based on a voltage doubler topology. The annular ring patch antenna was designed to operate at four frequency bands: 868 MHz, 915 MHz, 2.45 GHz, and 5.8 GHz. The rectifier circuit was designed using two Schottky diodes and two capacitors to achieve high rectification efficiency. The authors used a genetic algorithm to optimize the design parameters of the rectenna, including the outer and inner radii of the annular ring patch antenna and the spacing between the patch and ground plane. The optimized design achieved a maximum efficiency of 77% at 2.45 GHz and a minimum efficiency of 41% at 868 MHz [21].

6- In (2014), Valenta and Durgin presented a paper on millimeter-wave power transfer for wireless sensor networks (WSNs). The authors reported that the use of millimeter-wave frequencies for wireless power transfer is favorable due to the availability of large bandwidths and the potential for small antenna sizes. The authors proposed a millimeter-wave power transfer system based on a rectenna that can harvest energy from ambient millimeter-wave signals. The rectenna consisted of a patch antenna and a rectifier circuit based on a voltage doubler. The patch antenna was designed to operate at 30 GHz, which is a millimeter-wave frequency. The rectifier circuit was designed using two Schottky diodes and two capacitors to achieve high rectification efficiency. The authors performed simulations and experiments to evaluate the performance of the designed rectenna. The simulation results showed that the rectenna

had a wide operating bandwidth of 28 GHz to 38 GHz with a peak gain of 3.2 dBi. The experimental results showed that the rectenna achieved a maximum rectification efficiency of 10% [22].

7- In (2015), Niotaki et al. presented a paper on the design and analysis of a dual-band rectenna for energy harvesting applications. The authors reported that the design of a dual-band rectenna is challenging due to the need to achieve high efficiency over multiple frequency bands. The authors proposed a dual-band rectenna that can operate at both 915 MHz and 2.45 GHz frequency bands. The patch antenna was designed to have a dual-band response at both 915 MHz and 2.45 GHz frequency bands. The simulation results showed that the rectenna had a dual-band response with a peak gain of 3.2 dBi at 915 MHz and a peak gain of 7.8 dBi at 2.45 GHz [23].

8- In (2015), Song et al. presented a paper on the design and analysis of a broad-band rectenna for wireless power transmission and energy harvesting applications. The authors reported that the design of a broad-band rectenna is challenging due to the need to achieve high efficiency over a wide frequency range. The authors proposed a broad-band rectenna that can operate in the frequency range of 1.8 to 2.5 GHz. The rectenna consisted of a cross dipole antenna and a rectifier circuit based on a voltage doubler. The cross-dipole antenna was designed to have a broad-band response in the frequency range of 1.8 to 2.5 GHz. The simulation results showed that the rectenna had a broad-band response with a peak gain of 4.5 dBi and a 3-dB bandwidth of 680 MHz [24].

9- In 2018, Chuma et al. presented a paper on the design and analysis of a single-band rectenna for energy harvesting applications at 2.45 GHz frequency. The authors reported that the design of a single-band rectenna

is less complex than a dual-band or broad-band rectenna and can still achieve high efficiency. The rectenna consisted of a patch antenna and a rectifier circuit based on a voltage doubler topology. The patch antenna was designed to have a single-band response at 2.45 GHz frequency. The simulation results showed that the rectenna had a peak gain of 3.8 dBi and a 3-dB bandwidth of 120 MHz [25].

10- In (2018), Singh et al used numerous strategies and techniques for energy harvesting which have been proposed and investigated throughout the years using a variety of ways. However, the battery-free solution that uses energy harvesting to convert RF from the environment to DC power is significantly more efficient because it offers a dependable, clean, and environmentally friendly energy option for portable, low power devices. A rectenna consists of an impedance matching network, a rectifier, a sensing antenna, and DC output filter [26].

11- In (2019), Elwi used portable electronics that require regular charging, wireless energy harvesting (WEH) may be a practical way to meet the energy needs of wireless devices [27].

12- In (2019), Zheng et al. proposed a multiband RF energy harvesting system that could harvest energy from multiple frequency bands ranging from 700 MHz to 2.7 GHz. The system consisted of a broadband antenna, a matching network, and a rectifier circuit. The researchers reported that their system was able to harvest up to 5.5 mW of power in indoor environments and up to 20 mW in outdoor environments [28].

13- In (2019), Zhao et al. proposed a multiband RF energy harvesting system that could harvest energy from multiple frequency bands ranging from 0.9 GHz to 3.2 GHz. The system consisted of a broadband antenna, a matching network, and a rectifier circuit. The researchers reported that

their system was able to harvest up to 1.2 mW of power from a 2.4 GHz signal and up to 0.9 mW of power from a 1.8 GHz signal [29].

14- In (2019), Zhang et al. proposed a multiband RF energy harvesting system that could harvest energy from multiple frequency bands ranging from 2.3 GHz to 5.8 GHz. The system consisted of a broadband antenna, a matching network, and a rectifier circuit. The researchers reported that their system was able to harvest up to 1.1 mW of power from a 2.4 GHz signal and up to 0.6 mW of power from a 5.8 GHz signal [30].

15- In (2020), Sadeque Reza Khan et al. described modern multifunctional micro-electronic devices, like those used in biomedical implants may now be driven utilizing the methods, systems for Wireless Power Transmission (WPT). Designing and implementing high power transfer efficiency WPT systems meanwhile, hard when building WPT it is vital to consider the size of the system. The distance between the implanted medical devices location inside the body and the outside environment. The operating frequency and tissue safety due to power dissipation over the past 20 years, a broad variety of WPT systems have been investigated in order to improve overall system performance thorough analysis of this system is provided in this article [31].

16- In (2020), Alshehri et al. proposed a multiband RF energy harvesting system that could harvest energy from multiple frequency bands ranging from 1 GHz to 10 GHz. The system consisted of a broadband antenna, a matching network, and a rectifier circuit. The researchers reported that their system was able to harvest up to 2.5 mW of power from a 1 GHz signal and up to 1.5 mW of power from a 5.8 GHz signal [32].

17- In (2021), Yang et al. proposed a multiband RF energy harvester that could harvest energy from multiple frequency bands ranging from 900

MHz to 5.8 GHz. The harvester consisted of a broadband antenna, a matching network, and a rectifier circuit. The researchers reported that their harvester was able to harvest up to 1.8 mW of power from a 1 GHz signal and up to 0.6 mW of power from a 2.4 GHz signal [33].

1.3 Aims of the thesis

The aim of this work is to investigate the feasibility and performance of a multiband RF energy harvesting system using an antenna and voltage doubler rectifier. The primary objective is to design and optimize the antenna structure such as size of patch, substrate and type of material for efficient energy harvesting across multiple frequency bands. Additionally, the voltage doubler rectifier circuit will be optimized to maximize the conversion efficiency of the harvested RF energy. The thesis will also explore the potential applications of the proposed energy harvesting system, including wireless sensor networks. The research will involve theoretical analysis, simulation using electromagnetic simulation software, and experimental validation to demonstrate the performance and feasibility of the proposed system. Ultimately, the goal of this thesis is to contribute to the development of efficient and reliable energy harvesting technologies for wireless and IoT applications. These aims will be achieved by:

- 1- Study the output voltage and conversion efficiency of voltage doubler rectifier circuit with varying the input power using Advanced Design System (ADS) software.
- 2- Comparing the voltage doubler rectifier circuit for frequencies 2.4, 3.6, 5 GHz through the result of the output voltage efficiency with the goal of obtaining the highest efficiency and choosing the best among them.

3- Designing a suitable matching network between the source and the rectifier circuit to improve the system performance and reduce the reflections.

4- Designing RF antennas at frequency bands 2.4, 3.6, 5 GHz using Computer Simulation Technology (CST) microwave studio software that is employed to design and evaluate the performance of the proposed antennas. New fractal geometries will be employed for this purpose.

5- Manufacturing and fabricating the designed rectennas (rectifiers+ antenna) and testing their performance in the lab.

6- Comparing the simulated and measured result and drawing the main conclusion of this work.

1.4 Thesis Layout

The chapters of the thesis are present as follows:

- The first chapter discussed the introduction and literature reviews of multiband RF energy harvesting devices.
- The second chapter included reviews on multiband RF energy harvesting devices, comparison of different energy sources, discussion on Wireless Power Transfer (WPT), highlights on the characteristics of rectifier and demonstrated the design antenna equations for typical requirement RF energy harvesting systems.
- The third chapter discussed the simulation methodology of rectifier circuit where the efficiency and output voltage with varying input power are recorded for all circuits at operating frequency of 2.4, 3.6 and 5 GHz respectively.
- The fourth chapter focused on the design of antennas including multiband slot antennas and fractal antennas (hexagonal and

circular). The S-parameters, 2D radiation pattern, 3D radiation pattern of designed antennas were observed, recorded and discussed with a simple parametric study is conducted.

- The fifth chapter presented the conclusion of this work and the suggested future works.

CHAPTER TWO

THEORETICAL BACKGROUND

2.1 Introduction

Radio frequency (RF) energy harvesting is a process of collecting and converting RF energy from the environment into usable electrical energy. RF energy is a type of electromagnetic radiation that is commonly found in wireless communication devices, such as cell phones, routers, and other electronic devices. RF energy harvesting has gained significant attention in recent years due to the increasing demand for energy-efficient and sustainable wireless communication systems. The basic principle of RF energy harvesting is based on the conversion of electromagnetic waves into electrical energy using a device called an RF energy harvester. The harvester typically consists of an antenna, a rectifier, and a power management unit. The antenna is used to capture the RF energy from the environment and convert it into an alternating current (AC) signal. The rectifier then converts the AC signal into a direct current (DC) signal, which can be used to power electronic devices or stored in a battery for later use. The power management unit is used to regulate the voltage and current of the harvested energy to match the requirements of the electronic device.

One of the key advantages of RF energy harvesting is that it can operate without the need for a wired power source, which makes it suitable for small, low-power electronic devices. RF energy harvesting can also be used in various environments, including indoor and outdoor settings, and can harvest energy from a wide range of frequencies, ranging from a few MHz to several GHz. There are several challenges associated with RF energy harvesting, including the low power density of RF signals, which

means that only a small amount of energy can be harvested at any given time. In addition, the efficiency of RF energy harvesting is typically low, which means that a significant amount of RF energy is lost during the conversion process. To address these challenges, researchers are exploring new materials and designs to improve the efficiency of RF energy harvesters and to develop new techniques for capturing and converting RF energy. Overall, RF energy harvesting has the potential to revolutionize the way we power small electronic devices and enable the development of new wireless communication technologies that are more energy-efficient and sustainable.

2.2 Wireless Power Transfer (WPT)

Wireless Power Transfer (WPT) is a technology that enables the transmission of electrical power from a power source to an electrical load without the use of physical conductors. This technology has gained significant attention in recent years due to its potential to revolutionize the way of the power in electronic devices and vehicles. The concept of WPT has been around for over a century, with Nikola Tesla being the first to demonstrate wireless power transmission in the late 1800s. However, it is only in recent years that practical applications of WPT have begun to emerge, thanks to advancements in technology and engineering. In this introduction, we will explore the basics of WPT, including the different technologies used for WPT, the benefits and drawbacks of the technology, and the potential future applications of WPT. Wireless Internet of Things (IoT) systems and related applications have undergone tremendous growth over the past ten years [34][35], because of their enormous potential for linking tiny objects and the possibilities they provide to make our live more intelligent. Consequently, there will be a huge number of IoT devices used in contexts such as buildings, cities, adjacent car, healthcare, smart

commerce and others. Additionally, it is anticipated that as 5G and 6G technologies advance, this number of IoT will rise. In such a scenario, microwave wireless power transfer WPT and Energy Harvesting (EH) technology have garnered significant interest in last ten years, making the IoT devices more autonomous in terms of energy and removing the need for batteries or power supply resources as their maintenance are very complicated and expensive. Wireless power charging is currently necessary since many situations require the gadgets to be portable [36][37].

The rectenna is consist of the EH and WPT, which comprises of four blocks, an antenna that receive radio frequency RF signal from surrounding environment, a rectifying circuit is frequently utilized with a Schottky diode, which transform the RF power to direct current (DC) signal that travels across a load terminal, which represents the input impedance. A matching circuit is positioned between the rectifier and the antenna to optimize the power collected and avoid harmonics produced by diodes from being reradiated by the antenna (of the device that has to be powered up). The last section of block is the DC filter which smooths the output DC signal [38][39] as shown in Fig.2.1.

There are several rectenna designs now in use, according to the literature [40]-[46], rectennas described in references were made to work in linear polarization; hence they are sensitive to incident waves: this has a major impact on the effectiveness of energy collecting systems. However, an antenna with circular patterns can increase power collection and consequently conversion efficiency, because they can reduce polarization mismatch and improve tolerance to multipath interferences between transmitting and receiving antenna, therefor polarization and omnidirectional radiation pattern are highly sought [47][48].

2.3 Rectifier Characteristics

Rectifiers are electronic devices used to convert alternating current (AC) to direct current (DC). They are widely used in power supplies for electronic devices, allowing them to operate from AC power sources. Rectifiers come in various types and configurations, but they all share some common characteristics. This is achieved through the use of diodes, which are semiconductor devices that allow current to flow in only one direction. Another important characteristic of rectifiers is their efficiency in converting AC to DC. The efficiency of a rectifier is determined by the amount of power lost during the conversion process. This loss of power is due to the voltage drop across the diodes, which causes energy to be dissipated as heat. The voltage doubler rectifier was selected according to Fig.2.1, this circuit is made up of two diodes, a charging capacitor and smoothing capacitor. Fig.2.2 shows a response of a voltage doubler circuit that can provide twice the output voltage when compared to a single diode rectifier [49][50].

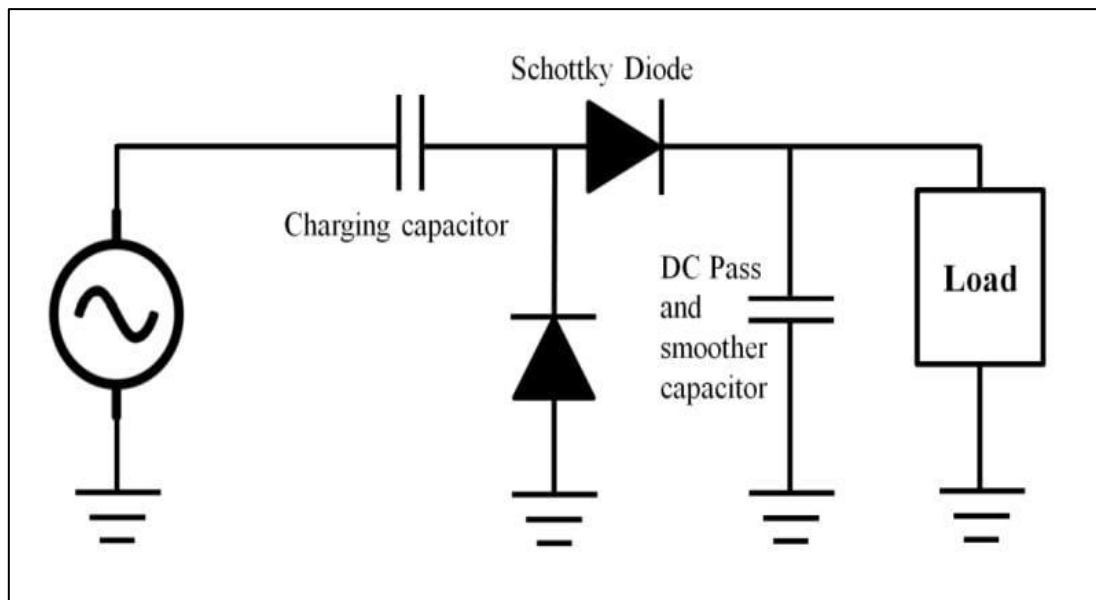


Fig.2.1: Voltage doubler rectifier circuit diagram [49].



Fig.2.2: Voltage doubler output as sweep of input power compared with single diode rectifier [50].

Diodes are selected for a special application based on a number of distinguishing features. Schottky diodes are continuously used in radio frequency application that expect low power input because they have a low forward voltage [51]. To increase power transmission an impedance matching network circuit is typically utilized between the antenna and the rectifier. Furthermore, a smoothing capacitor is extra supplied as a shunt to the rectifier output to offer a continuous DC output. Rectifier circuit typically includes one of the three essential topologies, a single diode rectifier is the primary topology [52][53]. Making use of this architecture, there are a half wave rectifier, ideal conversion efficiency for this type is 50% and diodes require some forward voltage to turn ON, as shown in Fig.2.3. Although the HSMS-2852 Diode has a forward threshold voltage of 0.15 V, this rectifier has a conversion efficiency of about 40%. The twin diode rectifier is the second kind. This rectifier is commonly used as a voltage doubler while still being regarded as a half wave rectifier [54], as shown in Fig.2.4.

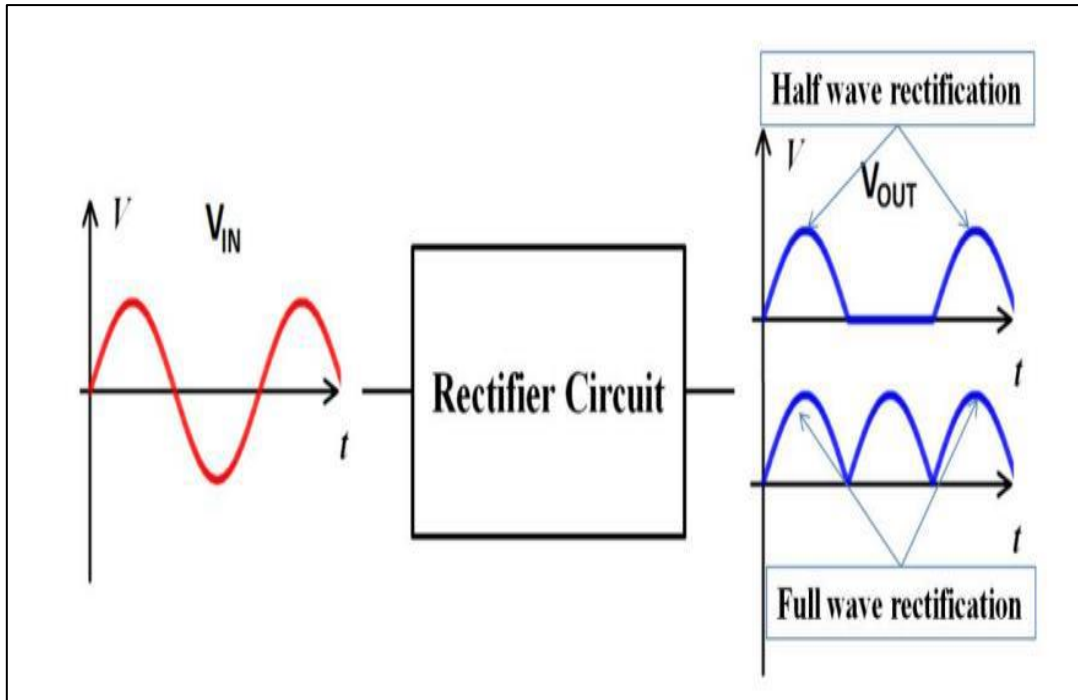


Fig.2.3: Diagram of the rectification process using half-wave and full-wave rectification [53].

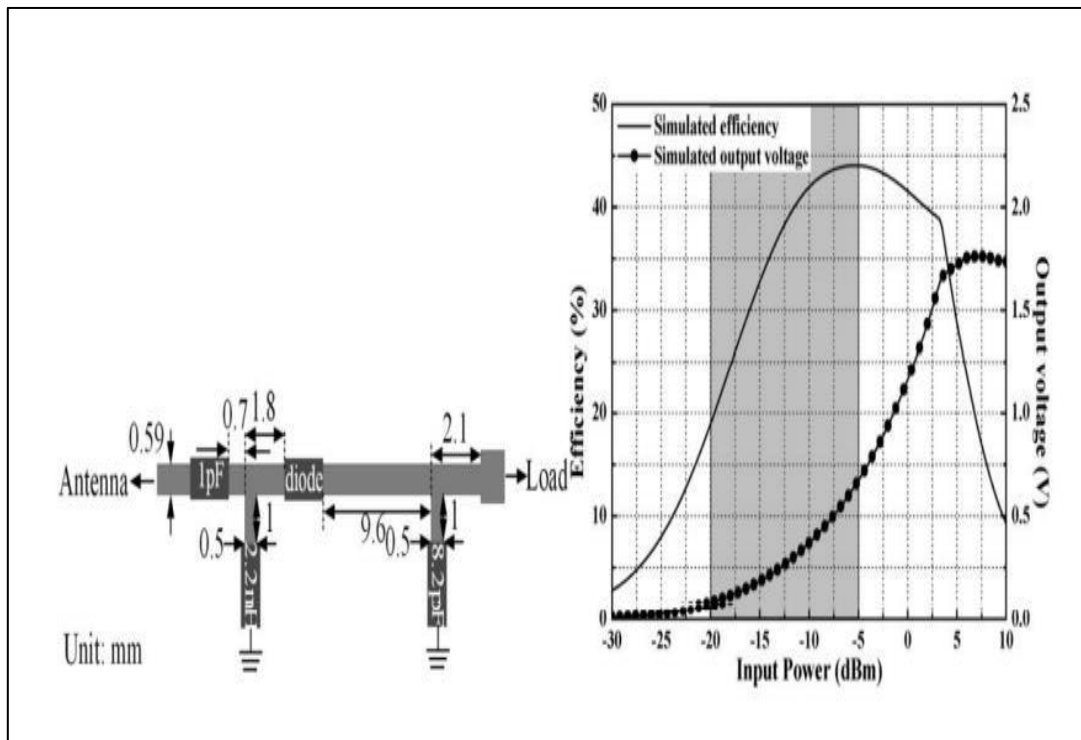


Fig.2.4: Diagram of a single diode rectifier showing the results of simulation[54].

2.4 Multiband Fractal Antennas

A multiband fractal antenna is a type of antenna that is designed to operate over multiple frequency bands using fractal geometry. Fractal geometry is a mathematical concept that describes objects with self-similar patterns at different scales. The design of a multiband fractal antenna involves using fractal patterns to create a complex antenna structure that can resonate at multiple frequencies simultaneously. The fractal geometry allows for the antenna to have a larger effective length, which enables it to operate at lower frequencies, while also providing higher resonant frequencies due to the complex pattern. One of the main advantages of multiband fractal antennas is their ability to operate over a wide frequency range. This makes them useful in applications where multiple frequency bands need to be covered, such as in wireless communication systems that use multiple frequency bands for different purposes. Another advantage of multiband fractal antennas are their compact size. The fractal geometry allows for the antenna to be designed with a smaller physical size compared to traditional antennas, while still maintaining high performance. There are several types of multiband fractal antennas, including the Sierpinski antenna, the Koch antenna, and the Minkowski antenna. Each of these antennas uses a different type of fractal geometry to achieve multiband operation. Overall, multiband fractal antennas are a promising technology for applications that require compact, high-performance antennas that can operate over multiple frequency bands. Eq. (2-1) [55] can be utilized to find the received power:

$$P_{RX} = P_{TX} + G_{RX} + G_{TX} - L_p - e_p \quad (2.1)$$

Where G_{TX} and G_{RX} are the gain of transmitting and receiving antenna respectively, L_p is the path loss, e_p is the polarization mismatch and P_{RX}

is the power received by the external receiver and P_{TX} is the power supplied to the in-body antenna [56]-[60].

2.4.1 Difficulties and requirements for the design of a multiband fractal antenna

Designing a multi-band fractal antenna can be challenging due to a number of factors. Here are some of the difficulties and requirements that need to be considered:

1. **Fractal Geometry:** Fractal antennas are based on complex geometric shapes that exhibit self-similarity, and designing these antennas requires a deep understanding of fractal geometry.
2. **Frequency Coverage:** Multi-band antennas require a wide frequency coverage, which can be challenging to achieve with a single antenna. The designer must carefully select the fractal geometry and optimize the antenna parameters to ensure that it can operate over multiple frequency bands.
3. **Impedance Matching:** The impedance of the antenna must be matched to the feed line to ensure efficient power transfer. This can be a difficult task when designing a multi-band antenna, as the impedance of the antenna will vary across different frequency bands.
4. **Size and Form Factor:** The size and form factor of the antenna must be optimized to ensure that it meets the requirements of the application. This can be a challenge when designing a multi-band antenna, as the antenna must be able to operate over multiple frequency bands while maintaining a compact form factor.
5. **Material Selection:** The performance of the antenna can be greatly influenced by the choice of materials used in its construction. The

designer must carefully select the materials to ensure that they provide the desired electrical properties and mechanical characteristics.

6. Manufacturing Complexity: Fractal antennas can be challenging to manufacture, especially when they have complex geometries. The designer must consider the manufacturing process and ensure that the antenna can be produced in a cost-effective and reliable manner.

In summary, designing a multi-band fractal antenna requires a deep understanding of fractal geometry, a wide frequency coverage, impedance matching, size and form factor optimization, material selection, and manufacturing complexity. Careful consideration of these factors is necessary to ensure that the antenna meets the requirements of the application.

The relationship between radiation efficiency and radiated power is calculated using the formula given in Eq. (2-2) [61]:

$$\eta = P_{rad} / P_{in} \% \quad (2.2)$$

where P_{in} [W] refers to the input power and P_{rad} refers to the radiated power.

2.4.2 Typical Requirements of Multiband Fractal Antenna Systems

1. Fractal Antenna Design: Multiband fractal antenna systems are designed using fractal geometry, which enables them to operate across multiple frequency bands. A review of these systems should therefore include a discussion of the types of fractal geometries that are commonly used in antenna design, as well as the design considerations that are important for achieving good performance across multiple bands.

2. Frequency Bands: Multiband fractal antenna systems operate in multiple frequency bands, so it's important to describe the frequency bands that are commonly used in these systems. This could include the range of frequencies that are typically used, the frequency allocation schemes used in different regions, and the types of devices that are commonly used to operate in these bands.

3. Antenna Performance Metrics: Antenna performance metrics such as efficiency, gain, bandwidth and radiation pattern are critical to multiband fractal antenna systems. A review of these systems should therefore include a discussion of the performance metrics that are important in these systems, as well as the tradeoffs between different performance metrics.

4. Signal Processing: Multiband fractal antenna systems often require signal processing techniques to extract useful information from signals received across multiple frequency bands. A review of these systems should therefore include a discussion of the types of signal processing techniques that are commonly used in these systems, as well as the performance tradeoffs associated with different techniques.

5. System Integration: Finally, a review of multiband fractal antenna systems should consider the challenges associated with integrating these antennas into a larger system. This could include a discussion of the types of interfaces that are commonly used in these systems, as well as the design considerations that are important for ensuring good overall system performance.

2.4.3 Antennas Parameters

Antenna parameters are characteristics of an antenna that describe its performance and behavior in transmitting or receiving electromagnetic waves. Some of the common antenna parameters include:

1. **Gain:** The gain of an antenna is a measure of how much it can increase the signal strength of the waves it receives or transmits in a particular direction compared to a reference antenna. Gain is usually expressed in decibels (dBi).
2. **Directivity:** Directivity is a measure of how well an antenna focuses its energy in a particular direction. It is expressed as a ratio of the maximum radiation intensity in a given direction to the average radiation intensity over all directions.
3. **Bandwidth:** The bandwidth of an antenna is the range of frequencies over which it can effectively transmit or receive signals; typically expressed as a percentage of the center frequency.
4. **Impedance:** Antenna impedance is the measure of the opposition to the flow of electric current through the antenna. It is usually expressed as a complex number comprising a resistance component (real part) and a reactance component (imaginary part).
5. **Polarization:** The polarization of an antenna refers to the orientation of its electric and magnetic fields relative to the direction of propagation of the electromagnetic waves. It can be linear, circular, or elliptical.
6. **Radiation pattern:** The radiation pattern of an antenna is a graphical representation of how the antenna radiates electromagnetic energy in different directions.

7. Efficiency: The efficiency of an antenna is the ratio of the power radiated by the antenna to the power supplied to it. It is usually expressed as a percentage.

2.4.4 Rectangular patch Antenna with inset feeding

The microstrip patch antenna design is accomplished according to the following equations [62] [63]:

Step 1: Calculation of the Width (W)

$$\text{The width of patch is given by } W_p = \frac{c}{2f_r \sqrt{(\epsilon_r + 1)/2}} \quad (2.3)$$

$$W_p = \frac{3 \times 10^8}{2 \times 2.4 \times 10^9 \sqrt{(4.3 + 1)/2}} = 38.37 \text{ mm}$$

Where, c is free space velocity of light. f_r is resonant frequency in GHz for the current design. ϵ_r is dielectric constant of the substrate (4.3 for FR-4).

Step 2: Calculation of effective dielectric constant

$$\epsilon_{reff} = \frac{\epsilon_r + 1}{2} + \frac{\epsilon_r - 1}{2} \left[1 + 12 \frac{h}{w} \right]^{-\frac{1}{2}} \quad (2.4)$$

$$\epsilon_{reff} = \frac{4.3 + 1}{2} + \frac{4.3 - 1}{2} \left[1 + 12 \frac{1.6 \times 10^{-3}}{38.39 \times 10^{-3}} \right]^{-\frac{1}{2}} = 3.99$$

Where, h is the height of the substrate or thickness of the substrate given as 1.6 mm.

Step 3: Now length effective is given by

$$L_{eff} = \frac{c}{2f_r \sqrt{\epsilon_{reff}}} = \frac{3 \times 10^8}{2 \times 2.4 \times 10^9 \times \sqrt{3.99}} = 31.28 \text{ mm} \quad (2.5)$$

Step 4: Calculation of the length extension ΔL , which is given by

$$\Delta L = 0.412h \frac{(\epsilon_{reff} + 0.3) \left(\frac{w}{h} + 0.265\right)}{(\epsilon_{reff} - 0.258) \left(\frac{w}{h} + 0.8\right)} \quad (2.6)$$

$$\Delta L = 0.412 \times 1.6 \times 10^{-3} \times \frac{(3.99 + 0.3) \left(\frac{38.39 \times 10^{-3}}{1.6 \times 10^{-3}} + 0.265\right)}{(3.99 - 0.258) \left(\frac{38.39 \times 10^{-3}}{1.6 \times 10^{-3}} + 0.8\right)}$$

$$\Delta L = 6.59 \times 10^{-4} \times \frac{101.8}{92.5} = 7.25 \times 10^{-4}$$

Step 5: Now length of patch is given by

$$L_p = L_{eff} - 2\Delta L \quad (2.7)$$

$$L_p = 31.28 \times 10^{-3} - (2 \times 7.25 \times 10^{-3}) = 29.85 \text{ mm}$$

Step 6: compute of Length of substrate is given by

$$L_s = 6h + L_p \quad (2.8)$$

$$L_s = 6 \times 1.6 \times 10^{-3} + 29.86 \times 10^{-3} = 41 \text{ mm}$$

Step 7: compute of width of substrate is given by

$$w_s = 6h + w_p \quad (2.9)$$

$$w_s = 6 \times 1.6 \times 10^{-3} + 38.39 = 44 \text{ mm}$$

Step 8: compute of the length of inset feed line is given by

$$D = \frac{L}{\pi} \text{Cos}^{-1} \left(\sqrt{\frac{Z_{feed\ line}}{Z_{antenna}}} \right) \quad (2.10)$$

$$D = \frac{29.86 \times 10^{-3}}{\pi} \text{Cos}^{-1} \left(\sqrt{\frac{50}{281}} \right) = 6 \text{ mm}$$

Where the value of D must be in radians

Step 9: compute of the width of inset feed line is given by

$$s = 1.46 \text{ mm}$$

2.4.5 Circular patch antenna

The radius (r) of circular patch can be calculated using the following equations [64][65].

$$r = \frac{F}{1 + \frac{2h}{\pi F \epsilon_r} [\ln\left(\frac{\pi F}{2h}\right) + 1.7726]^{\frac{1}{2}}} \quad (2.11)$$

where

$$F = \frac{(8.791 \times 10^9)}{(f_r \times \sqrt{\epsilon_r})} \quad (2.12)$$

$$F_{at (3 \text{ GHz})} = \frac{(8.791 \times 10^9)}{(3 \times 10^9 \times \sqrt{4.3})} = 1.413$$

$$r_{at (3 \text{ GHz})} = \frac{1.413}{1 + \frac{2 \times 1.6 \times 10^{-3}}{\pi \times 1.413 \times 4.3} [\ln\left(\frac{\pi \times 1.413}{2 \times 1.6 \times 10^{-3}}\right) + 1.7726]^{\frac{1}{2}}} = 14.1 \text{ mm}$$

ϵ_r is the dielectric constant of the substrate, f_r is the resonant frequency in GHz and h is the thickness of the substrate.

But there is a disadvantage in the above equation, and the radius of patch will be enhanced by following equation:

$$r_{eff} = r \left[1 + \frac{2 \times h}{\pi \times r \times \epsilon_r} \left\{ \ln\left(\frac{\pi \times r}{2 \times h}\right) + 1.7726 \right\} \right]^{\frac{1}{2}} \quad (2.13)$$

CHAPTER THREE

DESIGN AND SIMULATION OF SINGLE-STAGE RECTIFIER CIRCUITS

Voltage double rectifier and matching circuit design are simulated at 2.4 GHz, 3.6 GHz, and 5 GHz using Advanced Design System (ADS) Software. Wireless Power Transfer (WPT) is a reliable method of transferring power from a source to an end system without the need of cables or connections. This task is performed by rectennas, which are antennas coupled with rectifiers. Undoubtedly, the rectifier which converts RF power received into DC power is the most important component of the rectenna. Several rectifier topologies are designed for RF use (rectenna application) in this chapter. RF energy is taken in by the antenna and sent into the matching circuit. The antenna and rectifier's impedances have to be matched with aid of an intermediate matching circuit, while the Schottky diode type HSMS-2820 is utilized for rectification. It is worth mentioning that choosing the right diode is one of the most vital factors. The simulation results including DC output voltage (V_{out}) and efficiency with respect to the input power are recorded and plotted at three frequency bands throughout this chapter. The frequency response of Schottky diode type HSMS-2820:

- Typical operating frequency up to 6GHz.
- Intermodulation Distortion (IMD) Rating: -26 dBc (typical) at 2 GHz, 0 dBm input power levels.

The Forward Current vs. Forward Voltage and Reverse Current vs. Reverse Voltage at Temperatures as shown in Fig.3.1.

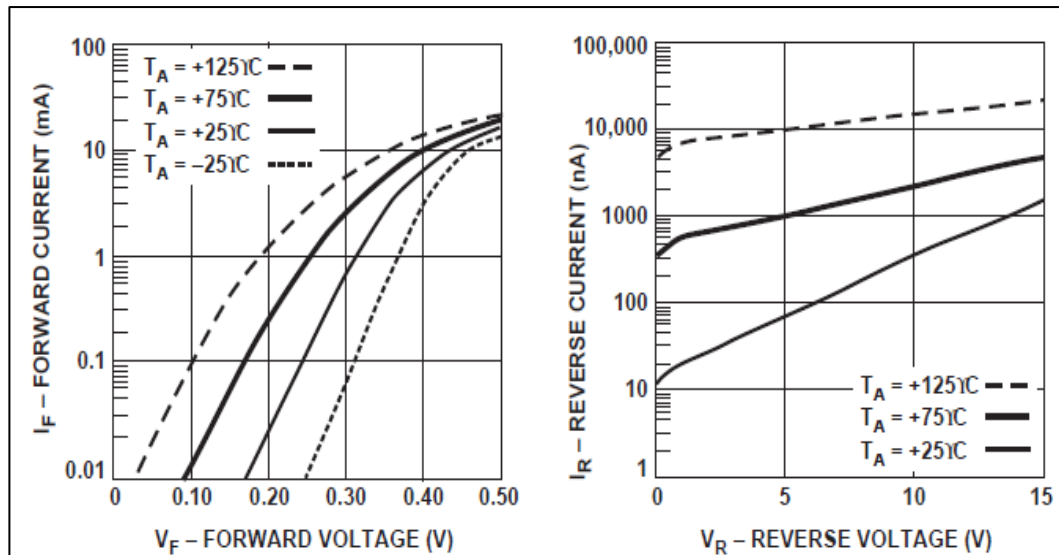


Fig.3.1: Forward Current vs. Forward Voltage and Reverse Current vs. Reverse Voltage at Temperatures.

3.1 Matching Circuit Methods

There are several methods for matching networks and only two of them will be discussed in detail in this chapter:

- 1- LC (Inductance and Capacitance)-Matching Method
- 2- TL (Transmission Lines)-Matching Method

3.1.1 LC- Matching Method:

There are four circuit configurations in this technique and one of them can be chosen depending on whether it is needed to pass the DC current or not and also depending on which one is higher resistance the input or load resistance as shown in Fig.3.1.

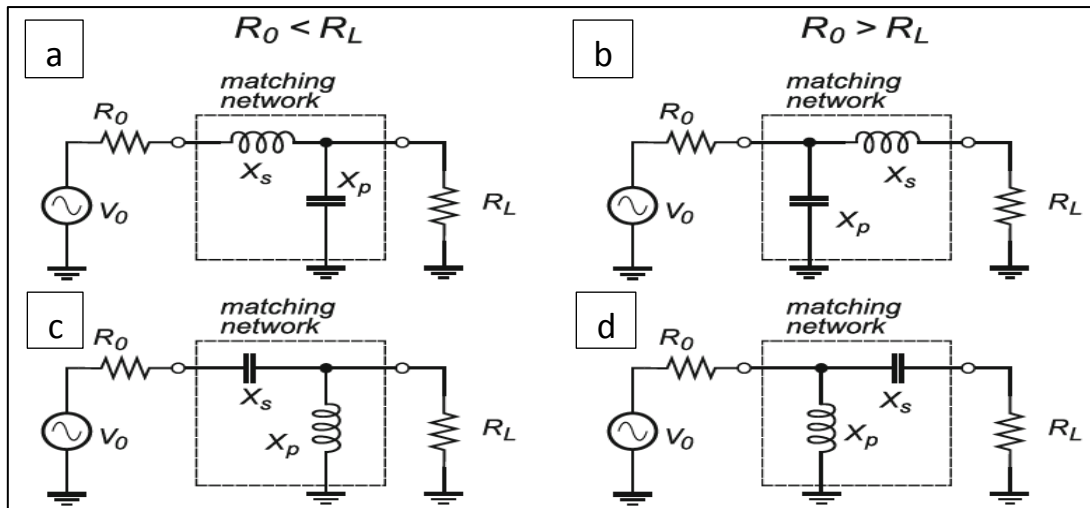


Fig.3.2: LC-Matching Method.

The common features of the LC-matching Method are:

- This one is solved using the Q matching technique.
- One of the drawbacks of this technique is its use of reactive components, meaning that the matching is possible at only one frequency.
- An LC section placed between two resistive terminations creates a serial subnetwork and a parallel subnetwork as shown in Fig.3.2. When the two subnetworks are conjugate matched to each other, their Q factors are equal.

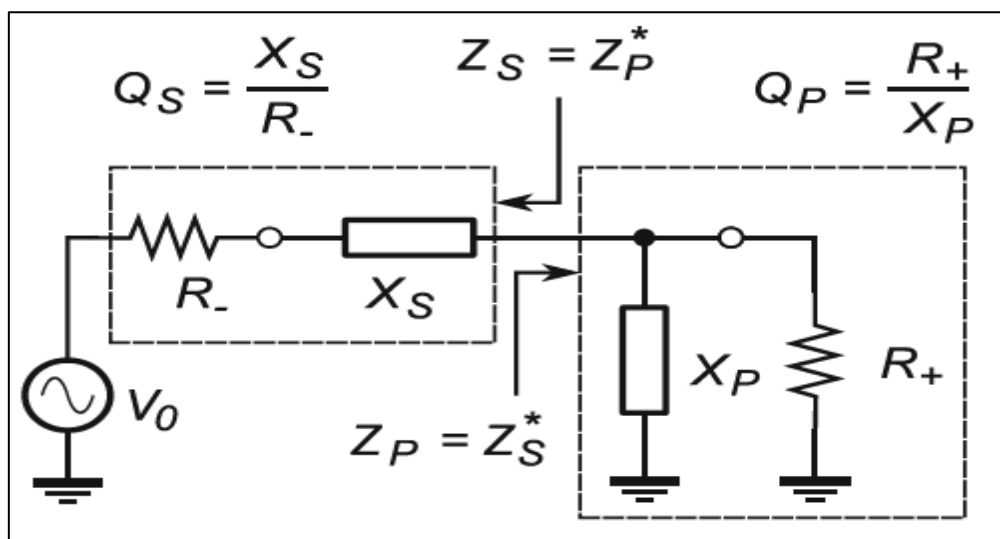


Fig.3.3: Equivalent Circuit for LC-Circuit.

Now, we will try to calculate the L and C values of the matching for the voltage double rectifier at 2.4 GHz for a 50Ω source (R_+) representing the antenna. The first step is to calculate the input impedance using ADS software. The voltage double circuit in Fig. 3.4 is simulated in ADS without using any matching method and the input impedance (Z_{in}) versus frequency is plotted as illustrated in Fig.3.5. The input impedance is recorded over the frequency range 1.2 GHz to 3.4 GHz and it is found that Z_{in} at 2.4 GHz is equal to $(3.196-j38.63 \Omega)$.

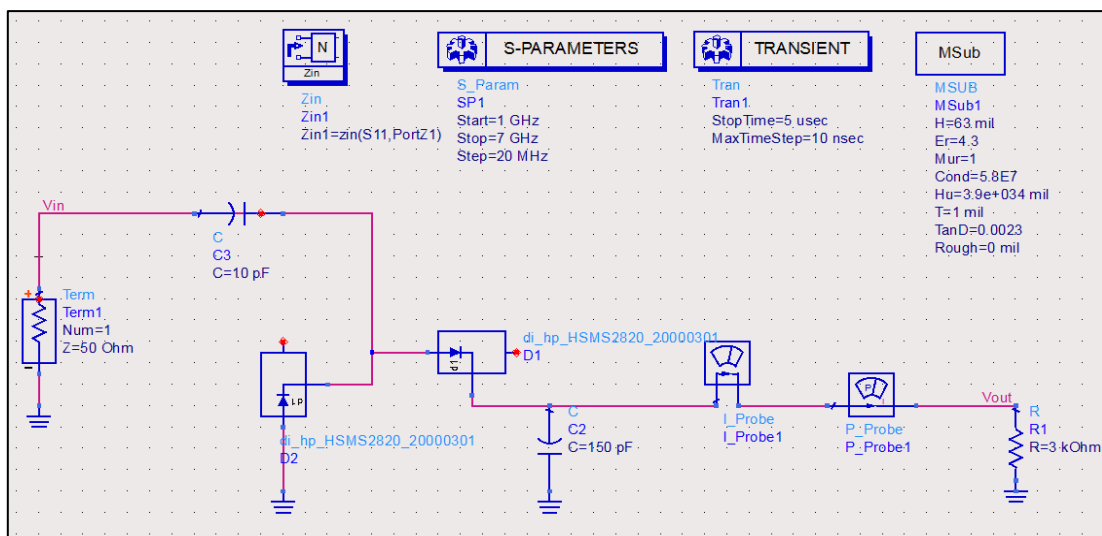


Fig.3.4: Simulated circuit to calculate Z_{in} at frequency band 2.4 GHz.

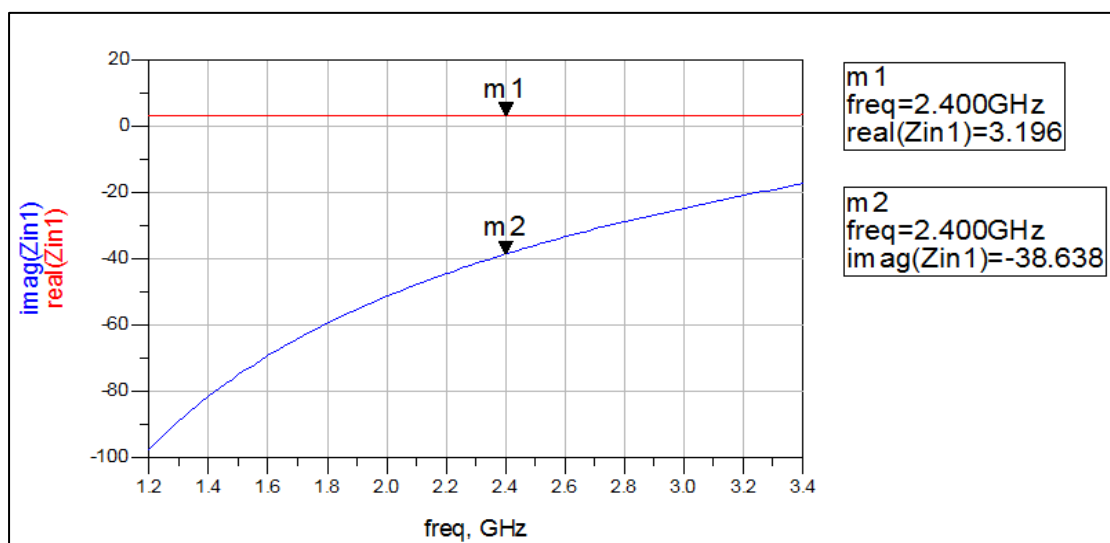


Fig.3.5: Simulated input impedance.

To validate the simulation results of Z_{in} , the value of input impedance is found analytically by using the equivalent circuit of the diode as shown in Figs.3.5 and 3.6.

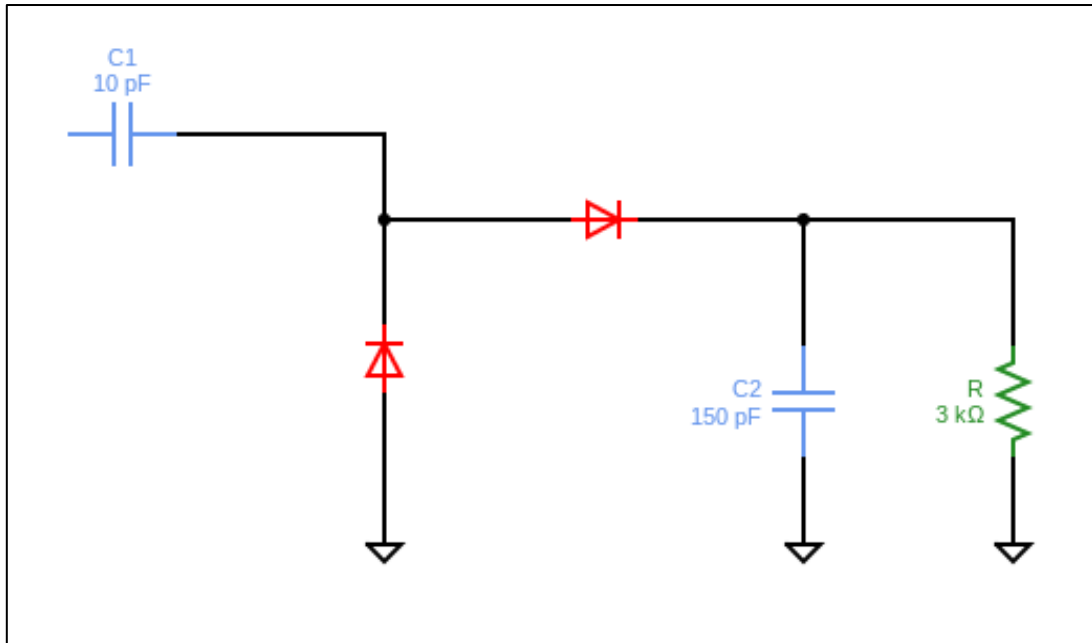


Fig.3.6: Voltage doubler rectifier Circuit.

Compensate for each Diode with the equivalent circuit shown in Fig.3.6.

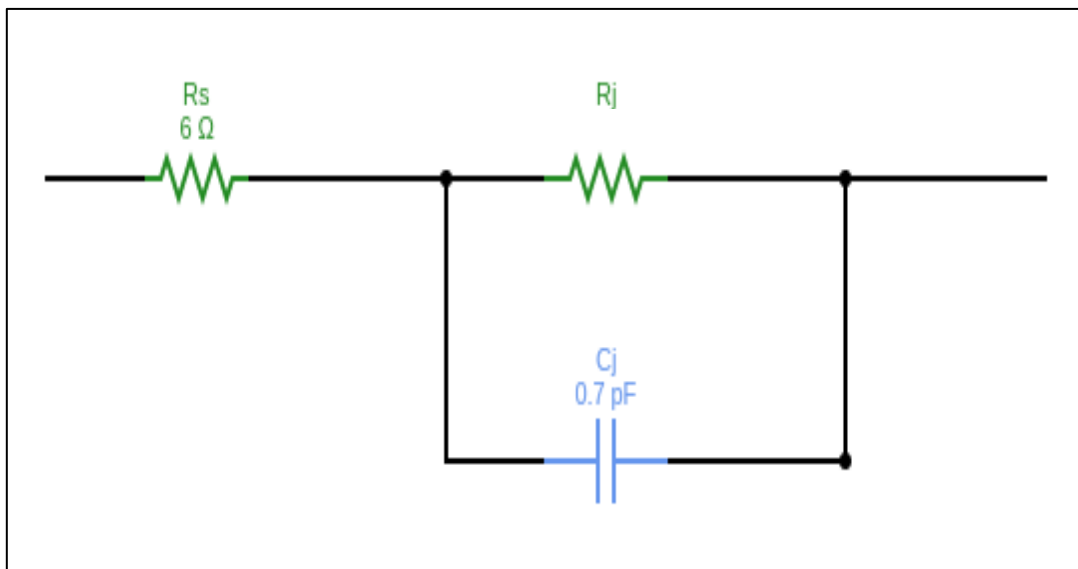


Fig3.7: Equivalent circuit for the employed diode.

This equation for computing R_j :

$$R_j = \frac{8.33 \times 10^{-5} \times n \times T}{I_s} \quad (3.1)$$

$$R_j = \frac{8.33 \times 10^{-5} \times 1.5 \times 300}{2.2 \times 10^{-8}}$$

$$R_j = 1.7 \text{ M}\Omega,$$

where $I_s = 2.2 \times 10^{-8} \text{ A}$, $n = 1.5$, $T = 300 \text{ c}$, $R_s = 6 \text{ }\Omega$ and $C_j = 0.7 \text{ pF}$. All values are taken from Data sheet for HSMS-2820 Schottky Diode.

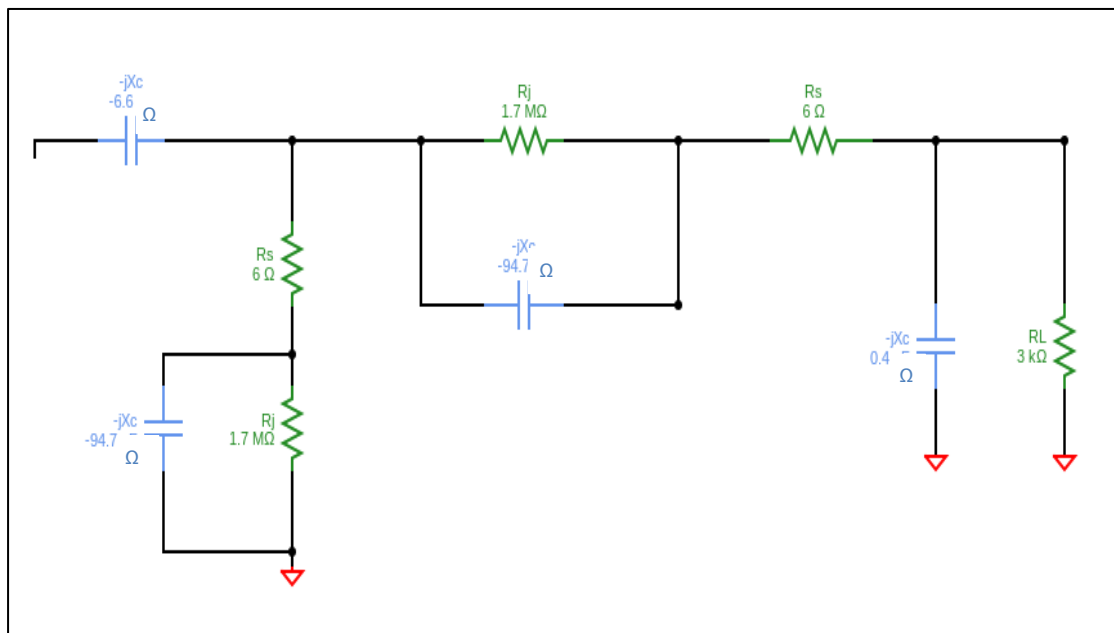


Fig.3.8: Analysis circuit to compute Z_{in} .

The value of R_j can be neglected because it has great value, then the circuit arrangement become as follows:

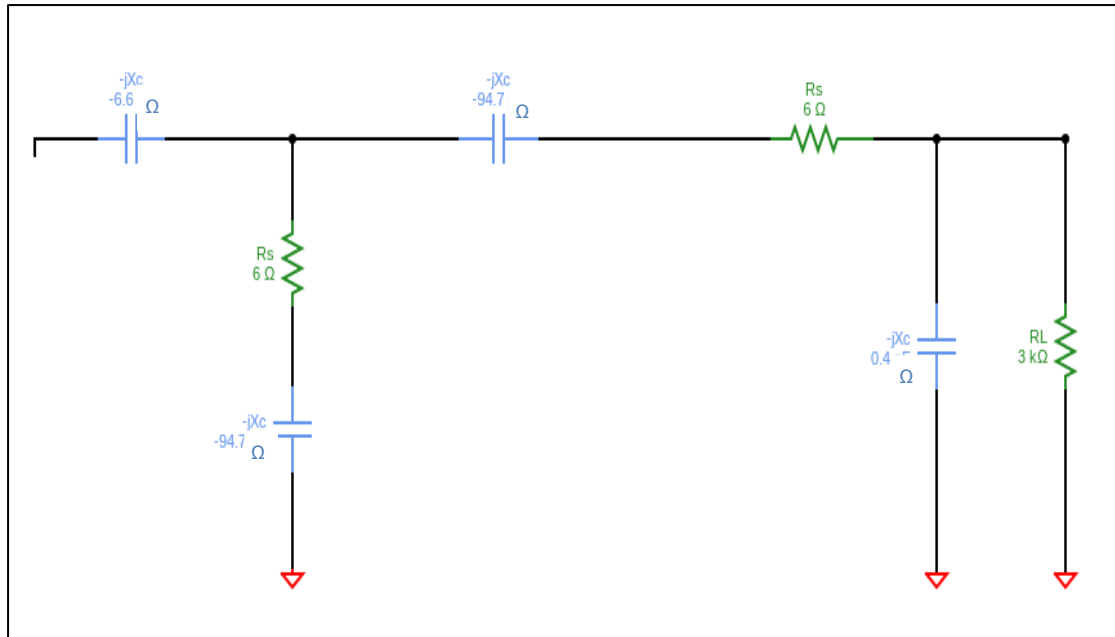


Fig.3.9: Simplified circuit after neglecting R_j .

$$Z_{in} = 6 - j95.14 \parallel 6 - j94.7$$

$$Z_{in} = \frac{(6 - j95.14) \times (6 - j94.7)}{(6 - j95.14) + (6 - j94.7)}$$

$$Z_{in} = \frac{8973.7 - j1139}{12 - j189.84} = 3 - j47.4 \Omega \quad \dots \text{ By analysis}$$

$$Z_{in} = 3.196 - j38.36 \Omega \quad \dots \text{ By simulation}$$

It is clearly seen that the analytical value of Z_{in} ($3 - j47.4 \Omega$) is very close to the simulated value ($3.19 - j38.6 \Omega$), which validates our simulation procedure. This value will be referred to as source resistance (R_s) in the calculation of the matching parameters.

Fig.3.2-b will be adopted as a matching method in this thesis since it fulfills the conditions of the voltage doubler rectifier used in this work.

Now, to compute the values of L and C of the matching method, use the following equations:

$$Q_s = Q_p = \sqrt{\frac{R_+}{R_-} - 1} \quad (3.2)$$

And then:

$$Q_s = \frac{X_s}{R_-} \quad (3.3)$$

$$Q_p = \frac{R_+}{X_p} \quad (3.4)$$

where R_- is the source resistance, R_+ is the load resistance, Q_s is the Serial Q Factor and Q_p is the parallel Q Factor

From the Eq. 3-2, the values of Q_s and Q_p can be calculated to be:

$$Q_s = Q_p = 3.826$$

$$Q_s = \frac{X_s}{R_-}$$

$$X_s = 3.826 \times 3.196 = 12.227$$

$$X_s = X_L = 2\pi fL \rightarrow 2 \times \pi \times 2.4 \times 10^9 \times L$$

$$L = \frac{12.227}{2 \times \pi \times 2.4 \times 10^9} = 0.81 \text{ nH}$$

$$Q_p = \frac{R_+}{X_p}$$

$$X_p = \frac{50}{3.826} = 13.06$$

$$X_p = X_C = \frac{1}{2\pi fC} \rightarrow 13.06 = \frac{1}{2 \times \pi \times 2.4 \times 10^9 \times C}$$

$$C = \frac{1}{2 \times \pi \times 2.4 \times 10^9 \times 13.06} = 5 \text{ pF}$$

Since the source impedance is pure resistance (50 Ω) and has no reactive part, the added value of the parallel capacitance will be 5 pF. On the other hand, for the load side, the calculated value of the series inductor is 0.81 nH. However, it can be seen that the load, which represents the equivalent impedance of the rectifier (3.19-j38.6 Ω) has a reactive part (-j38.6) and needs to be resonated out by adding a positive reactive part (+j38.6),

which can be achieved by an inductor that has a value of $L=2.56$ nH. Thus, the total added inductor to the circuit has to be $L=0.81\text{nH}+2.56\text{nH}=3.37$ nH.

3.1.2 TL (Transmission Lines) matching circuit

ADS is employed again to find the matching at a specific frequency, but this time a TL matching is used instead of the LC matching due to get better match and easy to fabricate. To adjust the Transmission Lines at a specific frequency such as a 2.4 GHz, the following procedure should be followed step by step:

Step (1): In the beginning use the smith chart palette with two impedance term as illustrated in circuit diagram in Fig.3.10.

Step (2): From Smith chart circuit select the frequency at 2.4 GHz, source impedance (z_{in}) at $50+j0$ and load impedance (z_l) at $3.196-j38.63$ and use two lines length and two open stub blocks to perform this task. The four blocks of TL will be calibrated, which appeared in the beginning the point of the (z_l) in the (Smith Chart Utility) and then pull out the TL1 from the point of (z_l) until reach to the first arc which faces of the Smith Chart and then pull out the TL2 from the end arc of the TL1 to the first arc which faces and also pull out the TL3 from the end arc of the TL2 to first arc which faces and finally pull out TL4 from the end arc of the TL3 until to meet the zero (reference) point of the Smith Chart and will be excellent match of S11 at 2.4 GHz as illustrated in below Fig.3.11.

Step (3): After adjusting the S11 at 2.4 GHz then from Smith chart click on the button (Build ADS Circuit) then the block diagram of transmission lines appear as illustrated in Fig.3.12.

Step (4): Based on of the previous information of block diagram of transmission lines compensate the value of Electric Field (E) for each block to find the dimensions (W and L) for four blocks that marked with TL1, TL2, TL3 and TL4 respectively by using the Synthesize property the LineCalc window of ADS as shown in Fig.3.13.

Step (5): Finally open the window of LinCalc to find dimensions (W and L) for all block of matching network circuit at 2.4 GHz consists of four blocks of TL as illustrated in Fig.3.14.

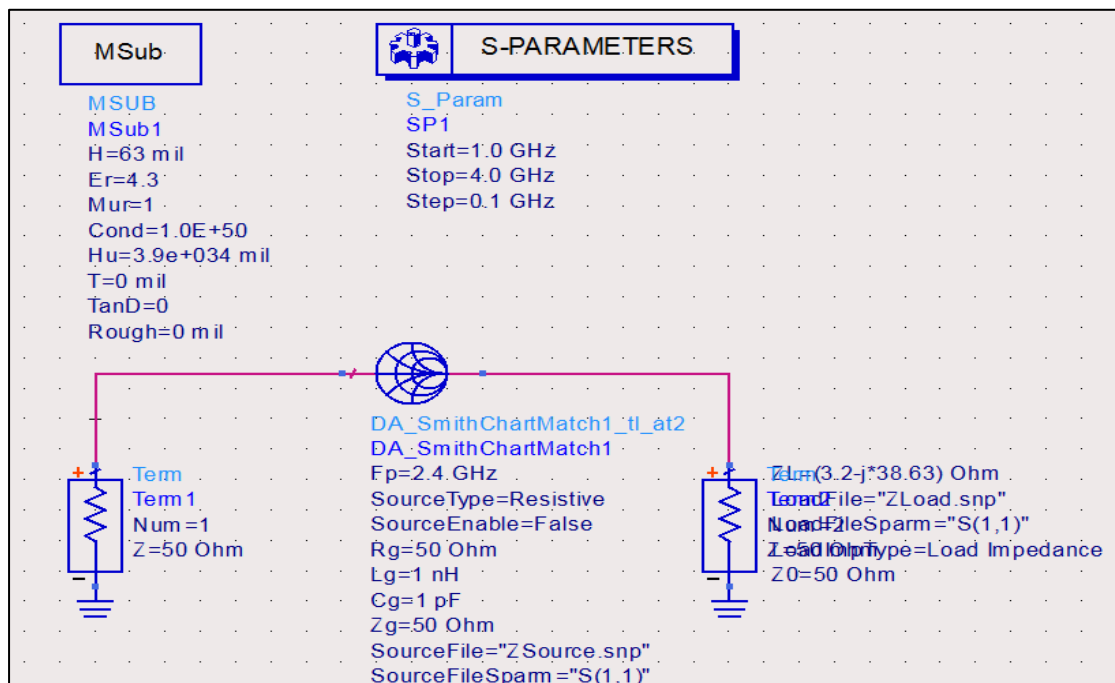


Fig.3.10: Tools of Smith chart.

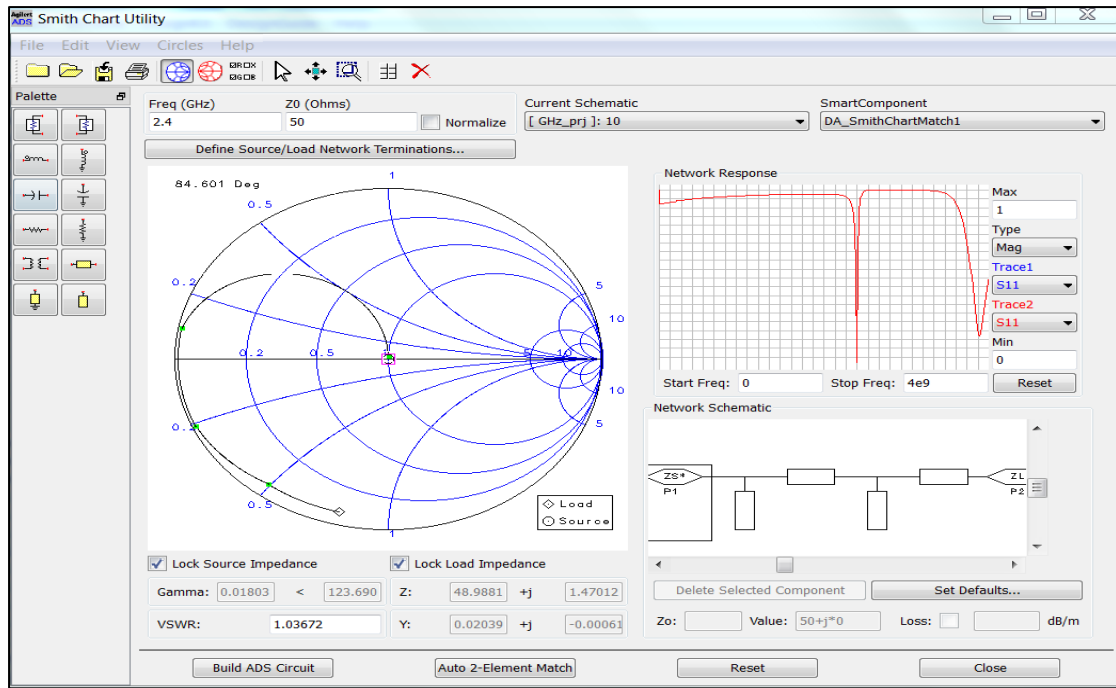


Fig3.11: Window of the Smith chart in ADS.

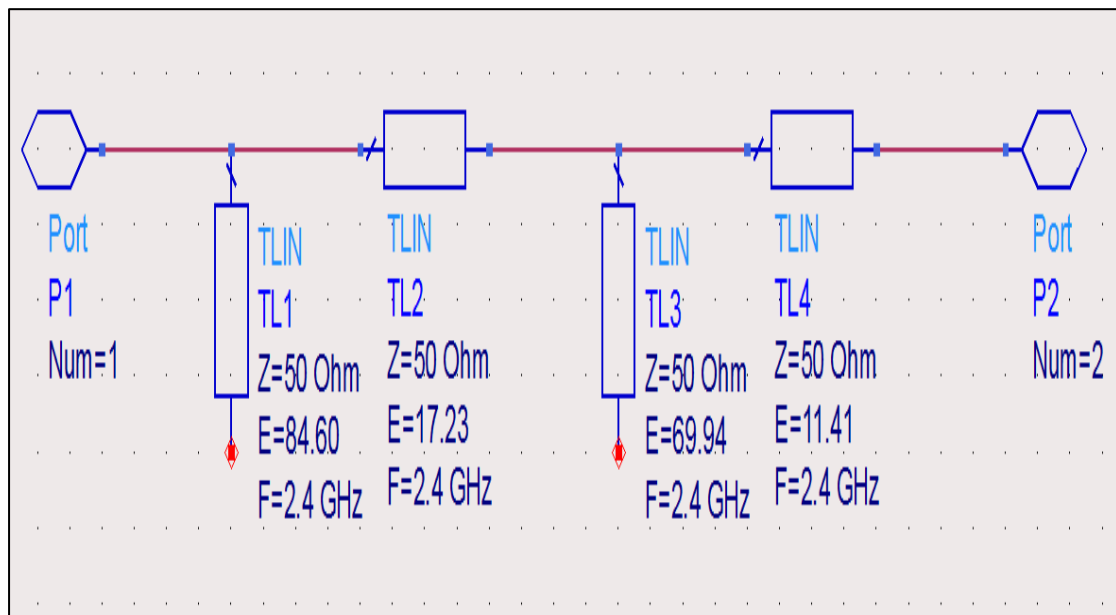


Fig.3.12: Block diagram of Transmission Lines.

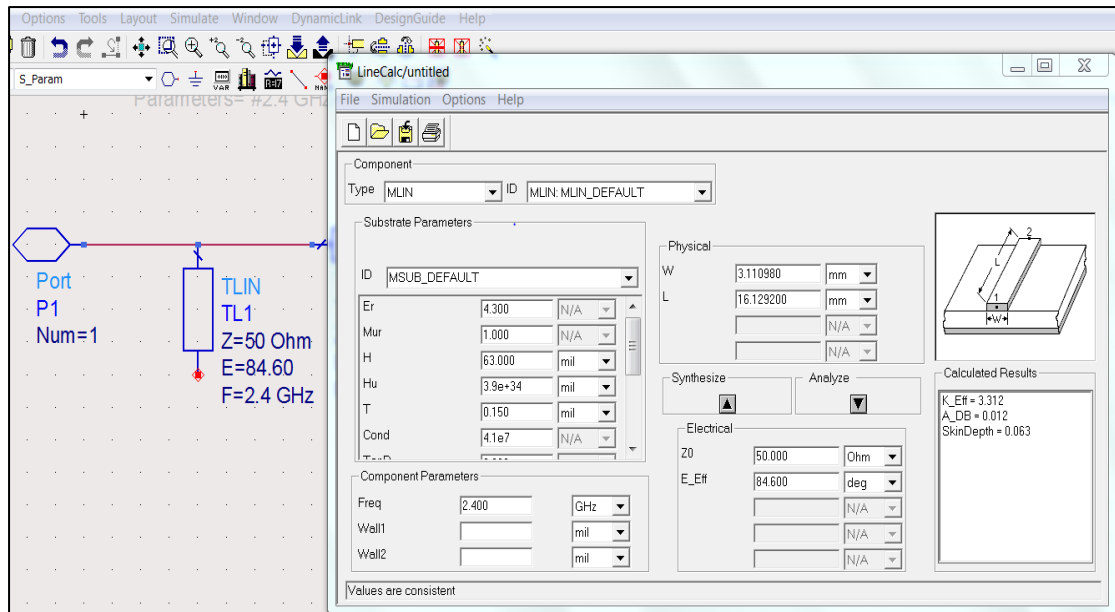


Fig.3.13: Window of the LineCalc to compute Width and Length.

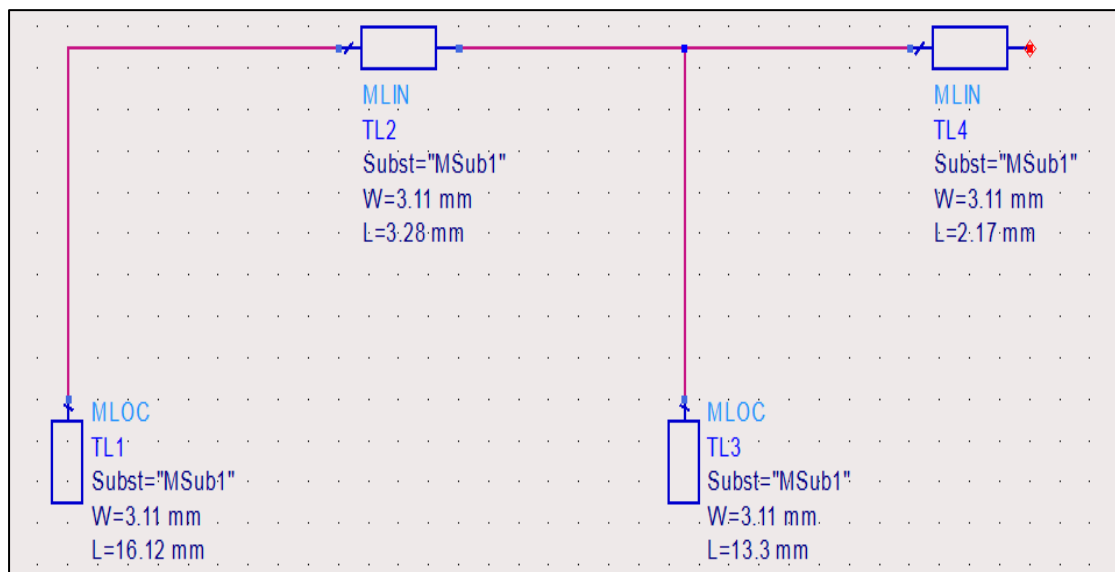


Fig.3.14: Simulated Block diagram of Transmission Lines (TL) at 2.4 GHz.

3.2 Rectifier Circuit operating at 2.4 GHz with LC-Circuit Matching Method

As shown in Fig.3.15, a single stage rectifier improved and simulated in Advanced Design System (ADS). The matching circuit for the rectifier circuit, which is LC-Circuit is chosen to match between an antenna and the rectifier. Furthermore HSMS-2820 diodes are used, which contribute to rectify the coming RF signal and transform it from alternating current AC to direct current DC. At the input, the series capacitance acts as a voltage doubler. Additionally, the output has a capacitance to smooth the DC output before it is fed to the load as a DC power or stored in a battery. It is necessary to note that the circuit in Fig.3.15 is intended to be printed on FR-4 substrate with a 4.3 dielectric constant and a thickness with 1.57 mm. Table 3.1, show DC Voltage output (V_{dc}) and Efficiency (η) for different input power (P_{in}) at 2.4, 3.6 and 5 GHz with using LC-Circuit.

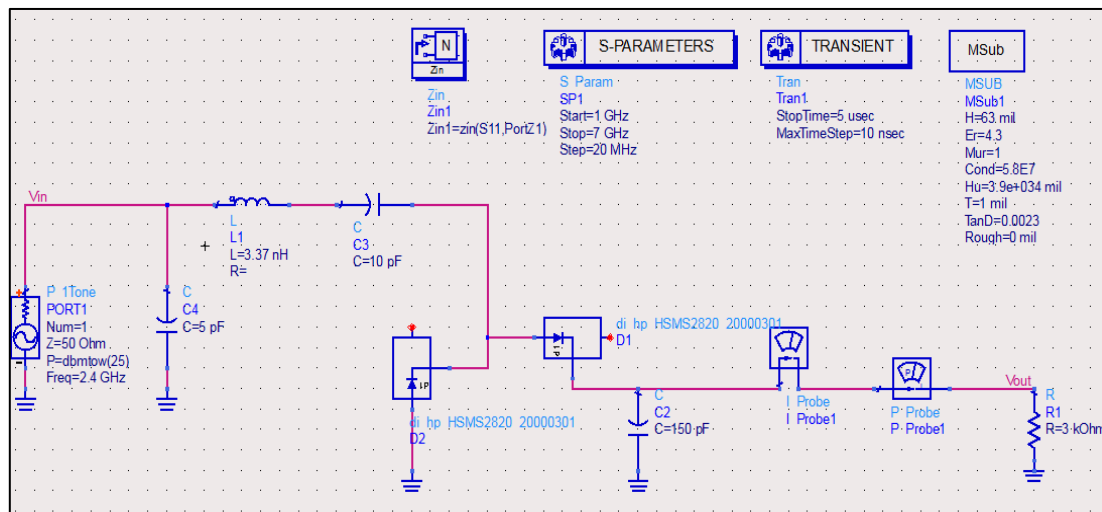


Fig.3.15: Rectifier circuit operating at 2.4 GHz with LC-Circuit as a matching method.

$$\eta_{at\ 10\ dBm} = \frac{P_{out}}{P_{in}} \times 100$$

$$\eta_{at\ 10\ dBm} = \frac{0.004522}{0.01} \times 100 = 45.22\ \%$$

Table 3.1: DC Voltage output (Vdc) and Efficiency (η) for different input power (Pin) at 2.4, 3.6 and 5 GHz with using LC-Circuit.

Pin (dBm)	Vout (dc)			Efficiency (η)		
	2.4GHz	3.6 GHz	5 GHz	2.4 GHz	3.6 GHz	5 GHz
-10	53 mV	16 mV	3 mV	0.88%	0.077%	0.0002%
-5	200 mV	170 mV	60 mV	21.7%	3.06%	0.35%
0	430 mV	500 mV	350 mV	6.2%	27.5%	3.9%
5	0.9 V	1 V	0.8 V	9.4%	10.2%	16%
10	2.2 V	1.6 V	1.7 V	45.22%	8.33%	27%
15	3.6 V	2.5 V	2.7 V	13.37%	6.7%	13.37%
20	5.9 V	3.7 V	4.5 V	11.2%	4.55%	11.2%
25	9 V	5.5 V	7 V	27.8%	3.33%	33.8%

The S11 curve versus frequency is plotted to show the influence of adding the matching network where it is clearly seen that the matching between the source and the rectifier circuit at 2.4 GHz is good and the Bandwidth (BW) = $f_H - f_L = 2.44 - 2.36 = 80$ MHz as shown in Fig.3.16.

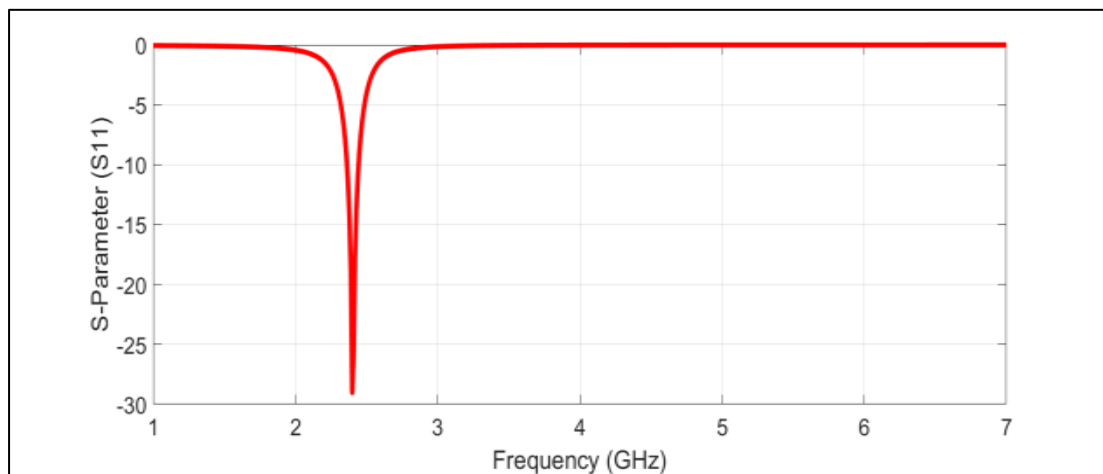


Fig.3.16: Simulated S11 of rectifier circuit at 2.4 GHz with LC-Circuit.

Fig.3.17 displays the input voltage waveform that is fed the rectifier circuit at 2.4 GHz frequency band, which is simulated by ADS.

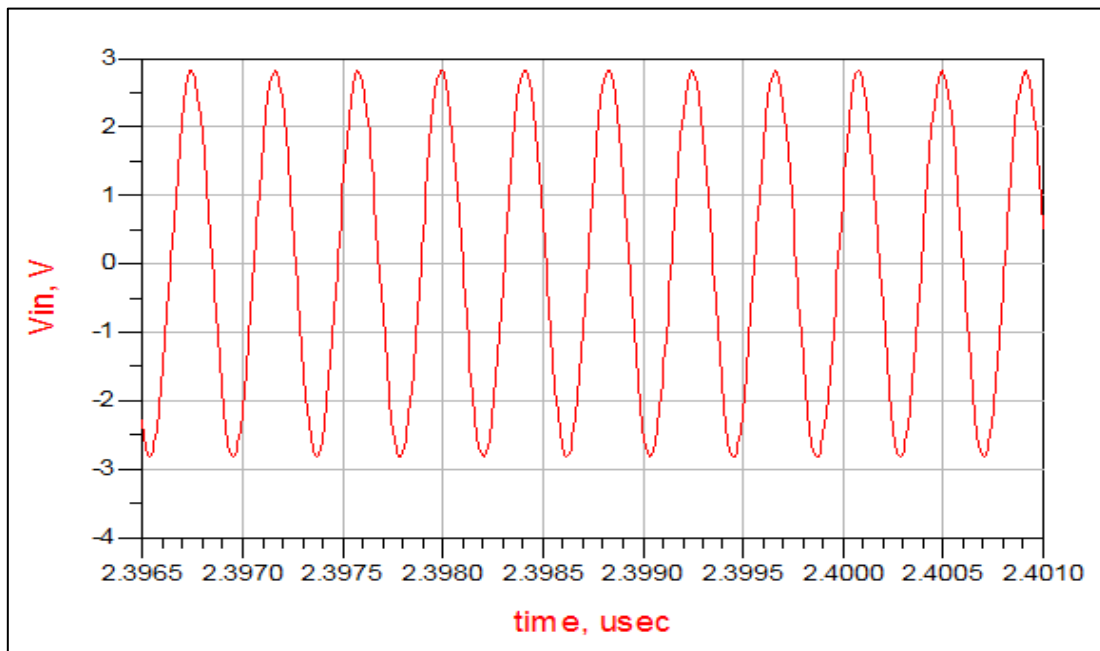


Fig.3.17: V_{in} (V) of Rectifier Circuit at 2.4 GHz with LC-Circuit.

Fig.3.18, as illustrated below the output voltage waveform for rectifier circuit at 2.4 GHz. The achieved DC output voltage is around 3 V, as may be shown in Fig.3.17 as observed that the ripple is acceptable and equal 3% in this application.

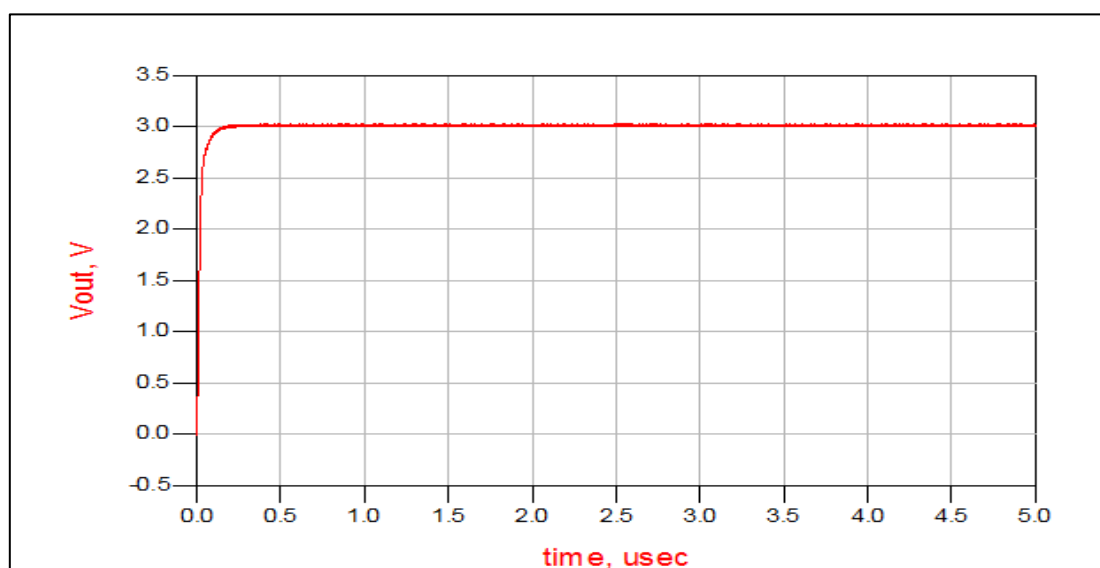


Fig.3.18: V_{out} (V) of Rectifier Circuit at 2.4 GHz with LC-Circuit.

Fig.3.19 displays the waveform of output current for the rectifier circuit at 2.4 GHz . The output current is about 9 mA, and with changing the load value changing the output current also.

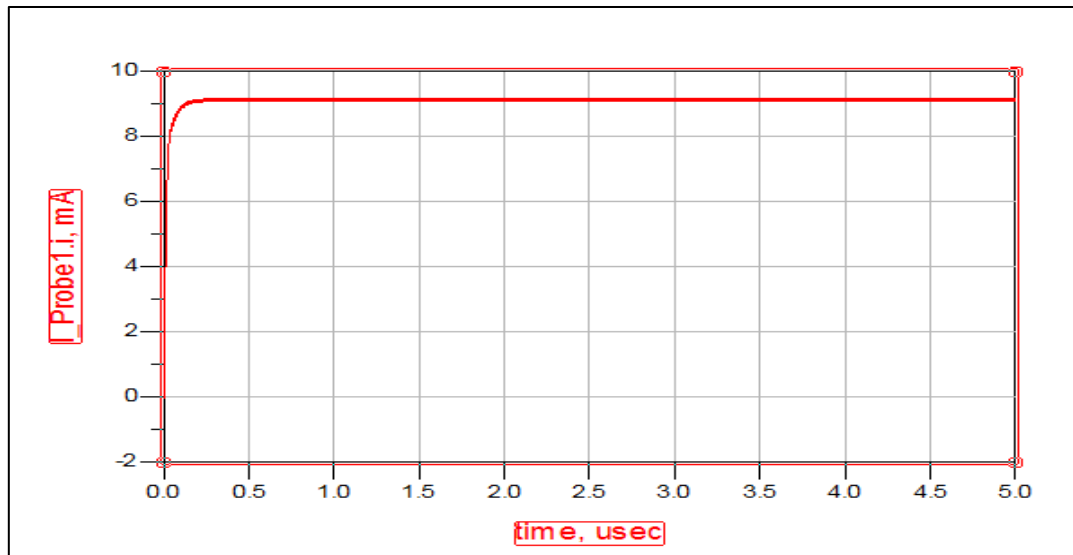


Fig.3.19: Output current of Rectifier Circuit at 2.4 GHz with LC-Circuit.

Fig.3.20 shows the measurement of the rectifier's performance. It has been investigated how the input power P_{in} impact the output voltage. The relationship between the input power (P_{in}) and the output voltage (V_{out}) of rectifier circuit at 2.4 GHz is recorded. It is clearly seen the output voltage increases exponentially with increasing the input power (P_{in}). A maximum output voltage is around 9 V is achieved at input power of 25 dBm, which is equivalent to 316.22 mW.

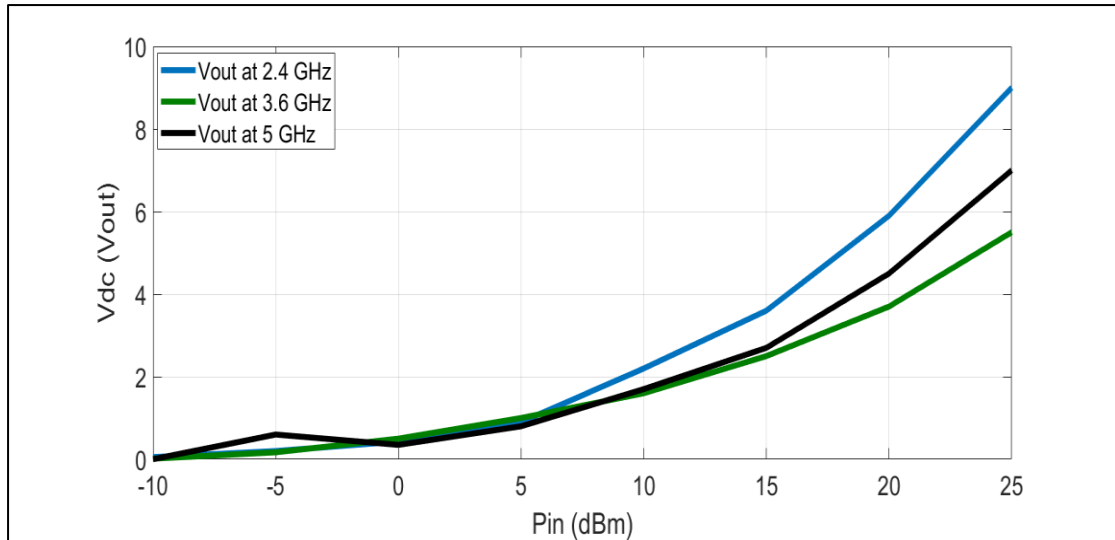


Fig.3.20: Vout (V) versus Pin (dBm) of Rectifier Circuit at 2.4, 3.6 and 5 GHz with LC-Circuit.

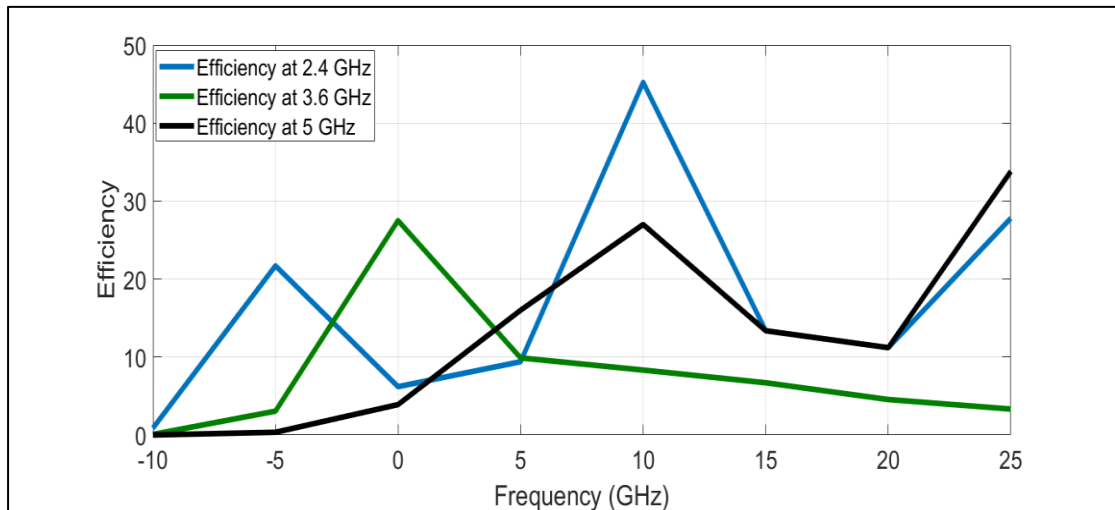


Fig.3.21: Efficiency versus input power of Rectifier Circuit at 2.4, 3.6 and 5 GHz with LC-Circuit.

Fig.3.21 shows that when the input power increases, the efficiency gradually rises. It also suggests that a slight increase must produce significant improvement in system performance. In other words, increasing the input power from -10 to 25 dBm produce an output voltage rise from 0 to 9 V and efficiency rise from 2% to 45% then drops to 27%.

3.3 Rectifier circuit operating at 3.6 GHz with LC-Circuit Matching Method

A rectifier circuit can be operated at 3.6 GHz by setting the power source frequency to 3.6 GHz as illustrated in Fig.3.22. The values of the L and C of the matching network were re-calculated using the new frequency 3.6 GHz. The S-parameters results show that the rectifier circuit has an excellent matching at 3.6 GHz due to the matching LC-circuit and the Bandwidth (BW) = $f_H - f_L = 3.7 - 3.53 = 170$ MHz as shown in Fig.3.23.

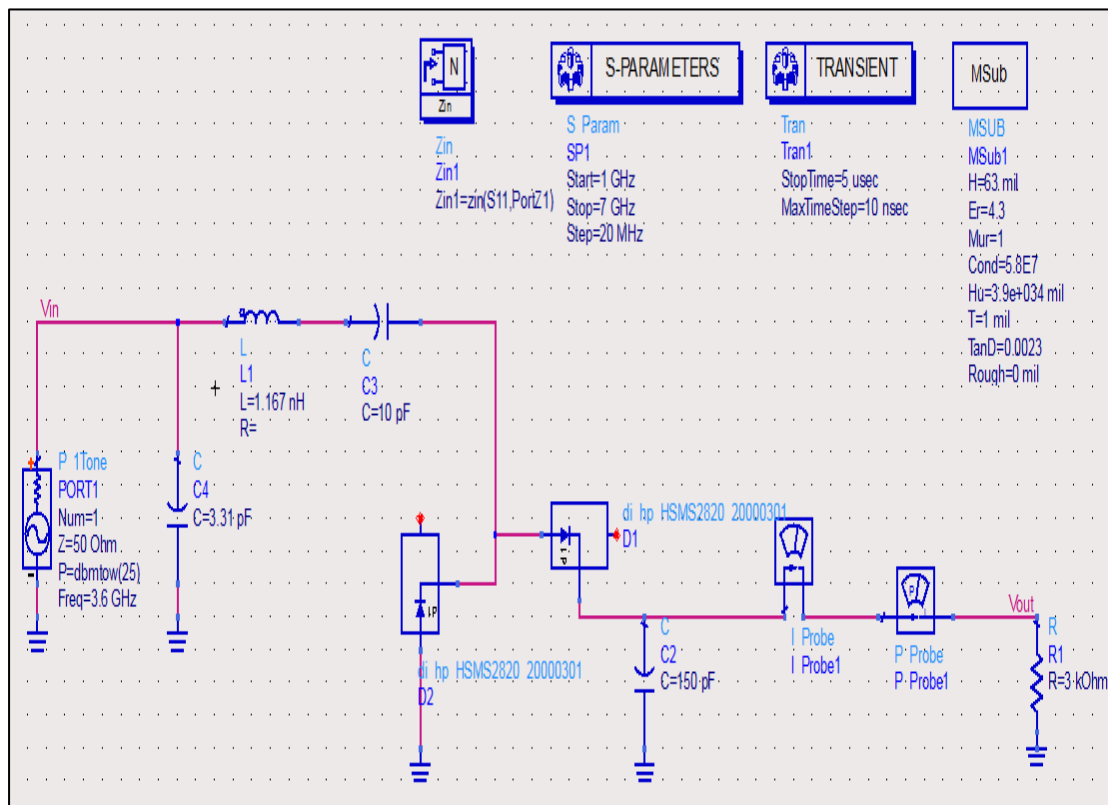


Fig.3.22: Rectifier circuit operating at 3.6 GHz with LC-Circuit.

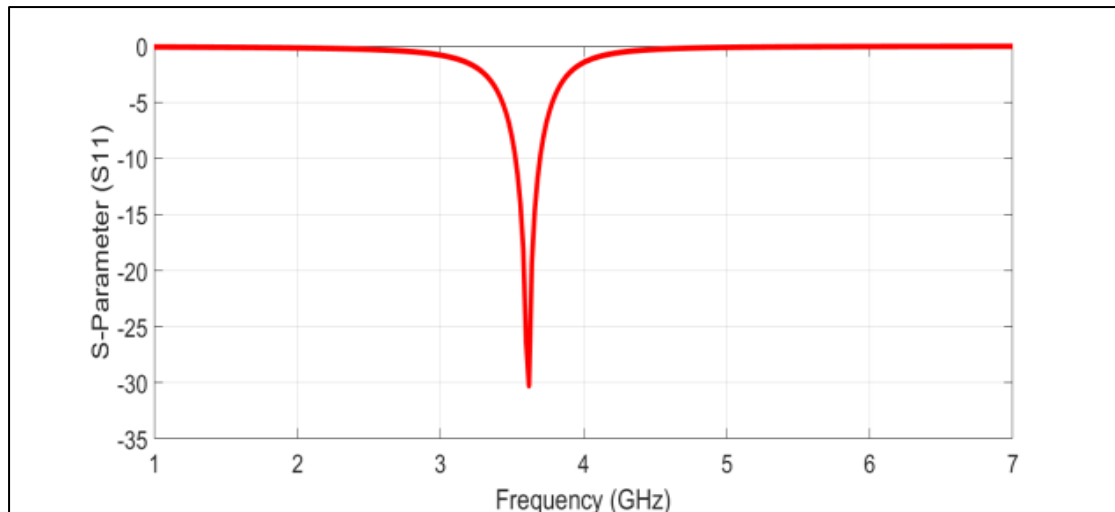


Fig.3.23: Simulated S11 of Rectifier Circuit at 3.6 GHz with LC-Circuit.

Fig.3.24 displays the input voltage waveform that is fed the rectifier circuit at 3.6 GHz frequency band, which is simulated by ADS.

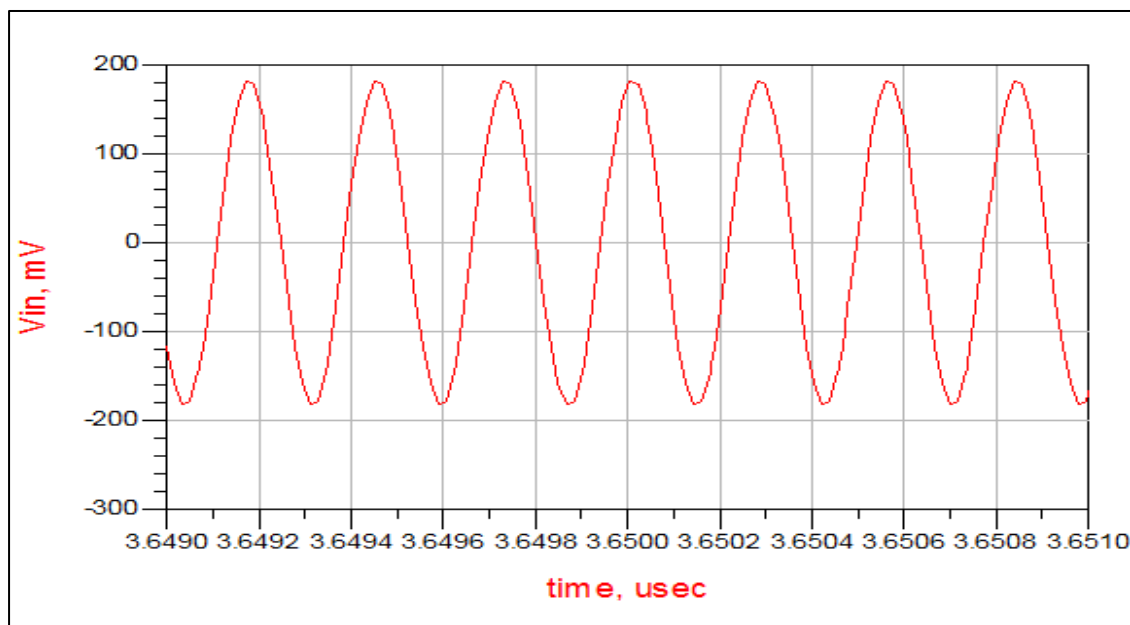


Fig.3.24: V_{in} (V) of Rectifier Circuit at 3.6 GHz with LC-Circuit.

Fig.3.25 illustrates the output voltage waveform for rectifier circuit at 3.6 GHz. The achieved DC output voltage is around 1.6 V and it is observed that the ripple is very small.

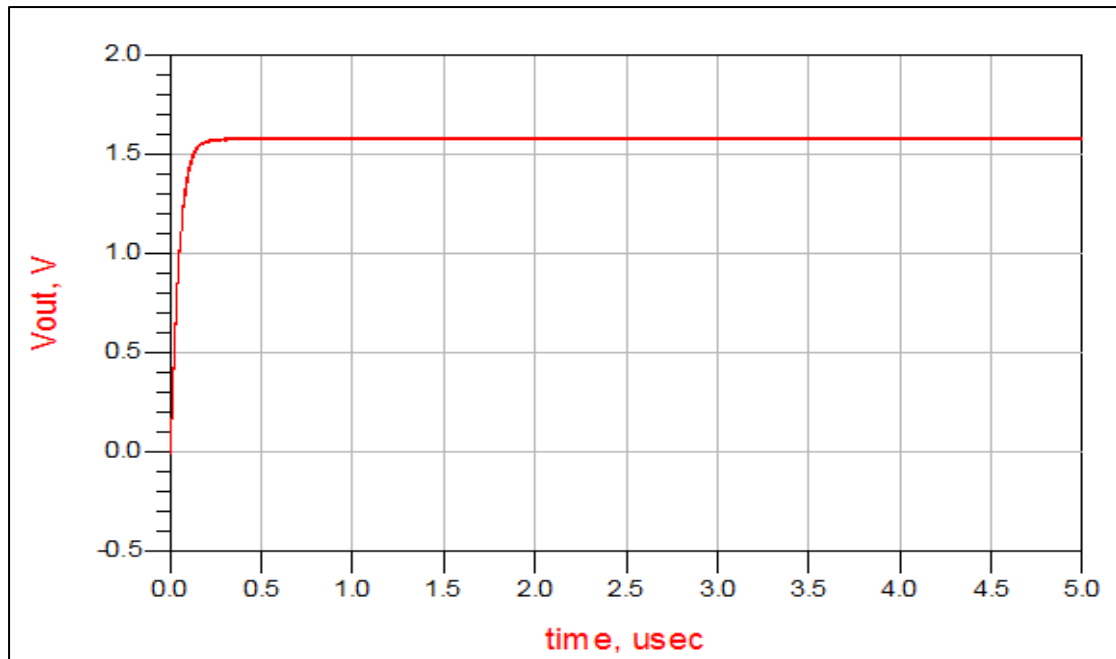


Fig.3.25: V_{out} (V) of Rectifier Circuit at 3.6 GHz with LC-Circuit.

Fig.3.26 displays the waveform of output current for the rectifier circuit at 3.6 GHz. The output current is about 530 μA .

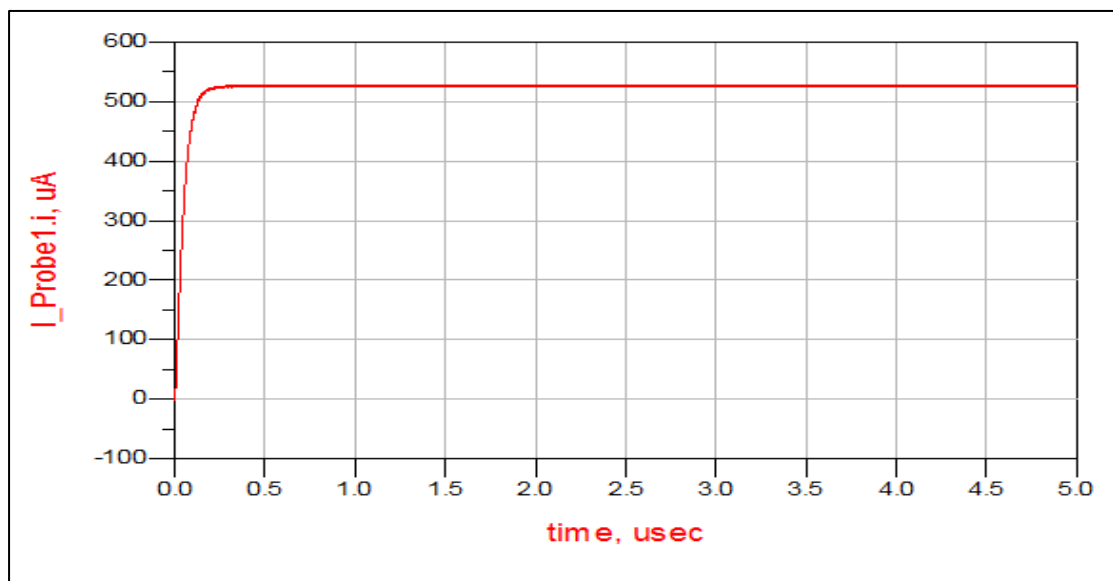


Fig.3.26: Output current of Rectifier Circuit at 3.6 GHz with LC-Circuit.

Fig.3.27 shows measure of the rectifier's performance in addition V_{out} value and quality. It has been investigated how the input power P_{in} affect the output voltage. The relationship between the input power (P_{in}) and the output voltage (V_{out}) of rectifier circuit at 3.6 GHz is depicted in

Fig.3.27. It may be clearly seen that the output voltage increases exponentially with increasing the input power (P_{in}). A maximum output voltage is around 5.6 V. It is achieved at input power of 25 dBm.

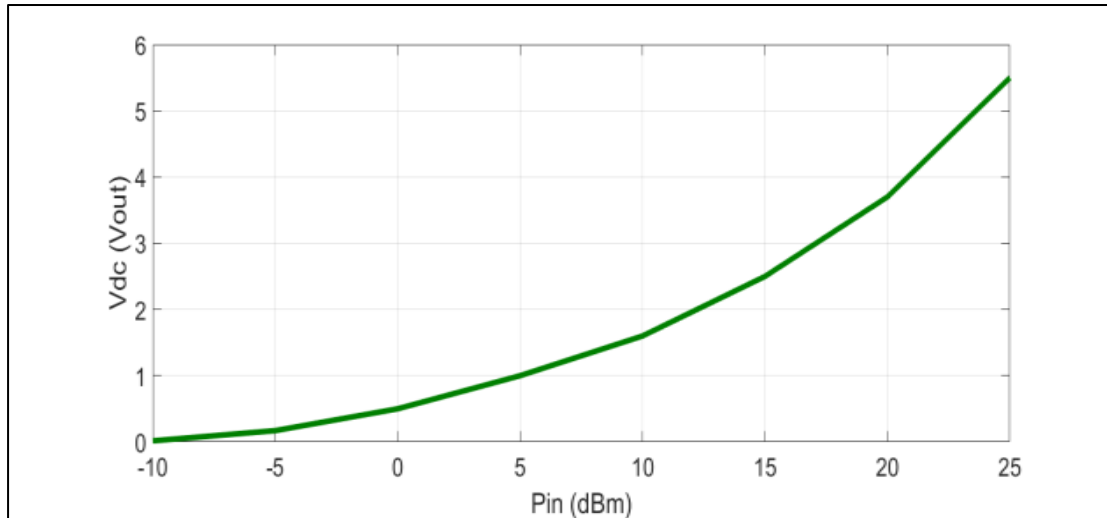


Fig.3.27: V_{out} (V) versus P_{in} (dBm) of Rectifier Circuit at 3.6 GHz with LC-Circuit.

Fig.3.28 shows that when the input power increases, the efficiency gradually rises. It also suggests that a slight increase could produce significant improvement in system performance. In other words, increasing the input power from -10 to 25 dBm may produce an output voltage rise from 0 to 5.7 V and efficiency rise from 0 % to 27 %.

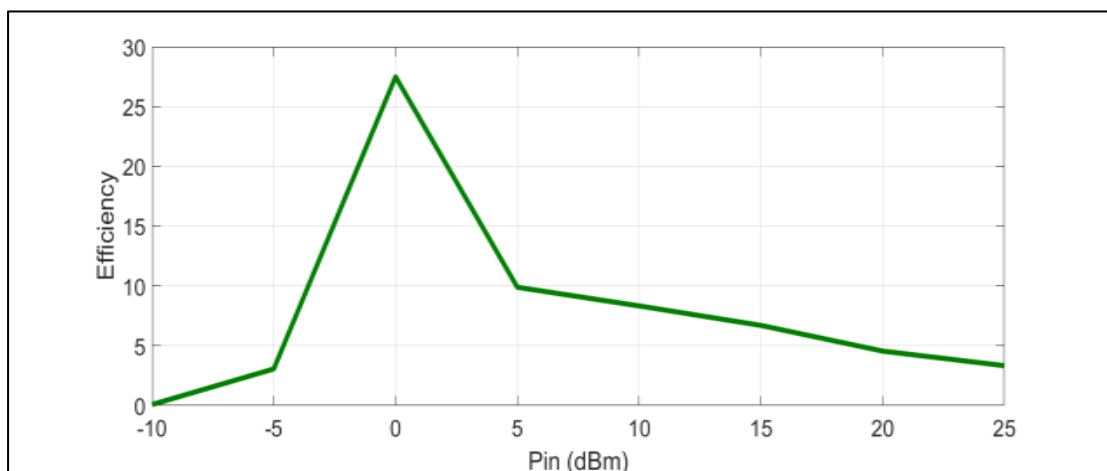


Fig.3.28: Efficiency versus input power of Rectifier Circuit at 3.6 GHz with LC-Circuit.

3.4 Rectifier circuit operating at 5 GHz with LC-Circuit Matching Method

A rectifier circuit can be operated at 5 GHz by setting the power source to 5 GHz as illustrated in Fig.3.29. The S-parameters results show that the rectifier circuit has a good matching at 5 GHz due to the matching LC-circuit as shown in Fig.3.30 and the Bandwidth (BW)= $f_H - f_L = 2.45-2.36 = 90$ MHz.

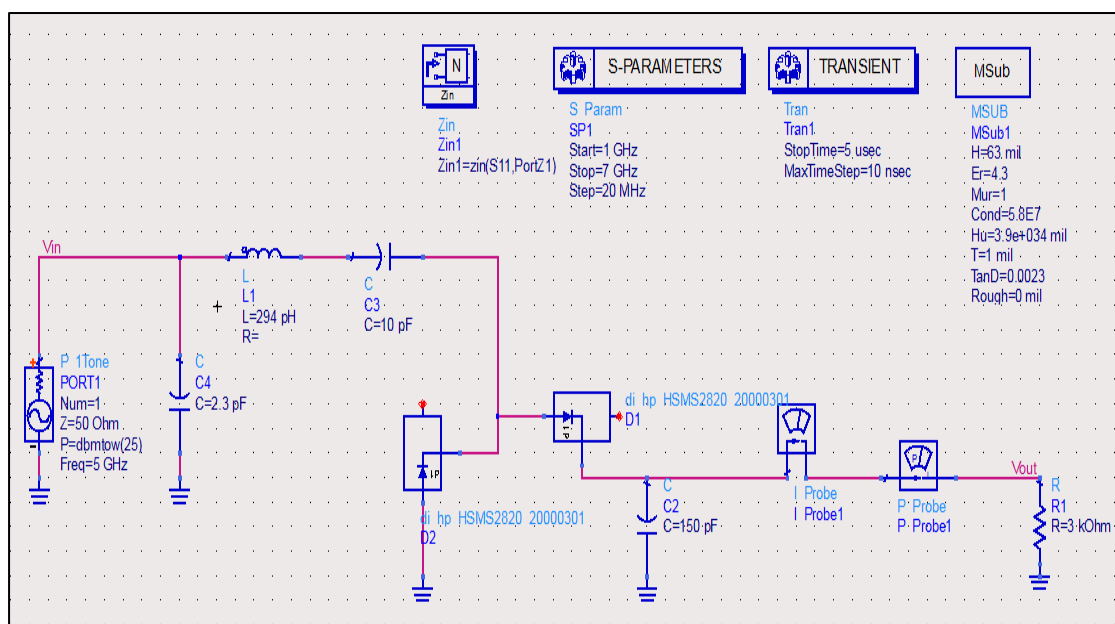


Fig.3.29: Rectifier circuit operating at 5 GHz with LC-Circuit.

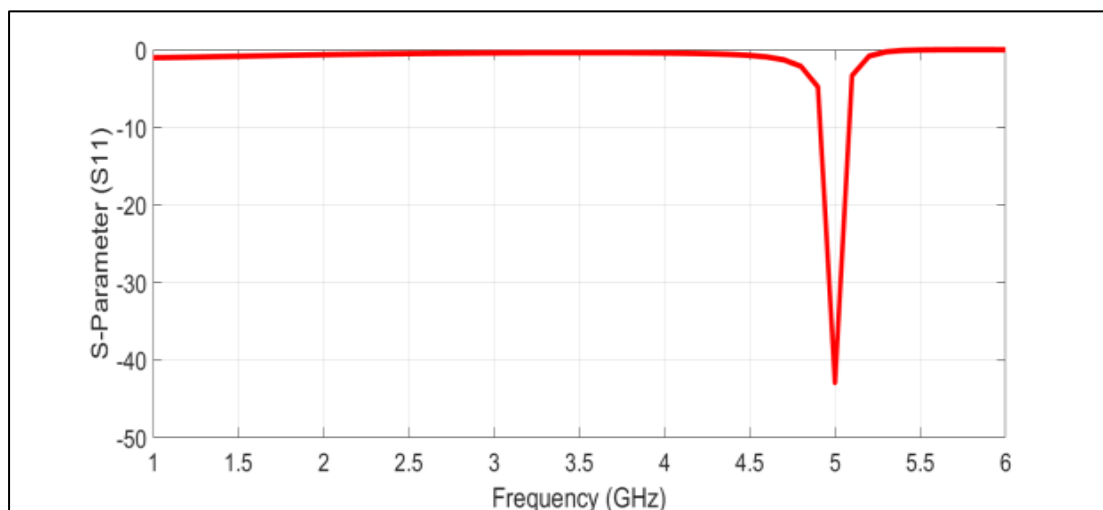


Fig.3.30: Simulated S11 of Rectifier Circuit at 5 GHz with LC-Circuit.

Fig.3.31 displays the input voltage waveform that is fed the rectifier circuit at 5 GHz frequency band, which is simulated by ADS.

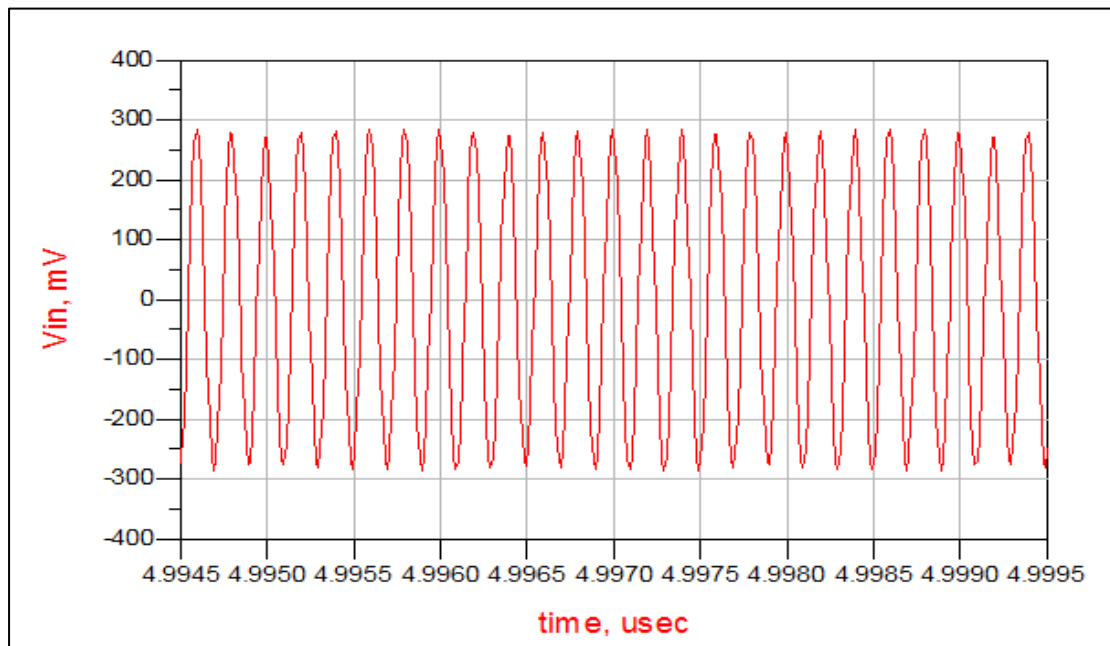


Fig.3.31: V_{in} (V) of rectifier circuit at 5 GHz with LC-Circuit.

Fig.3.32 illustrates the output voltage waveform for rectifier circuit at 5 GHz. The achieved DC output voltage is around 1.7 V, as can be seen in Fig.3.32.

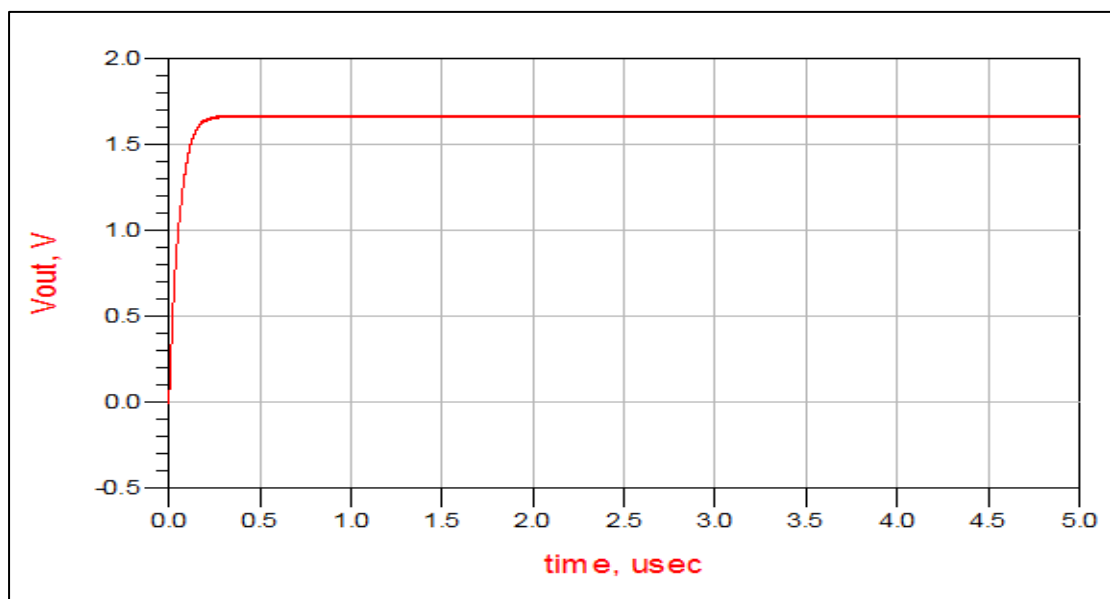


Fig.3.32: V_{out} (V) of rectifier circuit at 5 GHz with LC-Circuit.

Fig.3.33 displays the waveform of output current for the rectifier circuit at 5 GHz. The output current is about 550 μA , and with changing the load value will change the output current also.

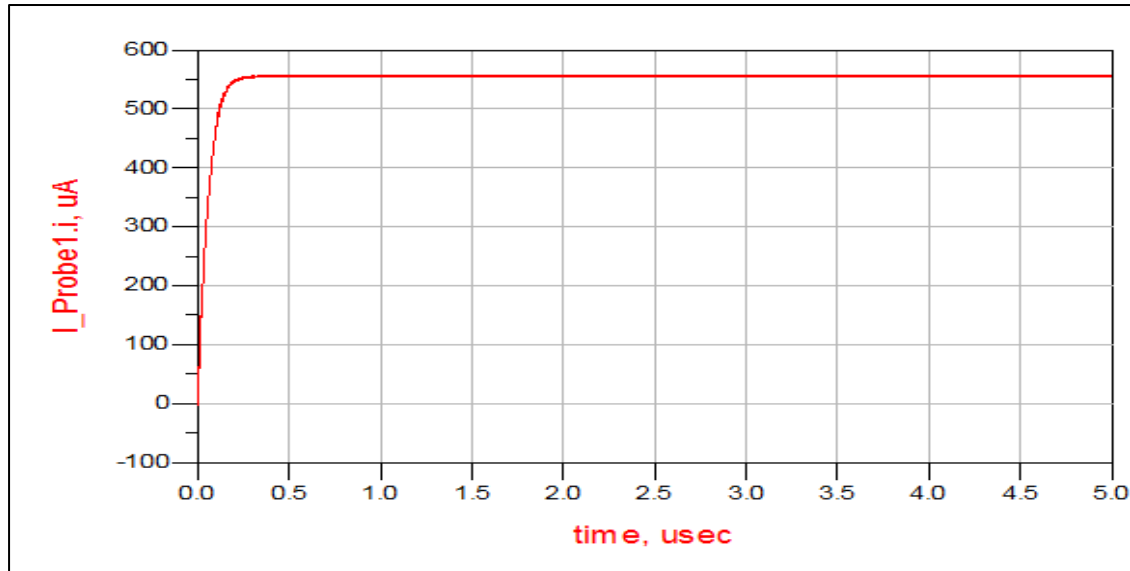


Fig.3.33: Output current of rectifier at 5 GHz with LC-Circuit.

Fig.3.34 shows measure of the rectifier's performance in addition to V_{out} value and quality. The relationship between the input power (P_{in}) and the output voltage (V_{out}) of rectifier circuit at 5 GHz is depicted in Fig.3.34. It can be clearly seen the output voltage increases exponentially with increasing the input power (P_{in}). A maximum output voltage is around 7 V is achieved at input power of 25 dBm.

In addition, Fig.3.35 shows that when the input power increases, the efficiency gradually rises. It suggests also that a slight increase must produce a significant improvement in system performance.

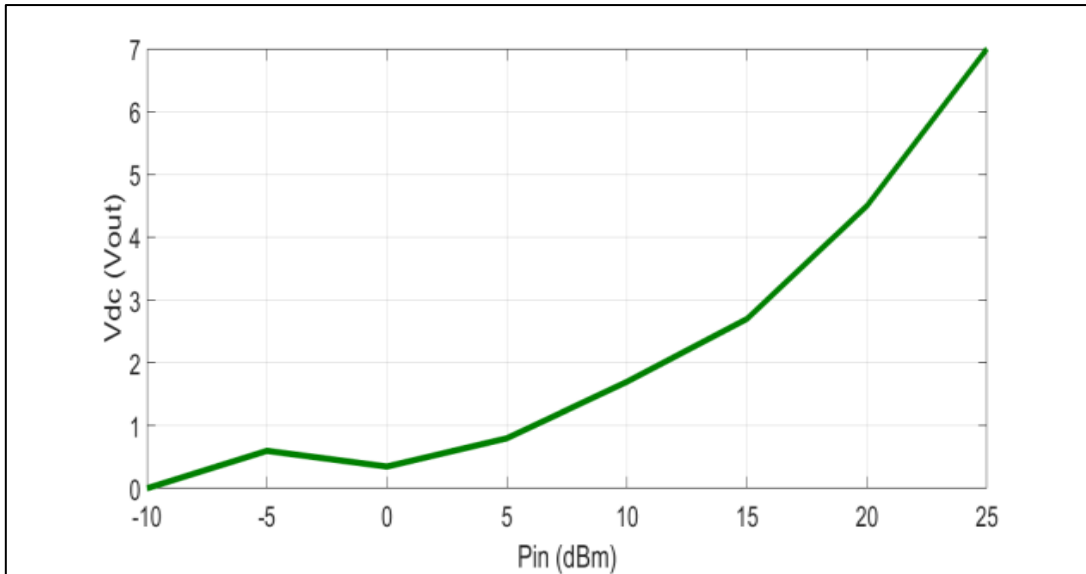


Fig.3.34: Vout (V) versus Pin (dBm) of rectifier circuit at 5 GHz with LC-Circuit.

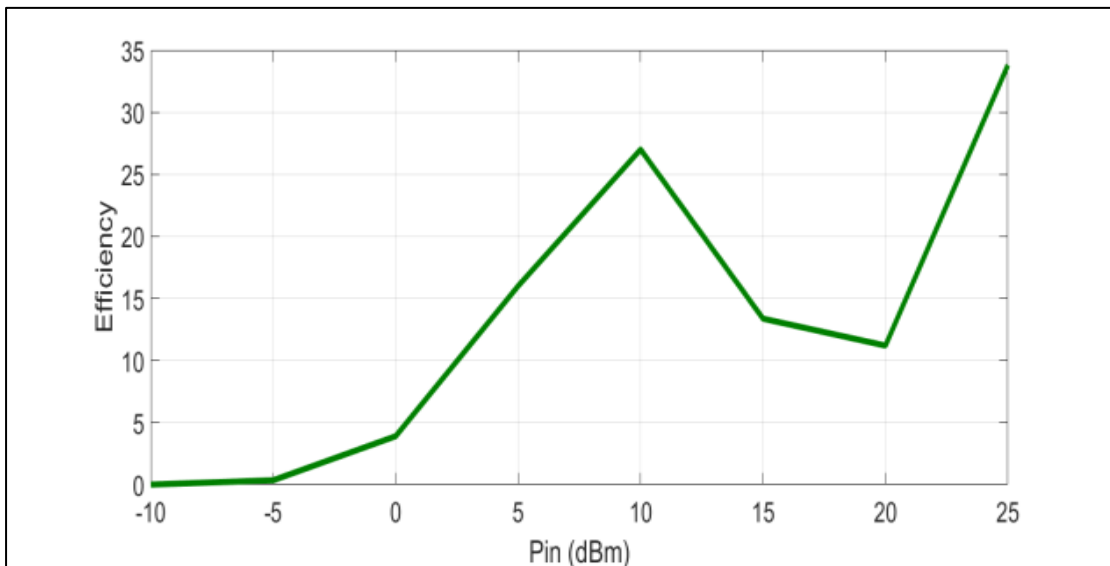


Fig.3.35: Efficiency versus input power of rectifier at 5 GHz.

3.5 Rectifier Circuit operating at 2.4 GHz with TL-Circuit Matching Method

Another way to perform impedance matching is applied by using the Smith Chart capability in ADS software. In this method, a transmission line stubs are employed at the input port of the circuit to match the source to the rectifier circuit as illustrated in Fig.3.36. The length (L) and width

(W) of these transmission line stubs play a crucial role in determining the quality of impedance matching. Fig.3.37 shows the simulated S11 of rectifier circuit at 2.4 GHz with TL-Circuit, where the return loss value went below -14 dB at the specified frequency and the Bandwidth (BW) = $f_H - f_L = 2.41 - 2.39 = 20$ MHz.

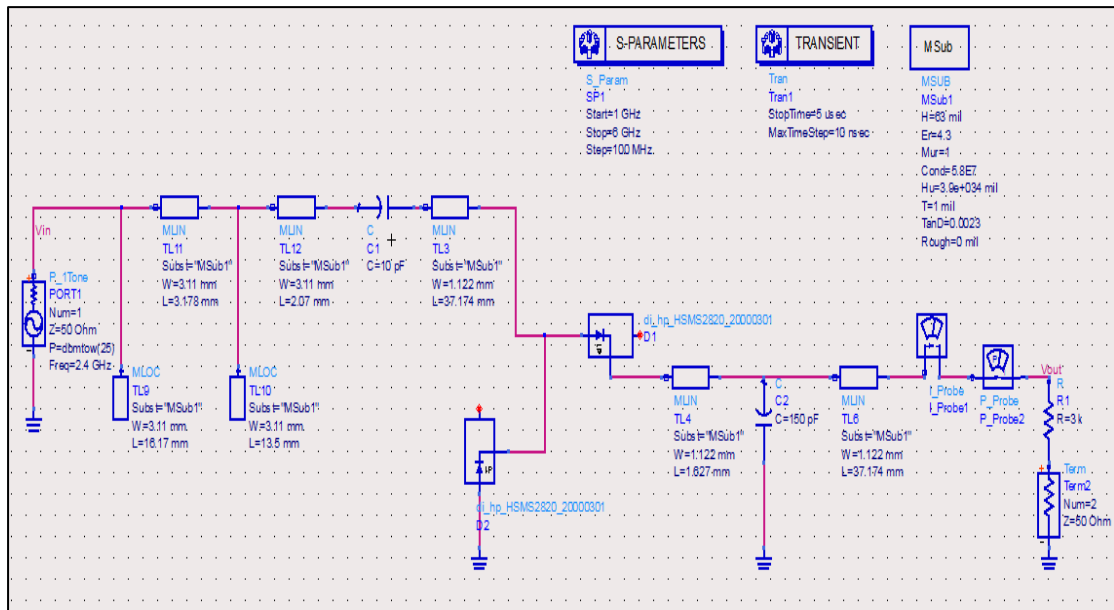


Fig.3.36: Rectifier circuit operating at 2.4 GHz with TL-Circuit.

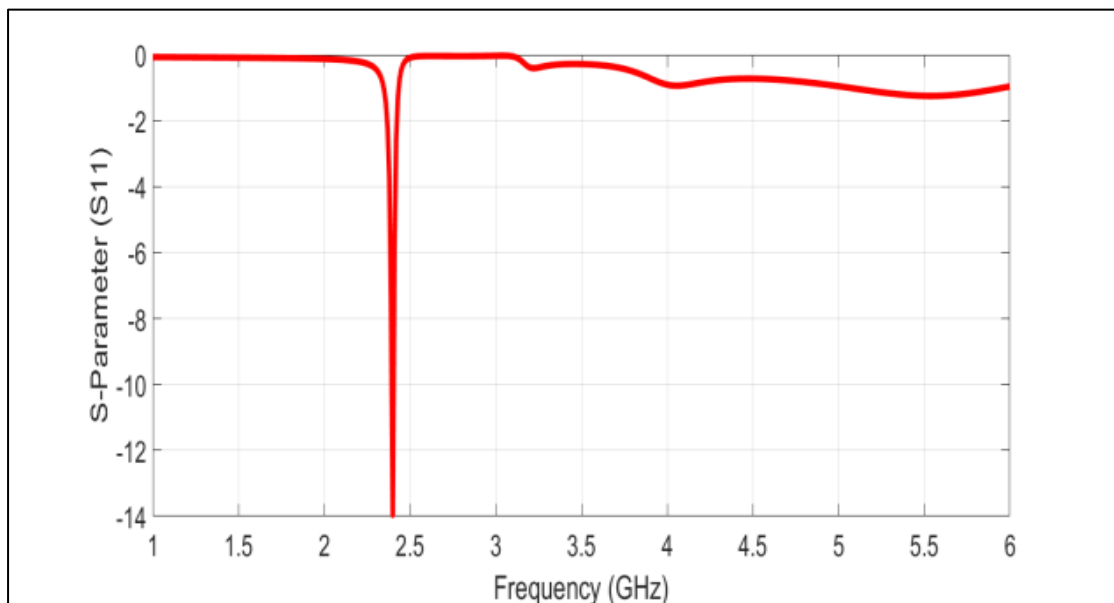


Fig3.37: Simulated S11 of Rectifier Circuit at 2.4 GHz with TL-Circuit.

The input voltage waveform that is fed to the rectifier circuit with TL-Circuit at 2.4 GHz frequency band is displayed in Fig.3.38, which is simulated by ADS.

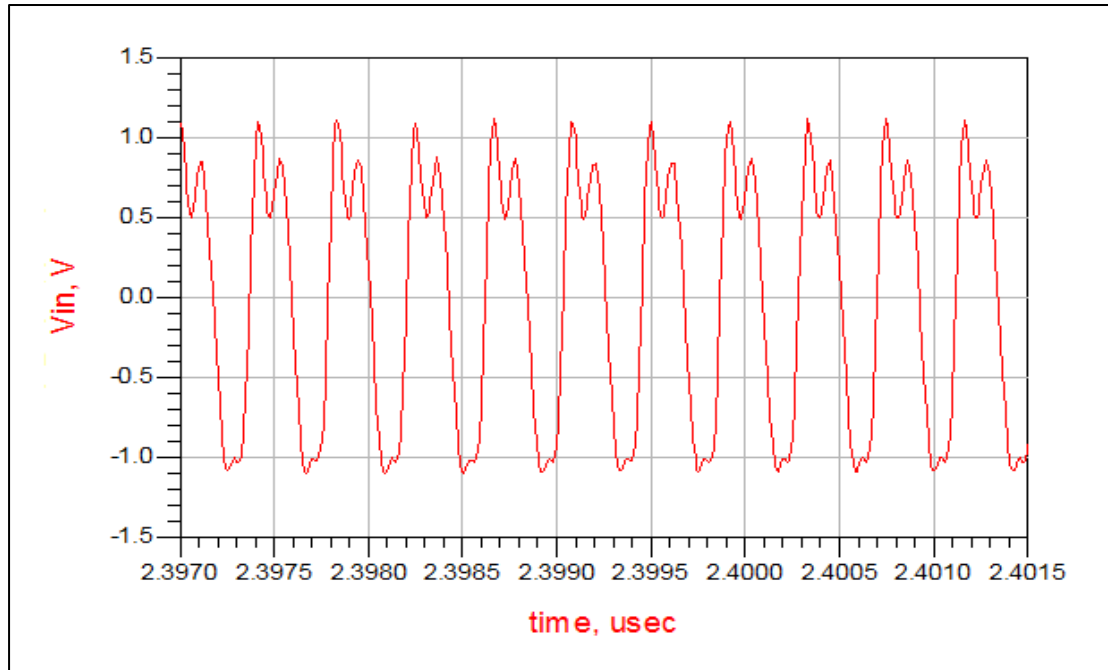


Fig.3.38: V_{in} (V) of rectifier circuit at 2.4 GHz with TL-Circuit.

Fig.3.39 illustrates the output voltage waveform for rectifier circuit with TL-Circuit at 2.4 GHz. The achieved DC output voltage is around 11.3 V as shown in Fig.3.39 with a very minimum ripple.

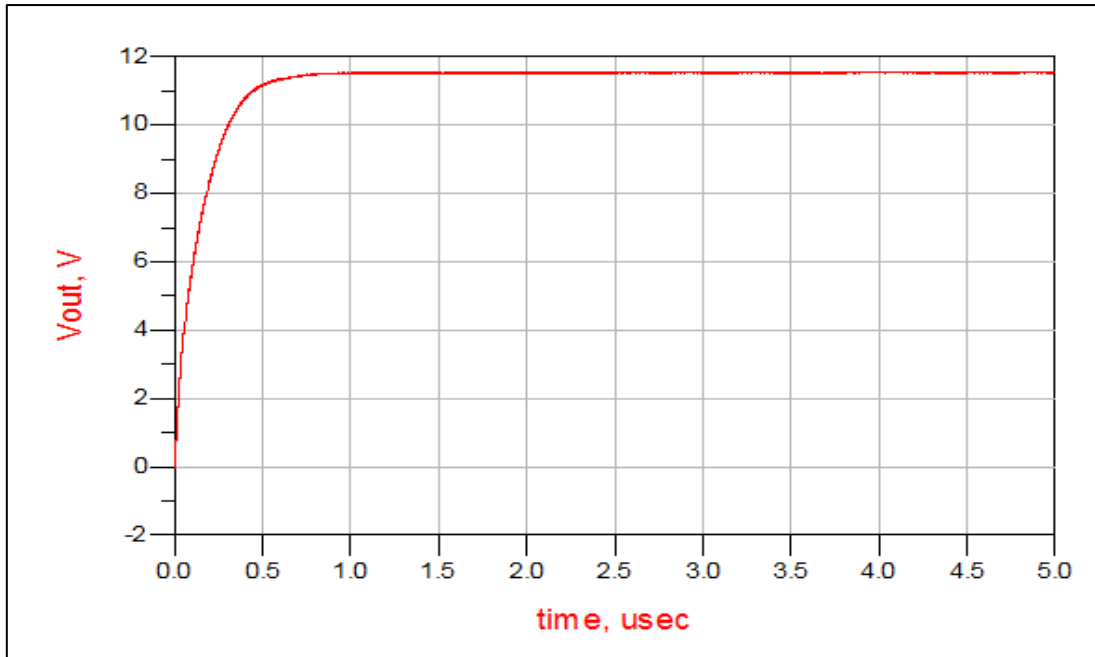


Fig.3.39: V_{out} (V) of Rectifier Circuit at 2.4 GHz with TL-Circuit.

Fig.3.40 displays the waveform of output current for the rectifier circuit with TL-Circuit at 2.4 GHz . The output current is about 3.44 mA.

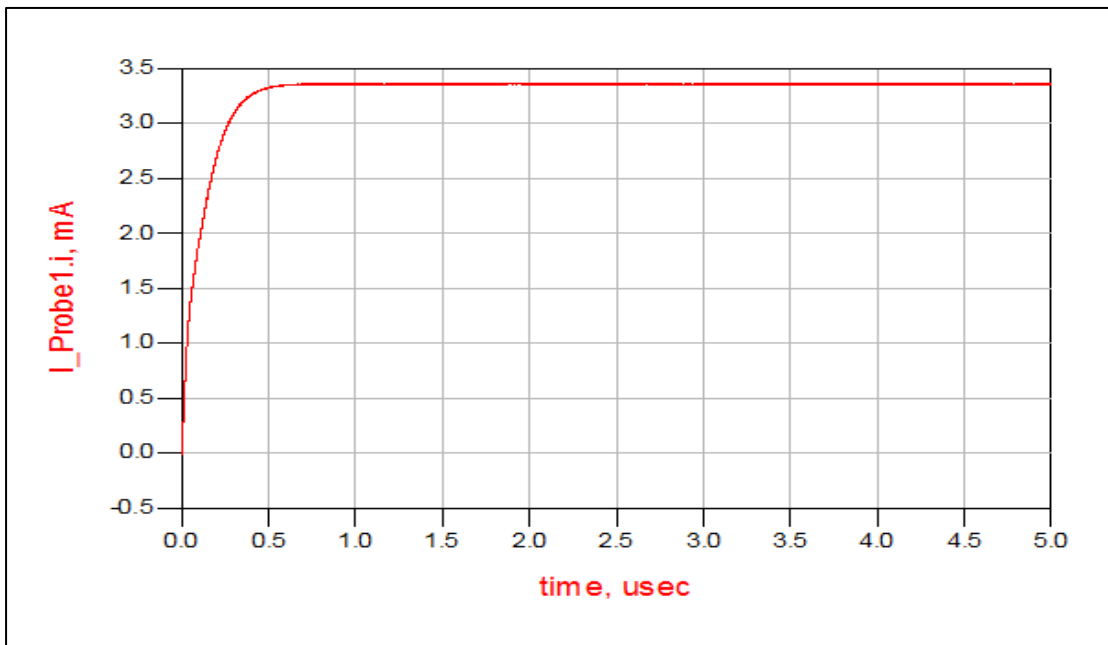


Fig.3.40: Output current of rectifier circuit at 2.4 GHz with TL-Circuit.

Fig.3.41 shows the measurement of the rectifier's performance. It has been investigated how the input power P_{in} impact the output voltage. The relationship between the input power (P_{in}) and the output voltage (V_{out})

of rectifier circuit with TL-Circuit at 2.4 GHz is recorded. It is clearly seen that the output voltage increases exponentially with increasing the input power (P_{in}). A maximum output voltage is around 10.5 V. It is achieved at input power of 25 dBm.

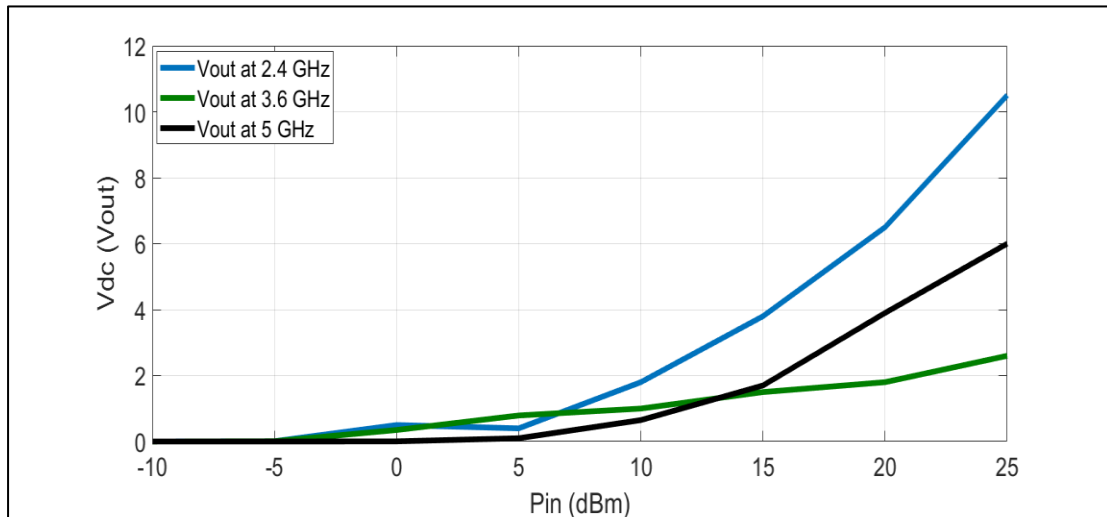


Fig.3.41: V_{dc} (V_{out}) versus input power of rectifier at 2.4, 3.6 and 5 GHz with TL-Circuit.

Fig.3.42 shows that when the input power increases, the efficiency gradually rises. It also suggests that increasing the input power from -10 to 25 dBm produce an output voltage rise from 0 to 10.5 V and efficiency rise from 2% to 27%.

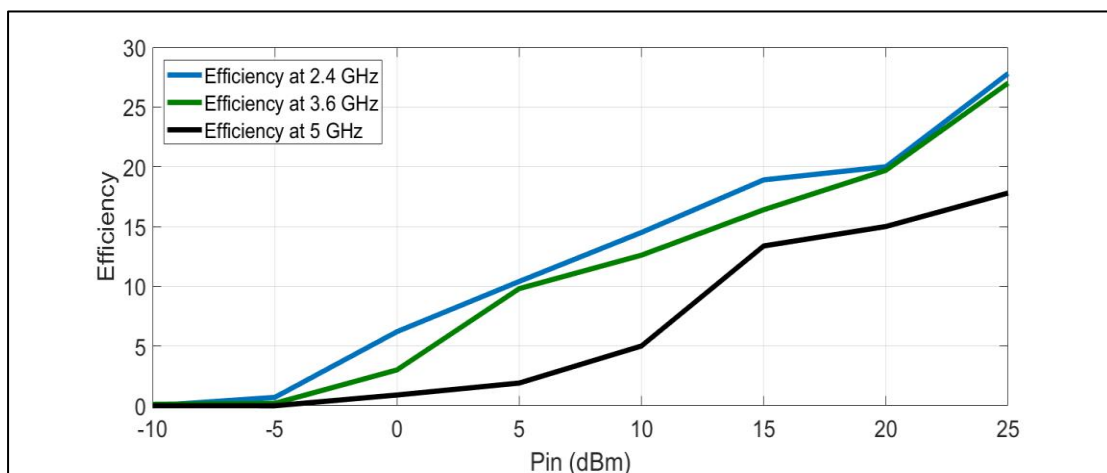


Fig.3.42: Efficiency versus input power of Rectifier Circuit at 2.4 GHz with TL-Circuit.

3.6 Rectifier circuit operating at 3.6 GHz with TL-Circuit Matching Method

The voltage doubler rectifier circuit with TL-circuit is operated at 3.6 GHz as illustrated in Fig.3.43. The simulated S11 is depicted in Fig.3.44, where the matching circuit has achieved the goal and the Bandwidth (BW)= $f_H - f_L = 3.65-3.55 = 100$ MHz.

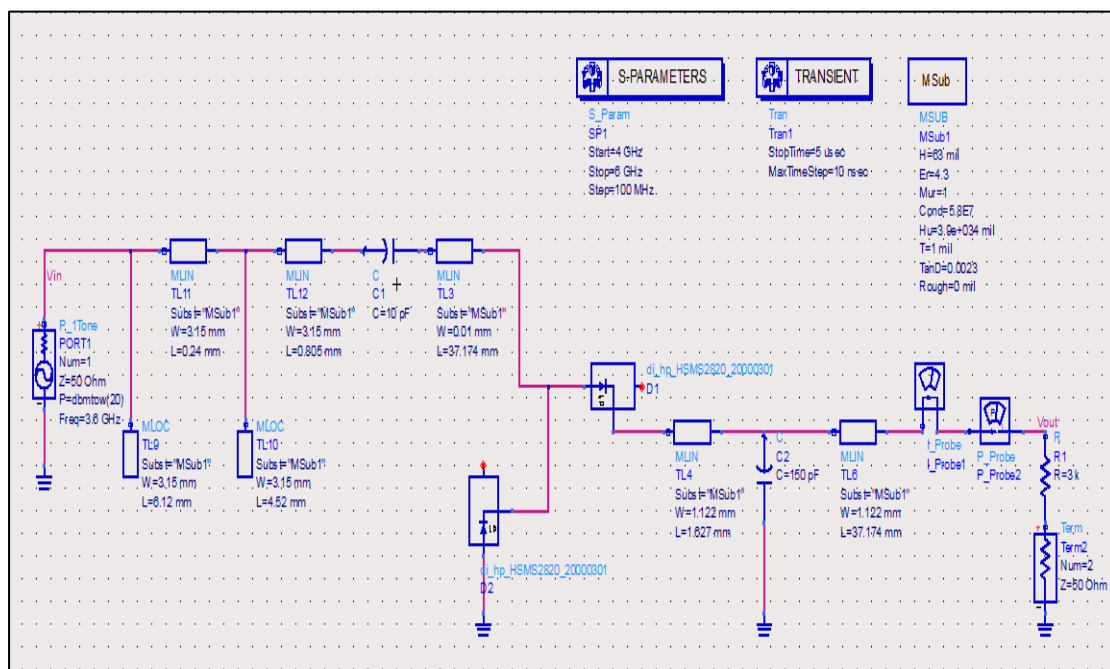


Fig.3.43: Rectifier circuit operating at 3.6 GHz with TL-Circuit.

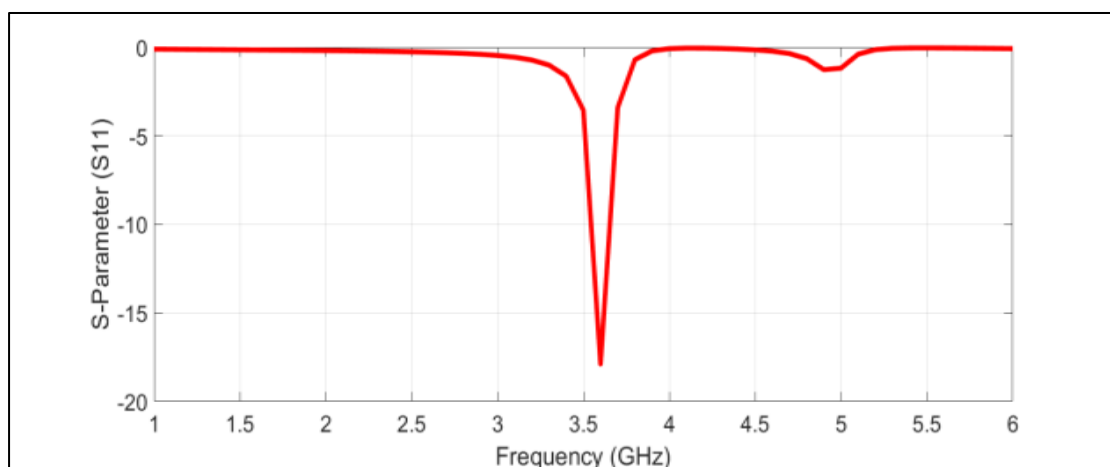


Fig3.44: Simulated S11 of Rectifier Circuit at 3.6 GHz with TL-Circuit.

Fig.3.45 displays the input voltage waveform that is fed to the rectifier circuit with TL-Circuit at 3.6 GHz frequency band.

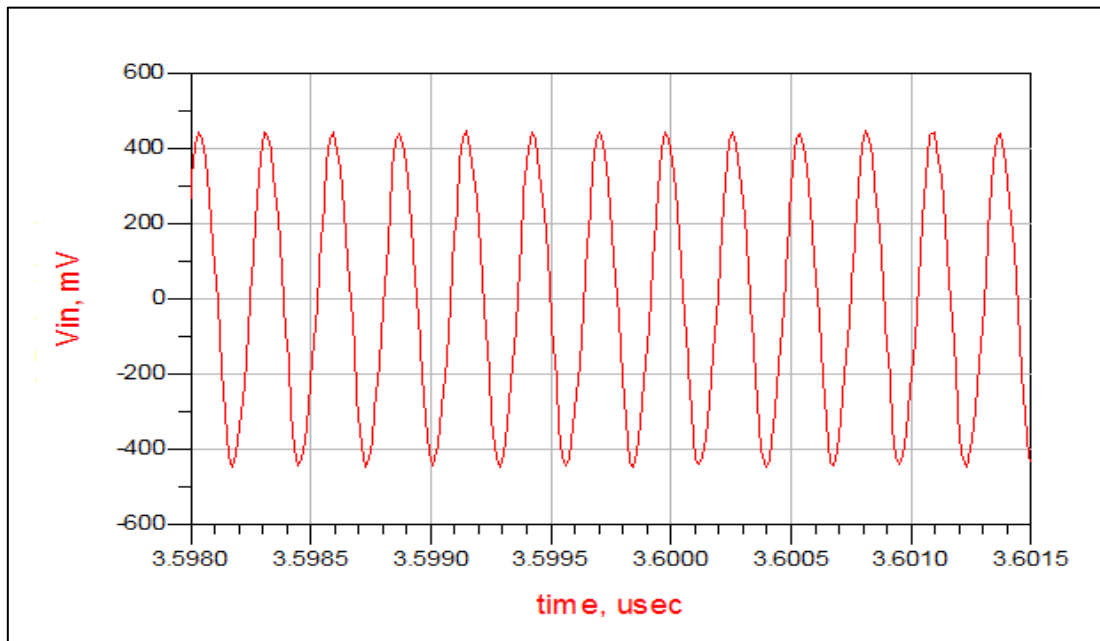


Fig.3.45: V_{in} (V) of rectifier circuit at 3.6 GHz with TL-Circuit.

Fig.3.46 illustrates the output voltage waveform for rectifier circuit with TL-Circuit at 3.6 GHz. The achieved DC output voltage is around 1.7 V as shown in Fig.3.46.

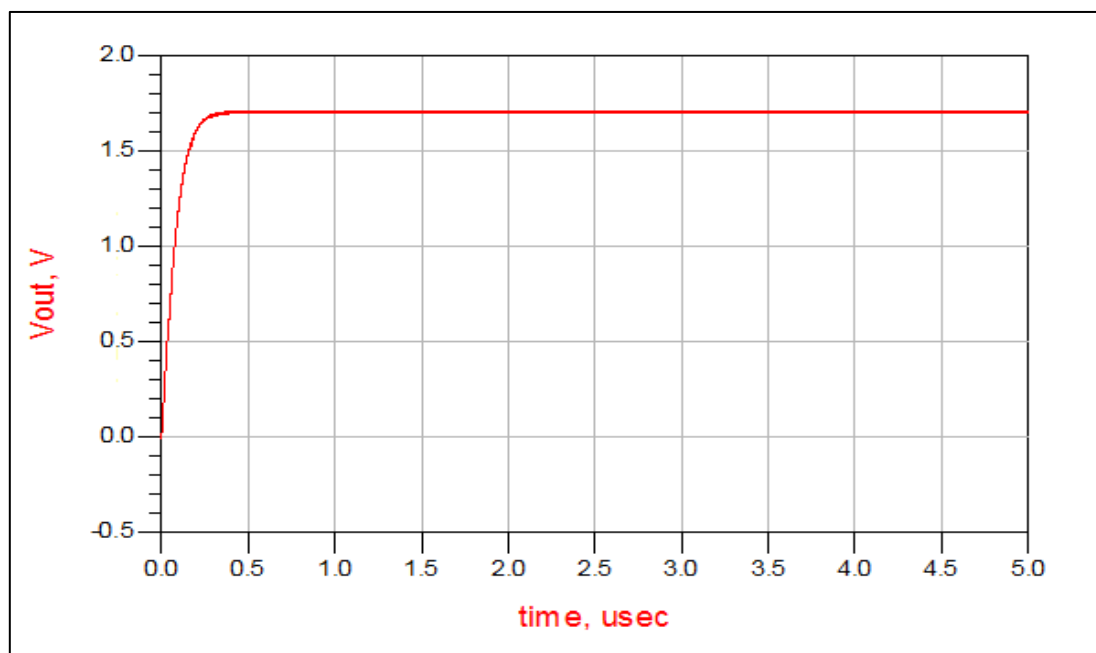


Fig.3.46: V_{out} (V) of rectifier circuit at 3.6 GHz with TL-Circuit.

Fig.3.47, Displays the waveform of output current for the rectifier circuit with TL-Circuit at 3.6 GHz . The output current is about 560 uA, and with changing the load value will change the output current also.

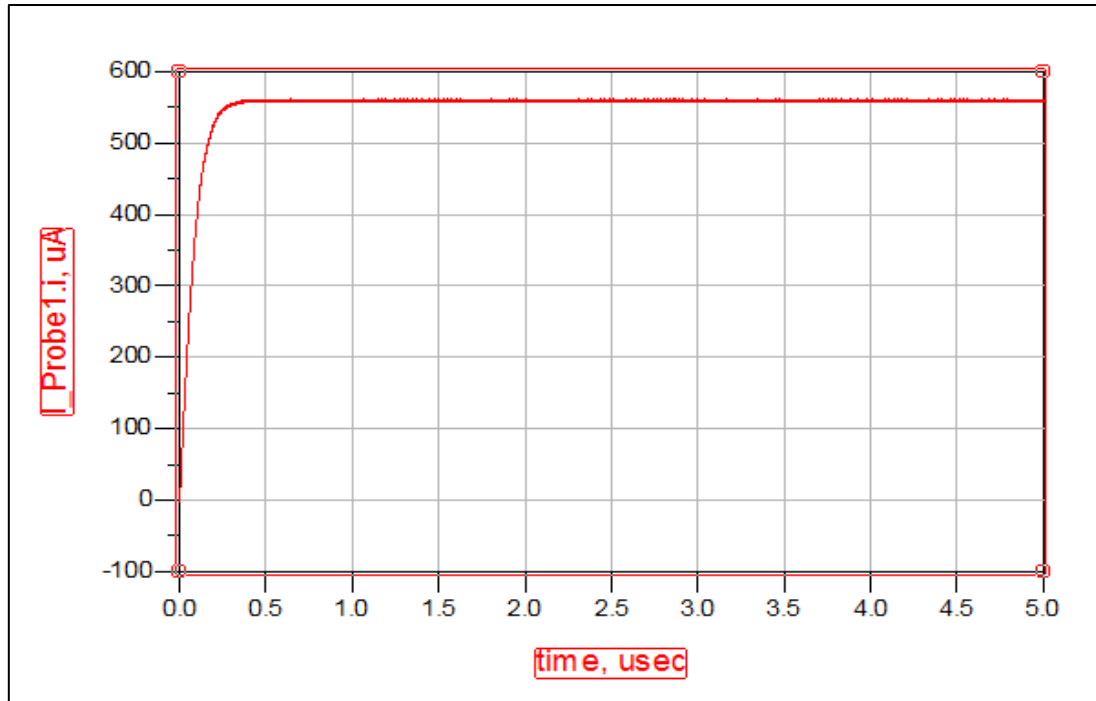


Fig.3.47: Output current of Rectifier Circuit at 3.6 GHz with TL-Circuit.

Fig.3.48 shows the measurement of the rectifier's performance. It has been investigated how the input power P_{in} impact the output voltage. The relationship between the input power (P_{in}) and the output voltage (V_{out}) of rectifier circuit with TL-Circuit at 3.6 GHz is recorded. It is clearly seen that the output voltage increases exponentially with increasing the input power (P_{in}). A maximum output voltage is around 2.6 V. It is achieved at input power of 25 dBm.

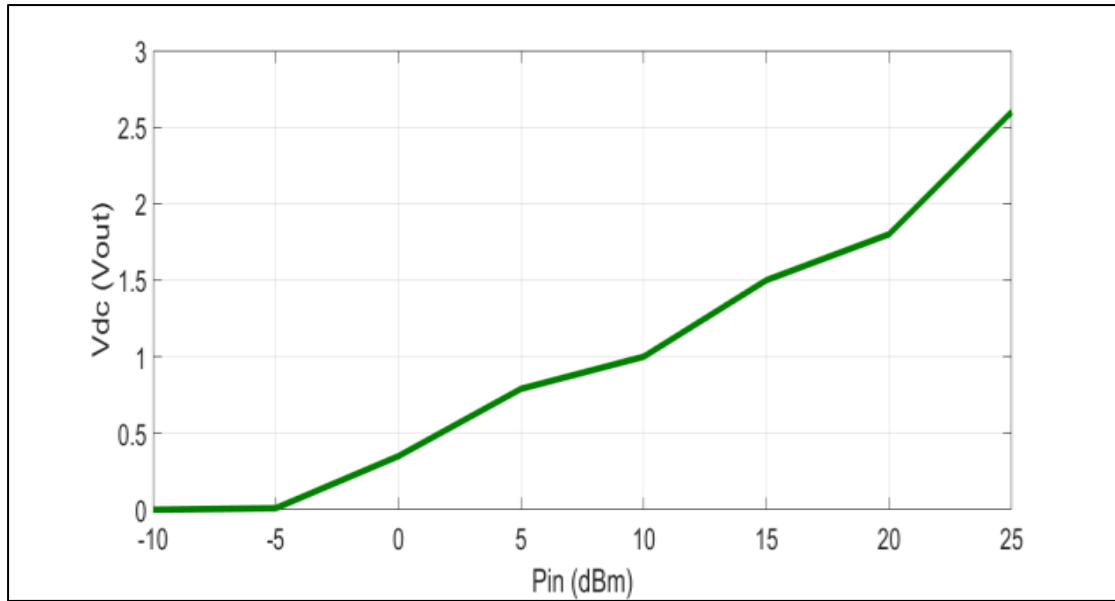


Fig.3.48: Vdc (Vout) versus input power of rectifier at 2.4 GHz with TL-Circuit.

The variation of efficiency versus input power is demonstrated in Fig.3.49. It is evident that increasing the input power from -10 to 25 dBm may produce an output voltage rise from 0 to 2.6 V and efficiency rise from 2% to 27%.

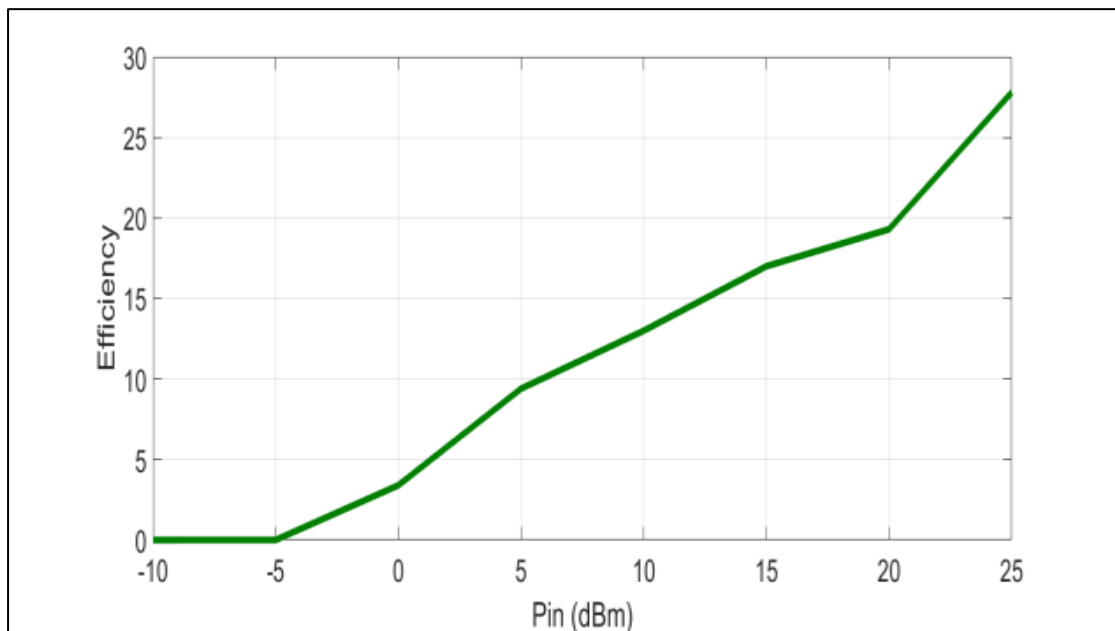


Fig.3.49: Efficiency versus input power of rectifier circuit at 3.6 GHz with TL-Circuit.

3.7 Rectifier circuit operating at 5 GHz with TL-Circuit Matching Method

The rectifier circuit is here operated at 5 GHz as illustrated in Fig.3.50 and the simulated S11 versus frequency and the Bandwidth (BW) = $f_H - f_L = 1$ MHz is depicted in Fig.3.51.

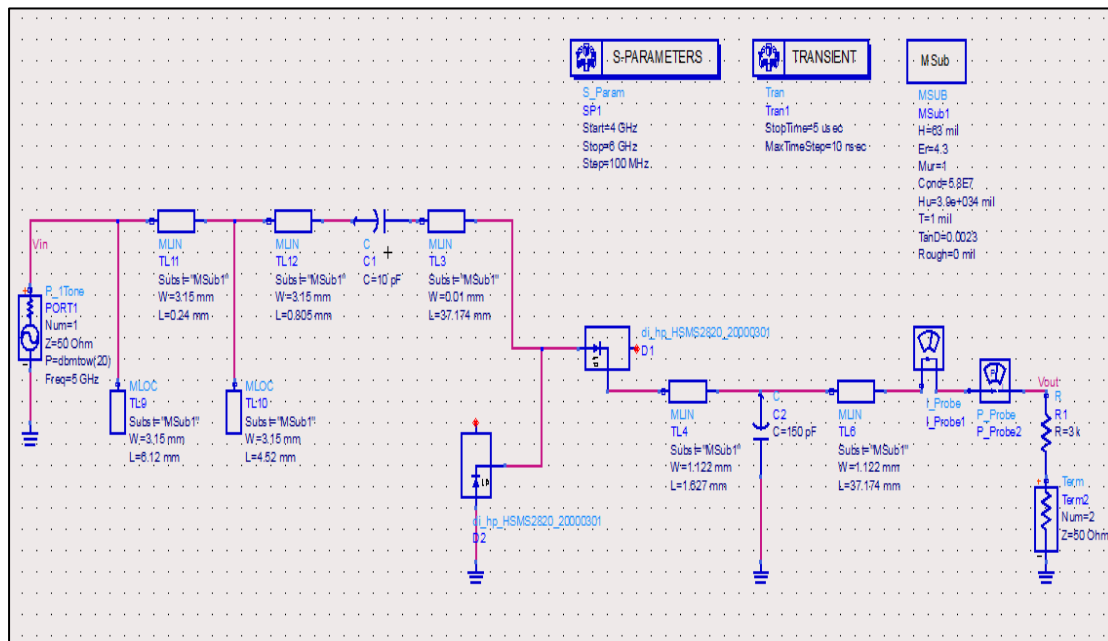


Fig.3.50: Rectifier circuit operating at 5 GHz with TL-Circuit.

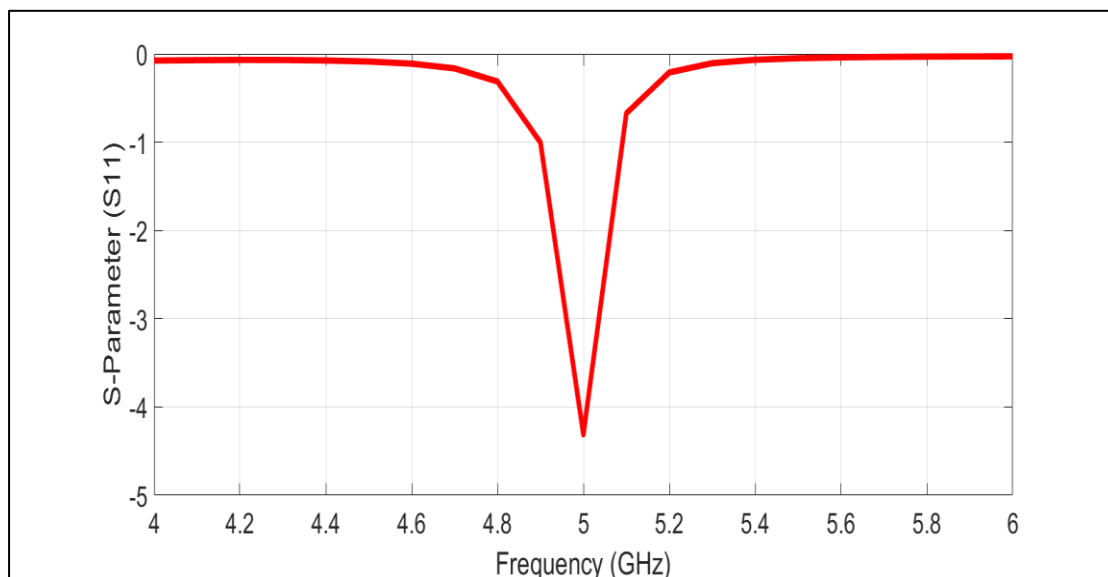


Fig3.51: Simulated S11 of Rectifier Circuit at 5 GHz with TL-Circuit.

Fig.3.52 displays the input voltage waveform that is fed to the rectifier circuit with TL-Circuit at 5 GHz frequency band.

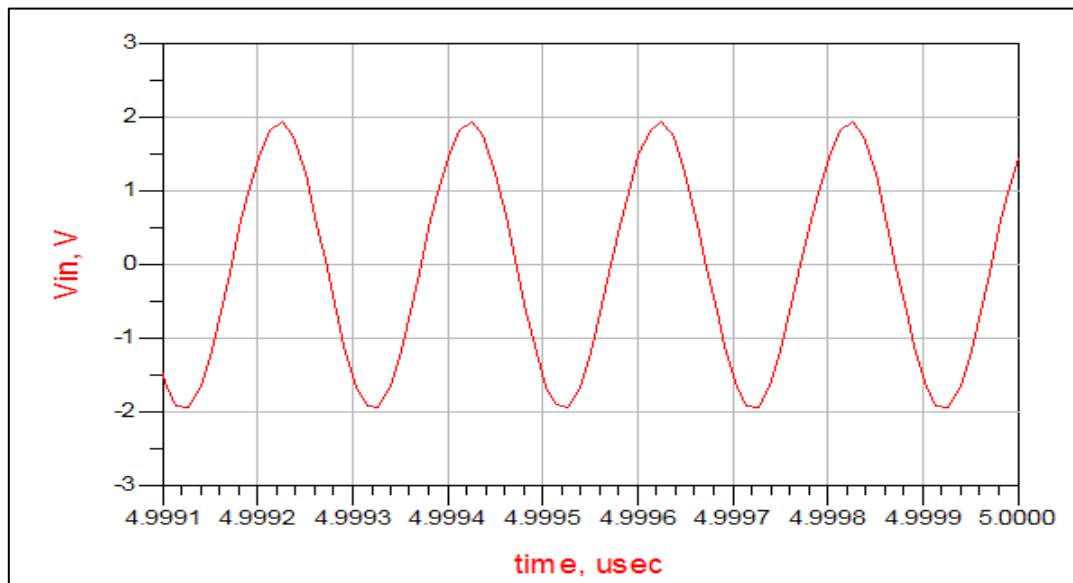


Fig.3.52: V_{in} (V) of Rectifier Circuit at 5 GHz with TL-Circuit.

Fig.3.53 illustrates the output voltage waveform for rectifier circuit with TL-Circuit at 5 GHz. The achieved DC output voltage is around 6.5 V as shown in Fig.3.53.

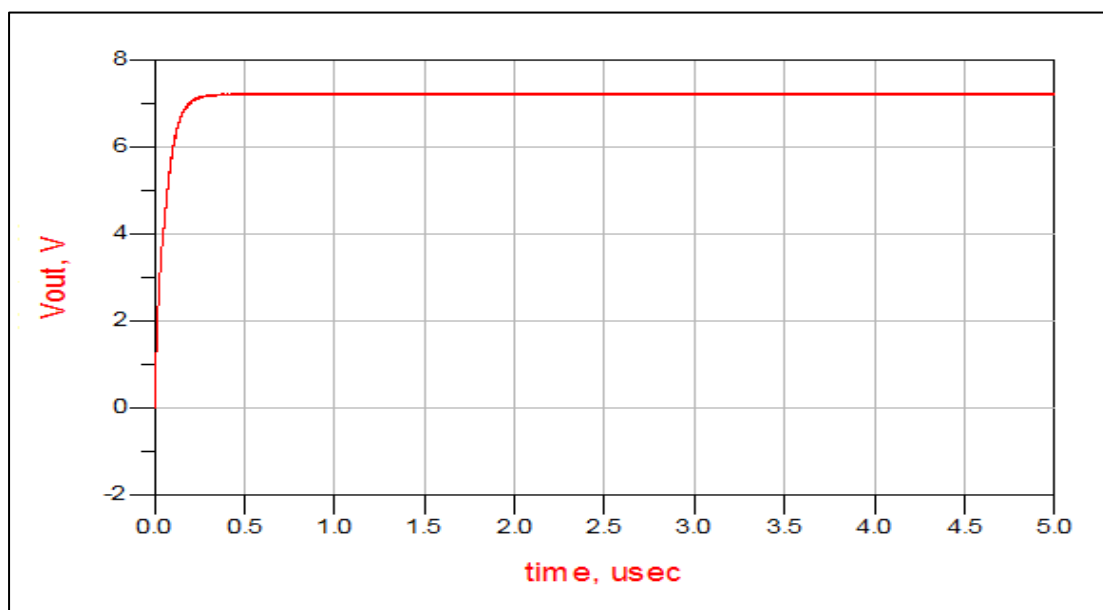


Fig.3.53: V_{out} (V) of Rectifier Circuit at 5 GHz with TL-Circuit.

Fig.3.54 displays the waveform of output current for the rectifier circuit with TL-Circuit at 5 GHz. The output current is about 2.4 mA.

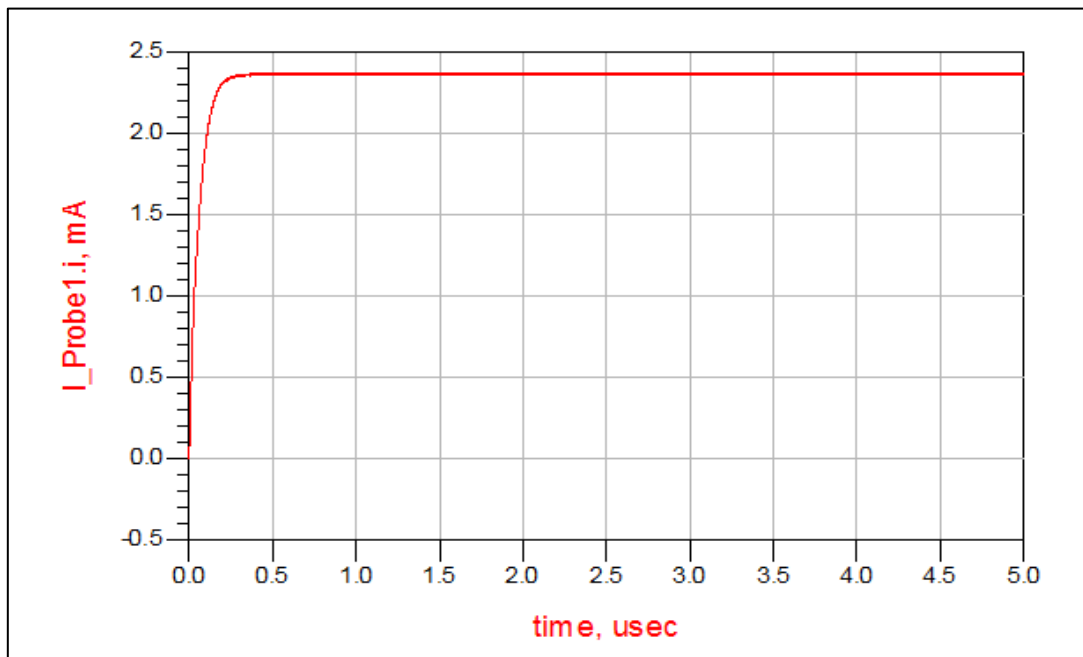


Fig.3.54: Output current of Rectifier Circuit at 5 GHz with TL-Circuit.

The relationship between the input power (P_{in}) and the output voltage (V_{out}) of rectifier circuit with TL-Circuit at 5 GHz is recorded in Fig.3.55. It is clearly seen that the output voltage increases exponentially with increasing the input power (P_{in}). A maximum output voltage is around 6 V. It is achieved at input power of 25 dBm.

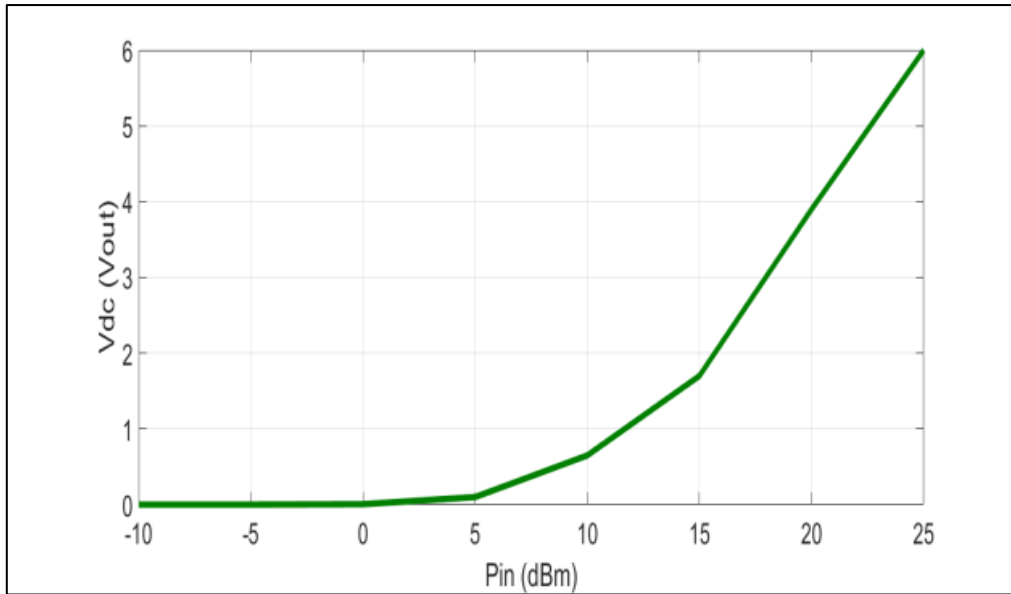


Fig.3.55: Vdc (Vout) versus input power of Rectifier Circuit at 5 GHz with TL-Circuit.

The variation of efficiency versus input power is demonstrated in Fig.3.56. It is evident that increasing the input power from -10 to 25 dBm produce an output voltage rise from 0 to 6 V and efficiency rise from 0% to 18%.

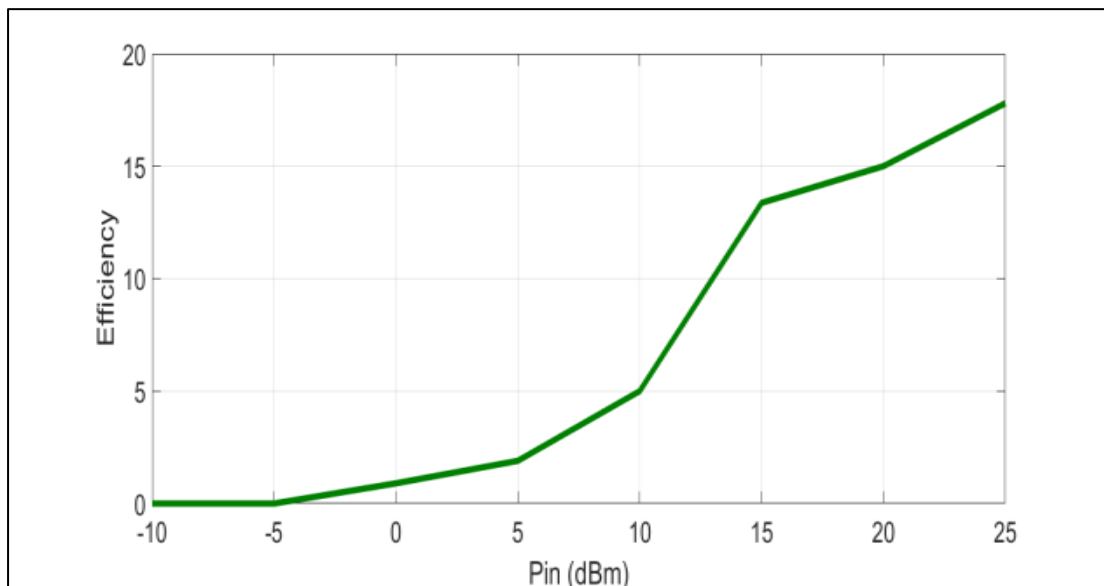


Fig.3.56: Efficiency versus input power of rectifier circuit at 5 GHz with TL-Circuit.

3.4 Fabrication and experimental validation

To validate the concept and for experimental validation, the rectifier circuit that operating at 2.4 was fabricated using PCB technology. FR-4 substrate with dielectric constant of 4.3 and thickness of 1.6 mm is employed. Fig.3.57 illustrates the PCB schematic diagram of the fabricated circuit where it is a double layer circuit with a full ground plane at the back of substrate. All the circuit components were available in the market.



Fig.3.57: Rectifier circuit layout for fabrication.

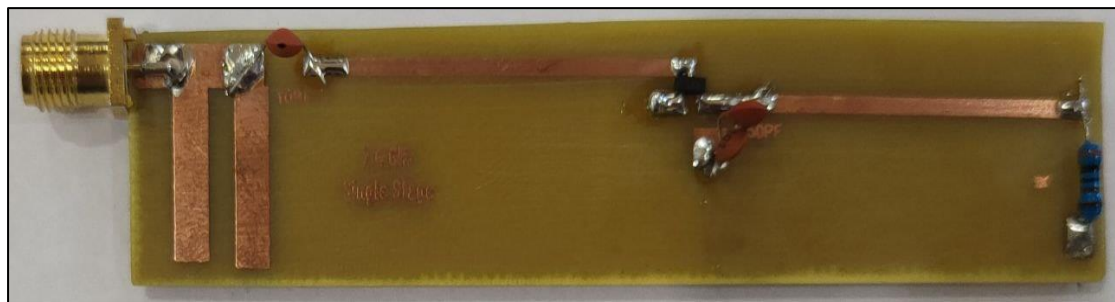


Fig.3.58: Photo of the front layer of rectifier circuit.



Fig.3.59: Photo of the back layer of rectifier circuit.

The fabricated rectifier circuit was fed by TGR6000 1GHz Synthesized RF Signal Generator with a variable input power level (in dBm) through a rigid microwave coaxial cable. Sub miniature Version A (SMA) connector is attached to the input port of fabricated circuit and the S11 (Reflection Coefficient) is measured by Network Analyzer as shown in Fig.3.60, and then the output voltage is measured using multipurpose digital AVO meter as illustrated in Fig.3.61. It can be seen from Fig.3.60 that best impedance matching is achieved at 1.87 GHz not 2.4 GHz due to losses of power in wires. This difference is due to the fabrication tolerance, which cause to slightly change the resonant frequency of the circuit and alter the impedance matching characteristics. Thus, in the measurement phase, the circuit was operated at 1.87 GHz and the output voltage is recorded at different input power. Furthermore, the employed TGR6000 1GHz Synthesized RF Signal Generator has a maximum input power of 7 dBm so that our measurements were limited to this value.

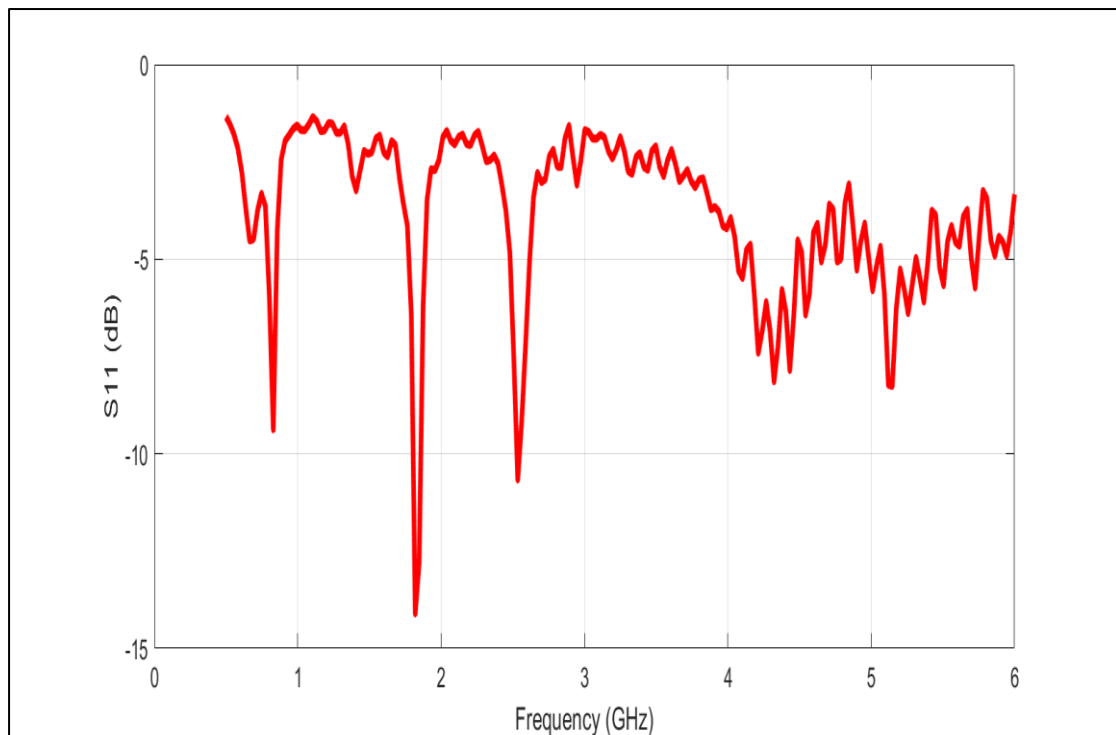


Fig.3.60: Measured S11 for the fabricated rectifier circuit.



Fig.3.61: Photograph of the experimental setup showing the measurement of V_{dc} (V_{out}) Versus P_{in} (dBm).

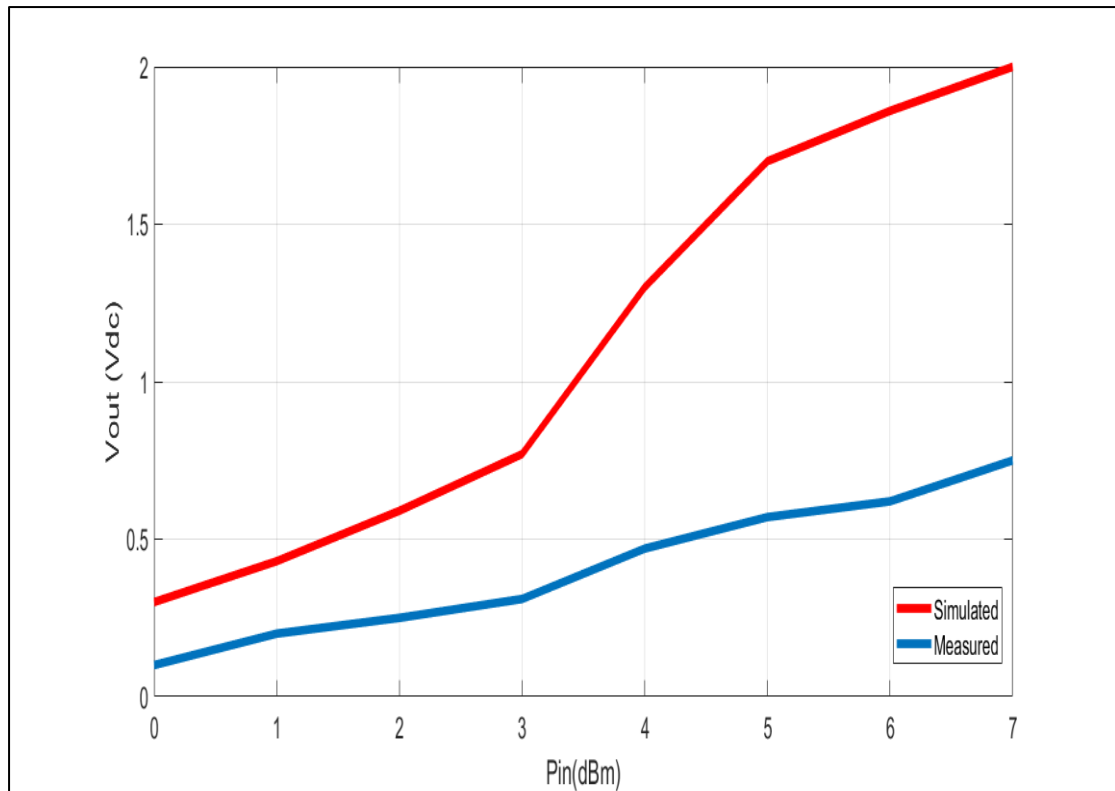


Fig.3.62: Comparison between simulated and Measured Vdc (Vout) versus Pin (dBm) at 3 kΩ.

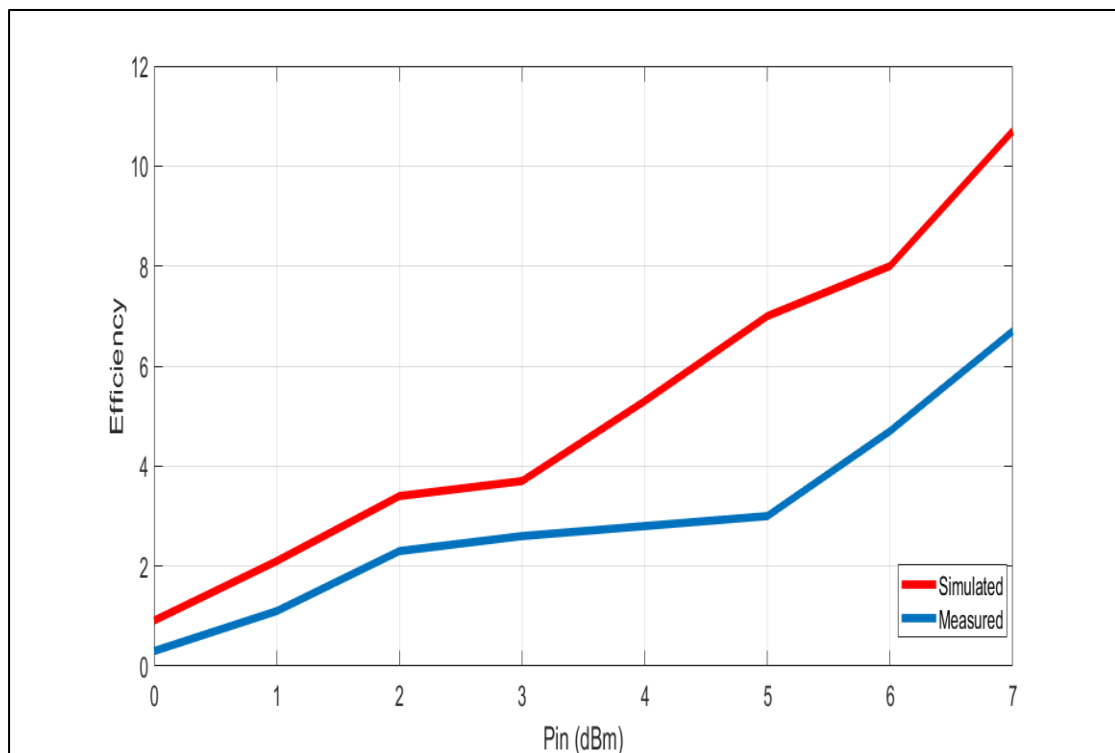


Fig.3.63: Comparison between simulated and Measured Efficiency (η) versus Pin (dBm) at 3 kΩ.

CHAPTER FOUR

Multiband and Wideband Antennas for Energy Harvesting Applications

4.1 Introduction

Antennas are employed to cover multiband operation at GHz frequencies to target wide range of applications such as Bluetooth, GSM, WLAN, Wi-MAX and satellite communication bands for energy harvesting systems. There are several proposed designs for antennas that exhibit multiband operation. In this work, the proposed designs are hexagonal and circular ring fractal antennas were simulated and fabricated. Both of designs will be placed on co-planer partial ground plane that is located on the front side of substrate. These types of antennas is selected due to its small size and compact nature compared with other types of antennas. In addition, there are other designs that operate with multiband and simulated such as rectangular patch with inset feeding without slot, rectangular patch with inset feeding and one slot on the front patch, rectangular patch with double slots, and UWB circular patch antennas. All the designs are simulated using the Computer Simulation Technology (CST) microwave software suite.

4.2 Antennas design

Microstrip patch antenna are popular due to their easy fabrication by using printed circuit board (PCB) technique, small size, light weight and low profile. Due to their compact and planar structure, these antennas are better to use for applications like wireless communications and satellite. The reflection coefficient of antenna is controlled by impedance matching of feed line and patch shape. The inset feeding is one of the famous techniques for achieving perfect matching.

4.2.1 Antenna 1 of rectangular patch with inset feeding

In the design process of a microstrip patch antenna, the selection of substrate is very crucial and important. The substrate's parameter such as weight, length, height and dielectric constant are very important for antenna performance. FR-4 substrate of thickness 1.6 mm, dielectric constant of $\epsilon_r = 4.3$ and a loss tangent (δ) of 0.02 is selected in this work. The size of patch in antenna is determined according to the Eq (2.3) and following Eqs (2.4)-(2.10) and shown in Fig.4.1. The width of patch is $W_p = 38.37$ mm and the length of patch is $L_p = 29.85$ mm. Furthermore, the width of substrate is $W_s = 44$ mm and the length of substrate is $L_s = 41$ mm. The antenna feeding should be designed carefully to provide a good impedance matching. The impedance of patch antenna should be equal to impedance of feeding line (typically 50Ω) to provide maximum power transfer and hence excellent results. The patch antenna was fed with a feed line connected to a point inside the patch where the input impedance is equal to 50Ω .

Fig.4.1 shows the structure of rectangular patch antenna with inset feeding. Fig.4.2 illustrates the design Antenna 1 with all dimensions marked. The reflection coefficient (S11) versus frequency is illustrated in Fig.4.3. It is noted that this antenna exhibits quad-band operation at frequencies 2.4, 3.6, 4.5 and 4.7 GHz with return loss of -50, -30, -17 and -15 dB and the Bandwidth (BW) = $f_H - f_L = 81.5, 84.6, 115$ and 124 MHz respectively. These results are matching the theoretical design process earlier in chapter two, which validate the design theory with simulation procedure.

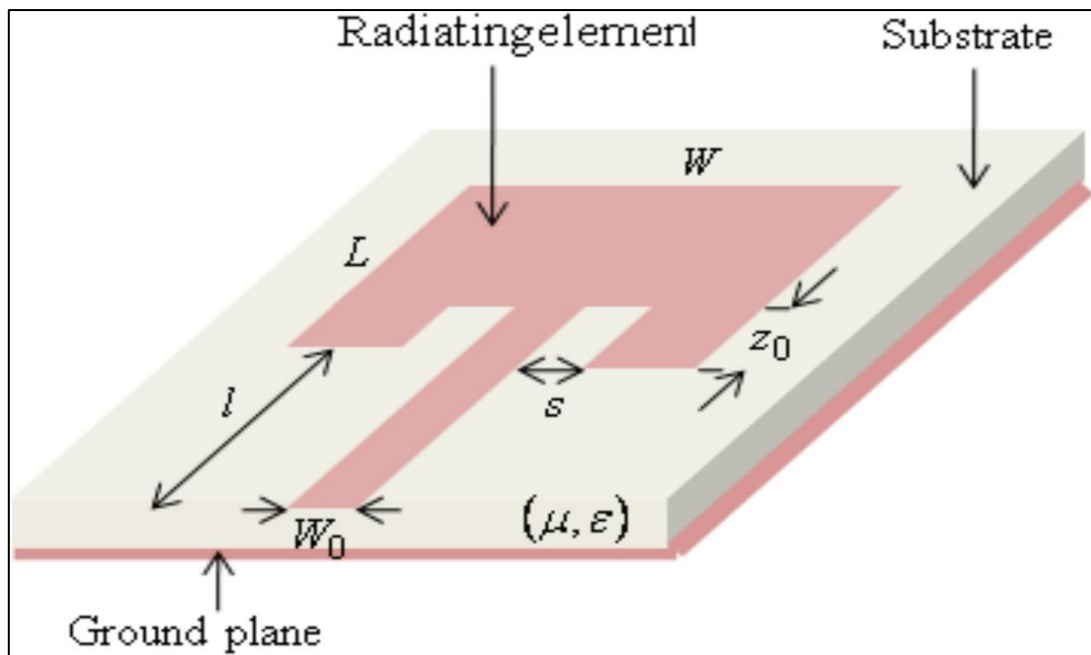


Fig.4.1: Rectangular patch antenna with inset feeding.

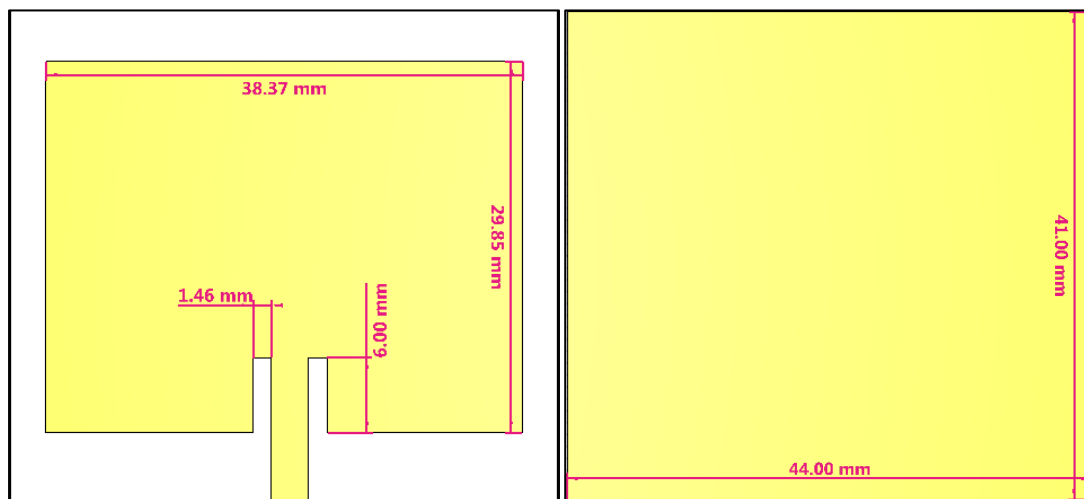


Fig.4.2: Antenna 1 of rectangular patch with inset feeding.

Table 4.1: Geometrical details of Antenna 1.

Name	Value (mm)
Width of substrate (W_s)	44
Length of substrate (L_s)	41
Width of patch (W_p)	38.37
Length of patch (L_p)	29.85
Width of ground plane (W_g)	44

Length of ground plane(Lg)	41
Width of feeding line (Wf)	3
Length of feeding line (Lf)	12.10
Width of inset feeding (Ws)	1.46
Length of inset feeding (LD)	6
Thickness of substrate (hs)	1.645
Dielectric constant of substrate ϵ_r	4.3
Thickness of copper (ht)	0.035

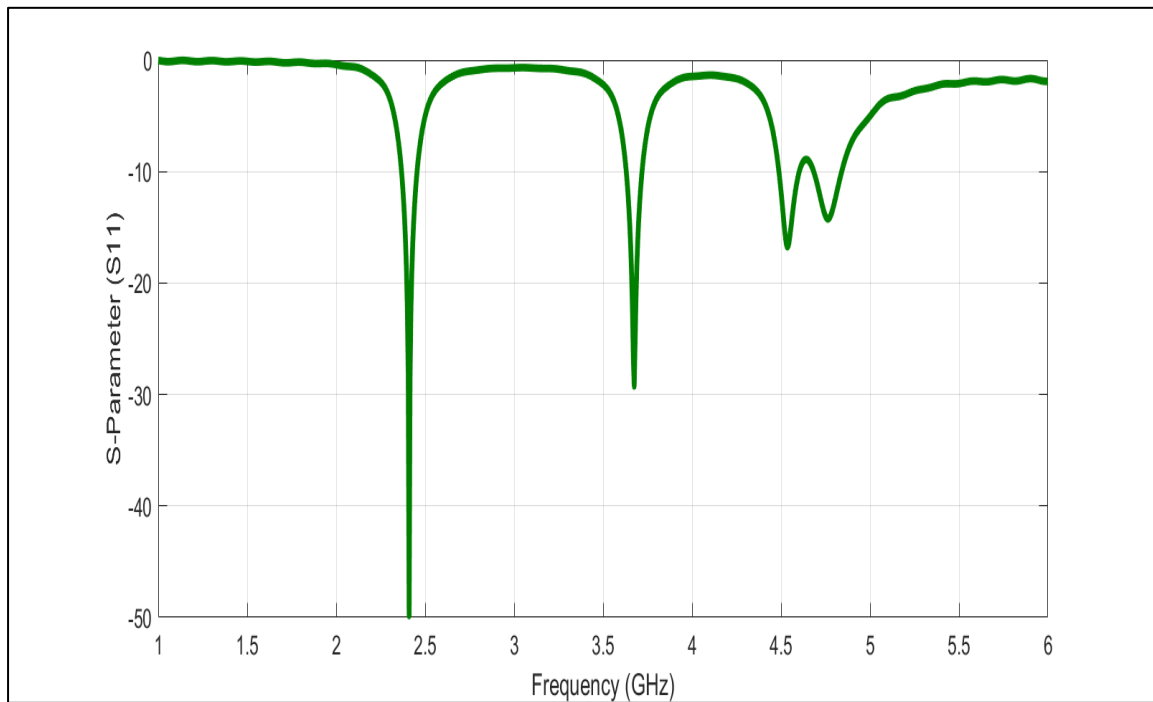


Fig.4.3: Simulated S11 versus frequency for Antenna 1.

The antenna's 3D radiation pattern at 2.4 GHz is shown in Fig.4.4. The antenna features have a directivity of about 5.509 dBi. The 2D (polar) radiation pattern of Antenna 1 at 2.4 GHz is depicted in Fig.4.5.

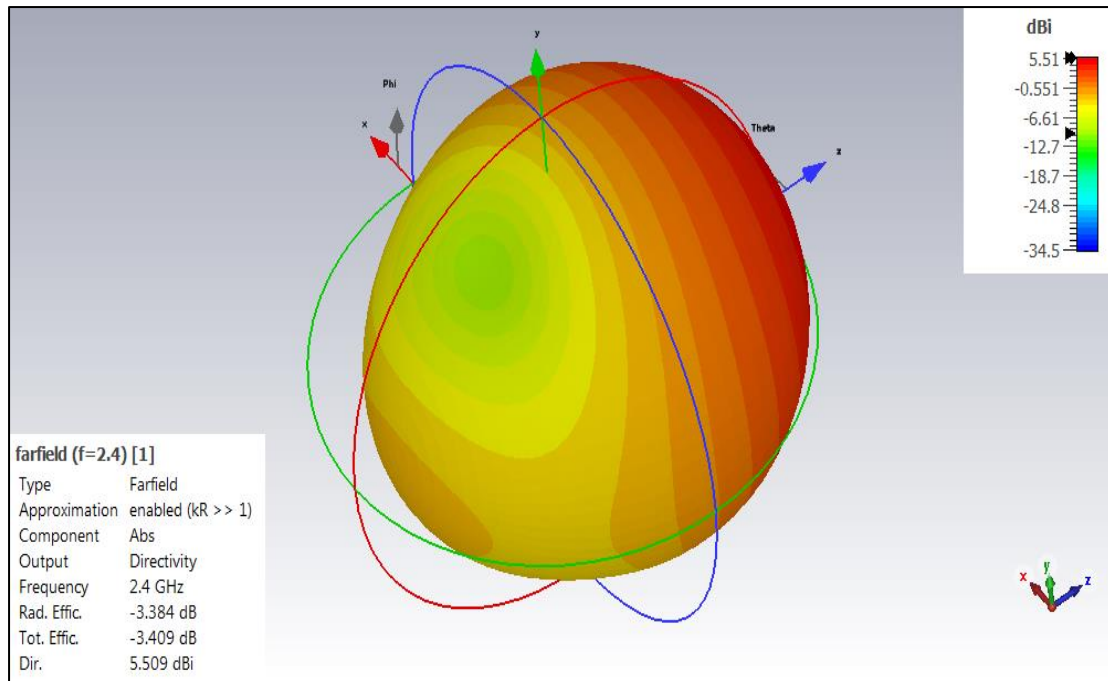


Fig.4.4: Simulated 3D radiation pattern at 2.4 GHz for Antenna 1.

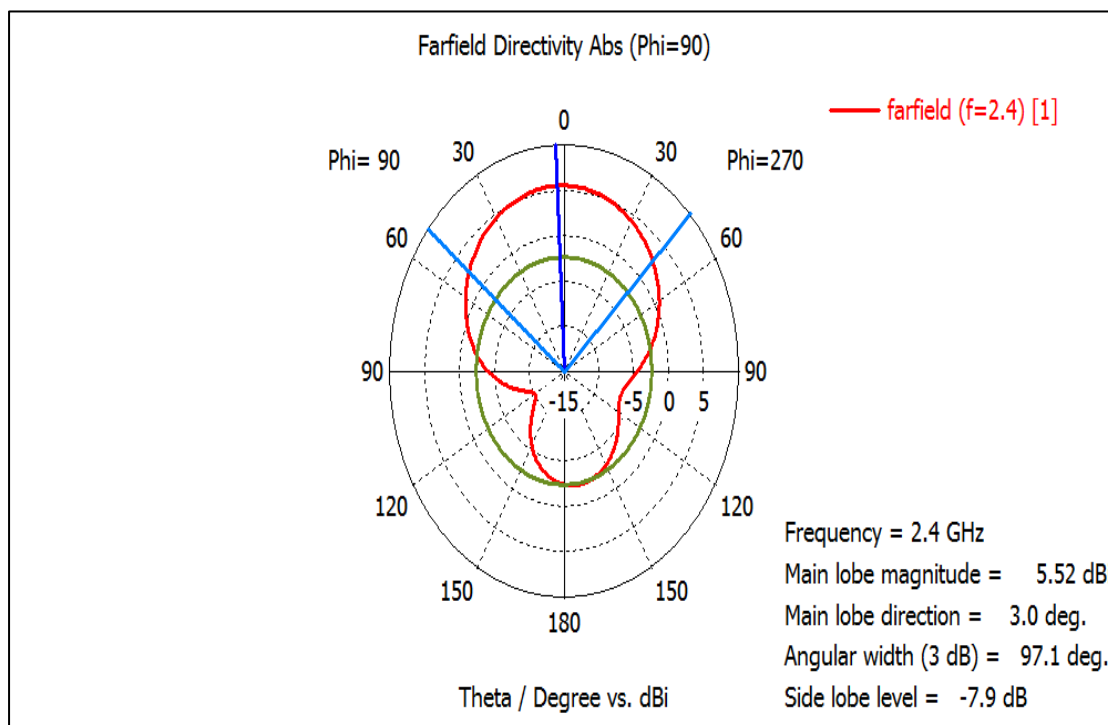


Fig.4.5: Simulated 2D radiation pattern at 2.4 GHz for Antenna 1.

Fig.4.6 shows the antenna's 3D radiation pattern at 3.6 GHz and Fig.4.7 shows the antenna's 2D radiation pattern at 3.6 GHz. The antenna features have a directivity about 4.284 dBi.

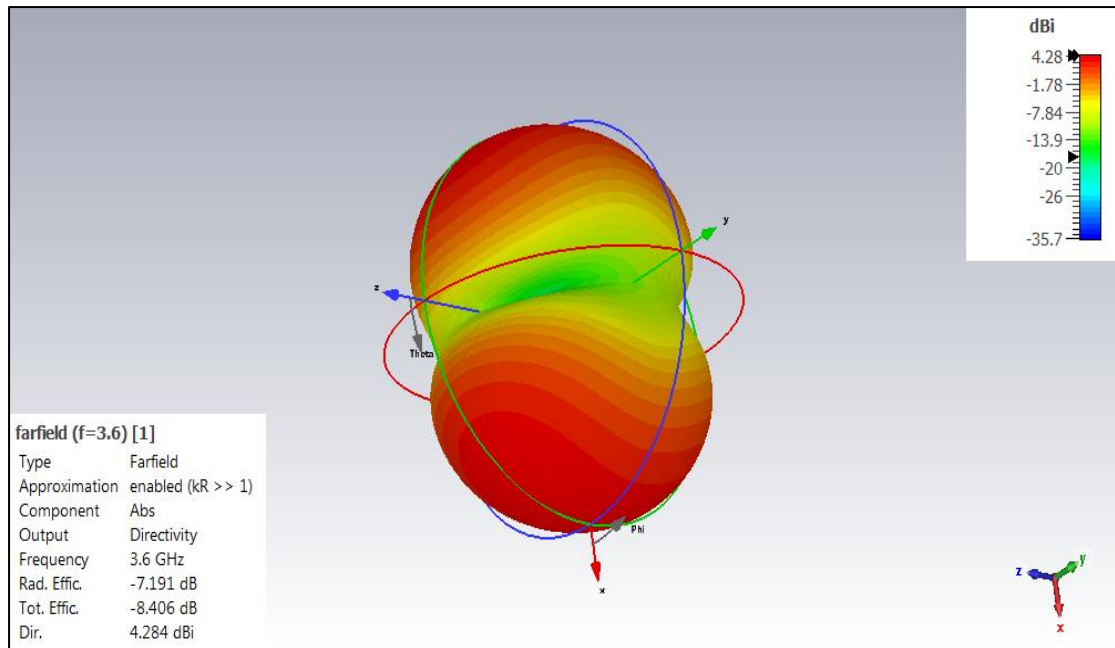


Fig.4.6: Simulated 3D radiation pattern at 3.6 GHz for Antenna 1.

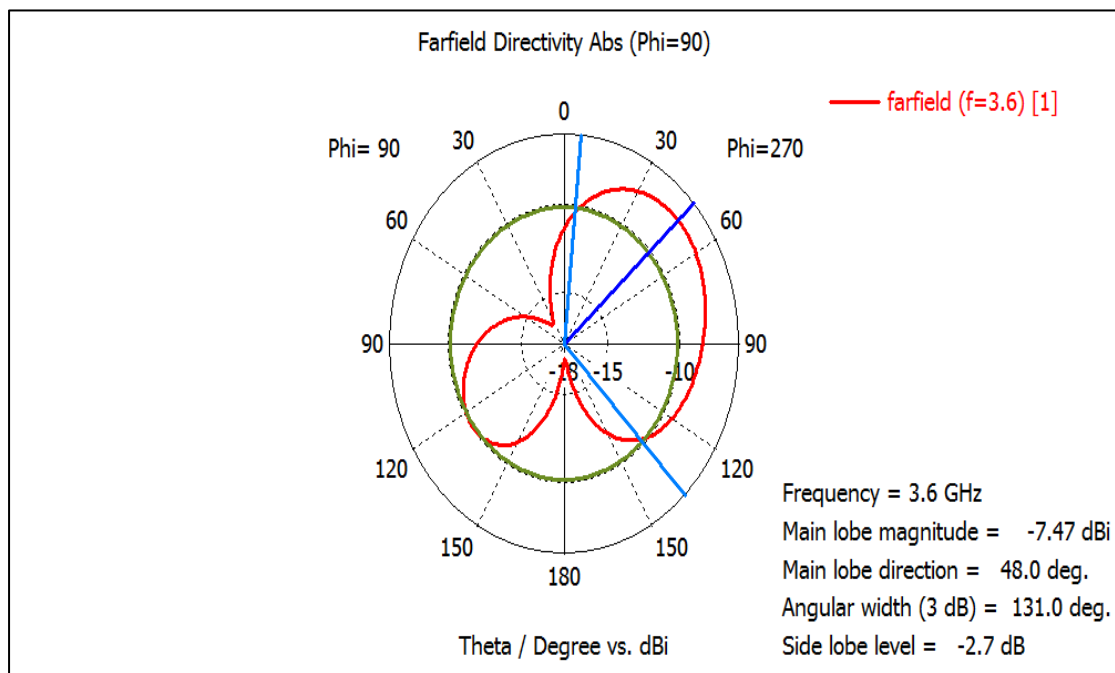


Fig.4.7: Simulated 3D radiation pattern at 3.6 GHz for Antenna 1.

Fig.4.8 shows the antenna's 3D radiation pattern at 4.5 GHz and Fig.4.9 shows the antenna's 2D radiation pattern at 4.5 GHz. The antenna features have a directivity about 4.135 dBi.

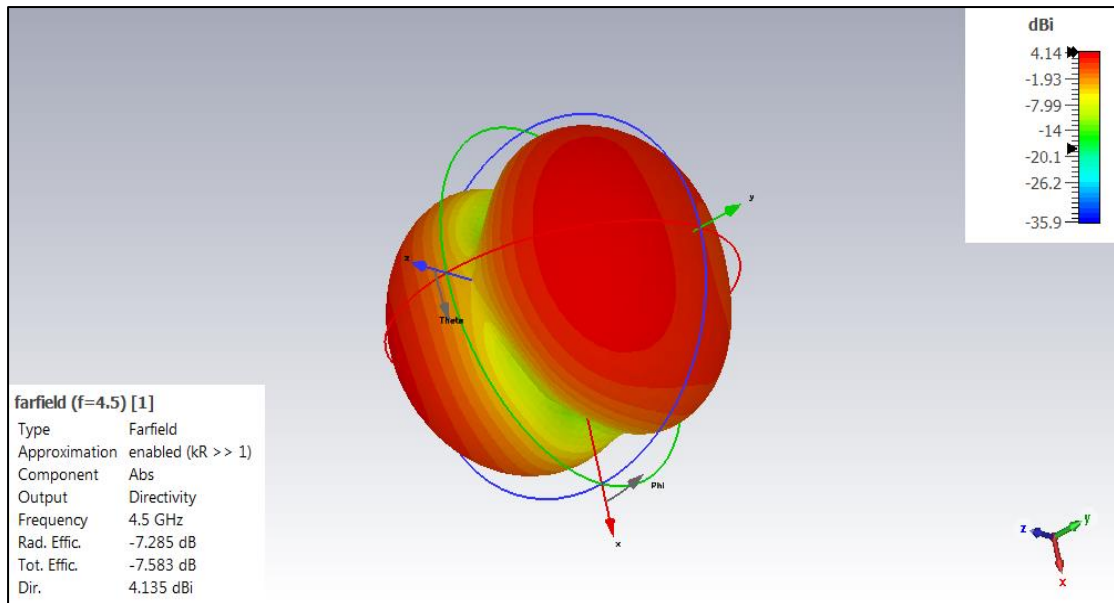


Fig.4.8: Simulated 3D radiation pattern at 4.5 GHz for Antenna 1.

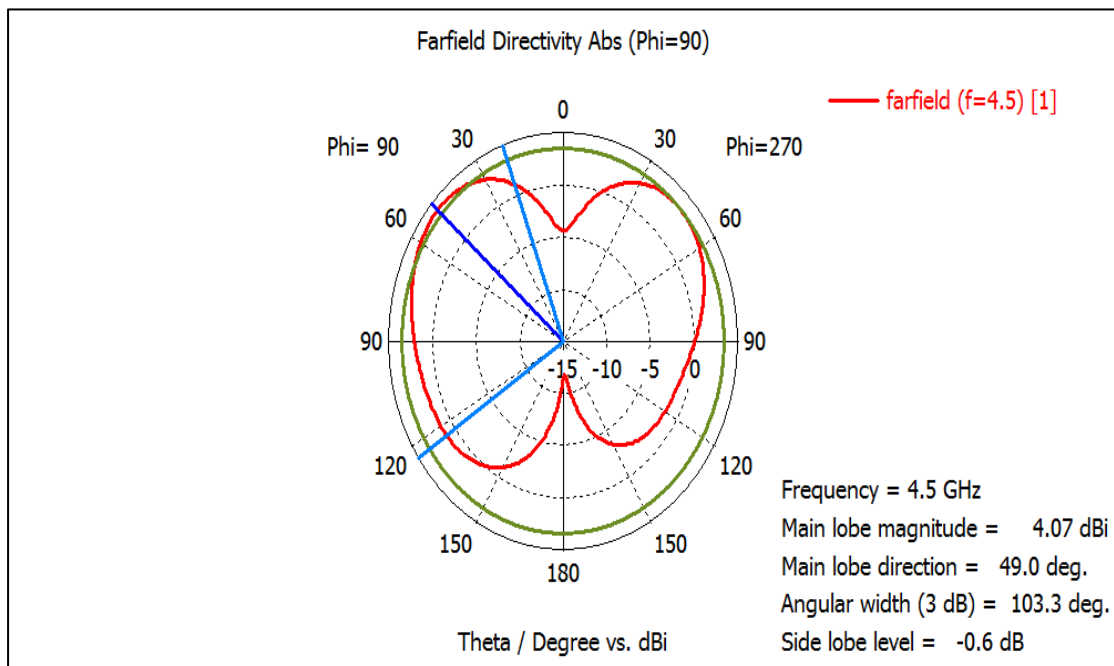


Fig.4.9: Simulated 2D radiation pattern at 4.5GHz for Antenna 1.

Fig.4.10 shows the antenna's 3D radiation pattern at 4.7 GHz and Fig.4.11 shows the antenna's 2D radiation pattern at 4.7 GHz.

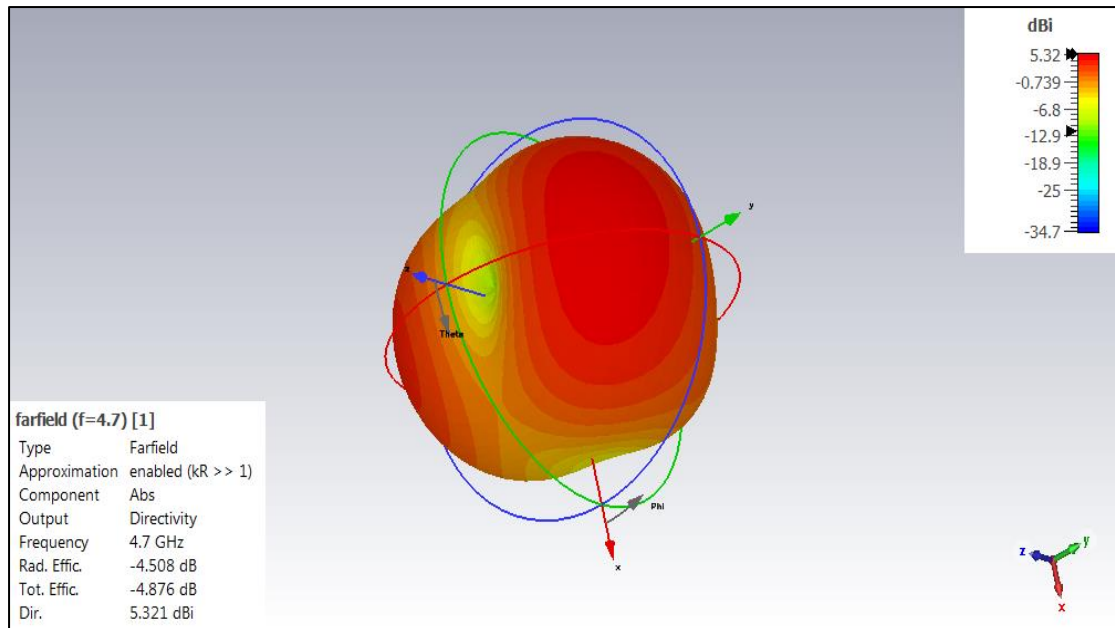


Fig.4.10: Simulated 3D radiation pattern at 4.7 GHz for Antenna 1.

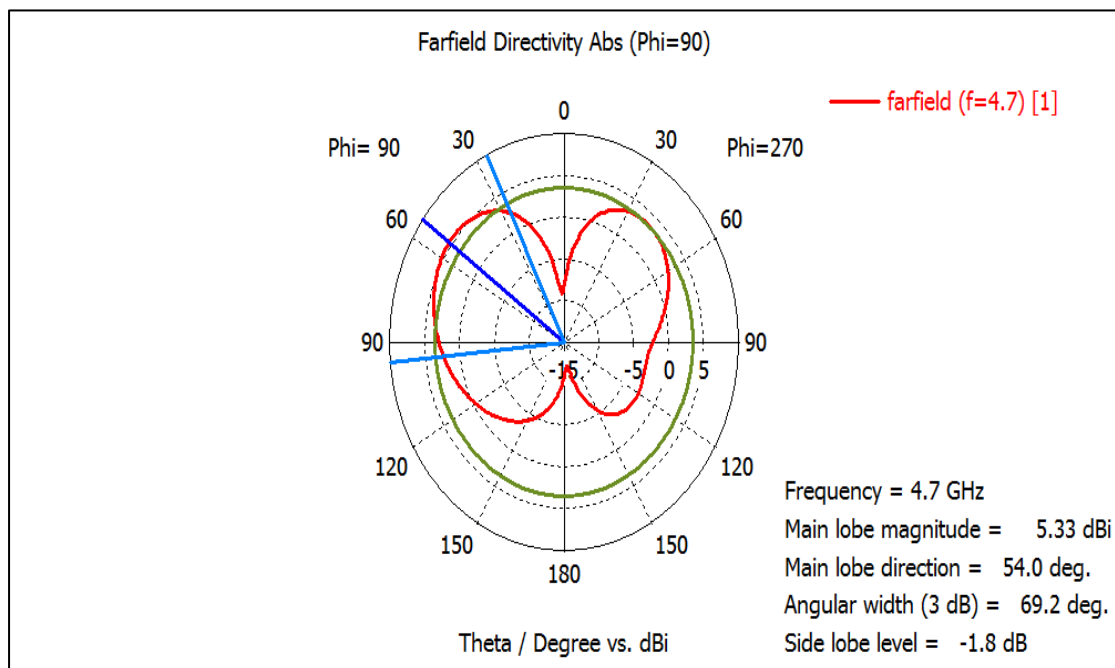


Fig4.11: Simulated 2D radiation pattern at 4.7 GHz for Antenna 1.

It can be seen from the figures of radiation pattern above that the shape of the radiation pattern and the value of directivity is different for each resonant frequency.

4.2.2 Antenna 2 of rectangular patch with inset feeding and slot

A slotted rectangular patch antenna with inset feeding is designed and simulated. The antenna structure has two slots: the first slot has a rectangle shape and lies on the front patch, while the second slot lies on the ground plane as shown in Fig.4.12. Adding slots to the antenna design contributes to adding more frequency band. The antenna is placed on FR-4 substrate with $\epsilon_r = 4.3$, a thickness of 1.6 mm and a loss tangent (δ) of 0.02. The triple band are located at resonant frequencies 2.32, 3.8 and 4.9 GHz and the Bandwidth (BW) = $f_H - f_L = 77.5, 80.6, 111$ MHz respectively.

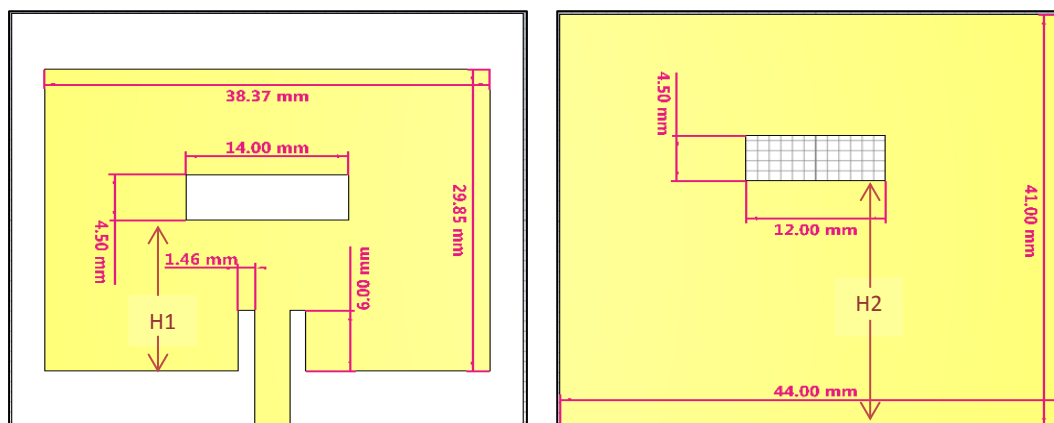


Fig.4.12: Antenna 2 Rectangular patch antenna with inset feeding and two slots.

Table 4.2: Geometrical details of Antenna 2.

Name	Value (mm)
Width of substrate (W_s)	44
length of substrate (L_s)	41
Width of patch (W_p)	38.37
Length of patch (L_p)	29.85

Width of ground plane(W_g)	44
length of ground plane(W_g)	41
Width of feeding line (W_f)	3
Length of feeding line (L_f)	12.10
Height the locate of front slot (H_1)	14.38
Height the locate of back slot (H_2)	24.5
Width the locate of back slot (L_3)	12
Width of inset feeding (W_s)	1.46
length of inset feeding (L_D)	6
Thickness of substrate (h_s)	1.645
Dielectric constant of substrate (ϵ_r)	4.3
Thickness of copper (h_t)	0.035

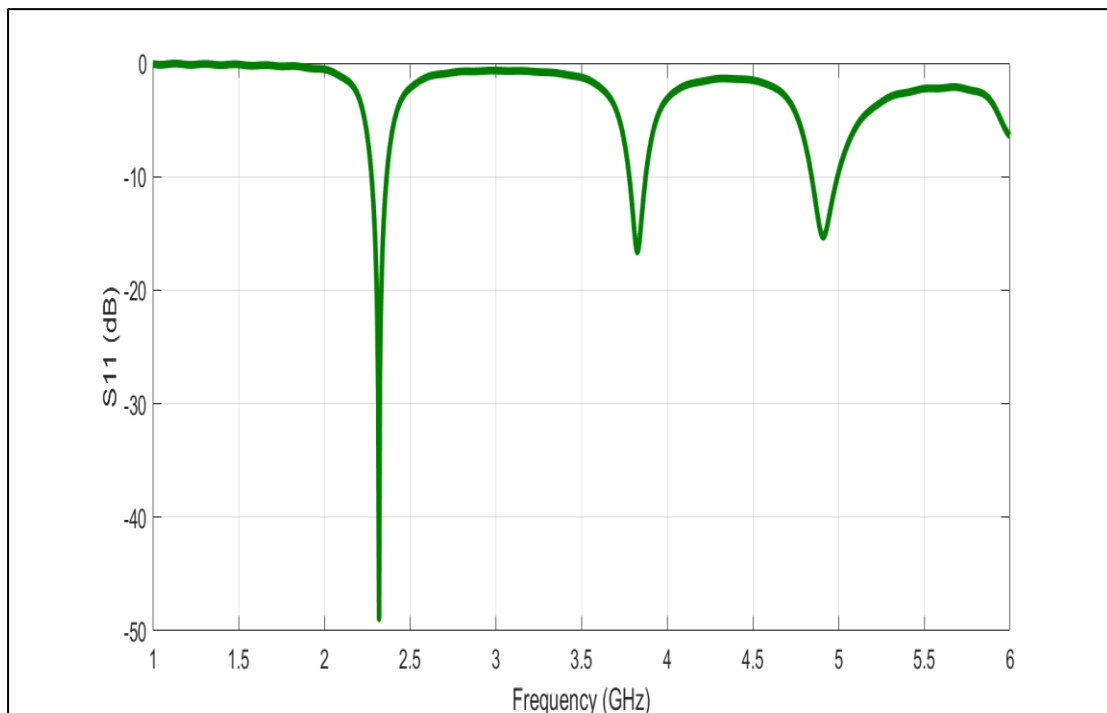


Fig.4.13: Simulated S11 for Antenna 2 (rectangular patch antenna with inset feeding).

A parametric study on the impact of the slot location is conducted. The aim is to study the possibility of controlling the resonant frequency of the antenna by changing the slot characteristics. To this end, the height (H1) of the front slot (i.e. distance between the slot and the bottom of the patch antenna). The results showed that increasing H1 will reduce the resonant frequency of all bands with decreasing the value of S11 as shown in Fig.4.14. On the other hand, the height (H2) of the back slot is increased from 24.5 mm to 32.5 mm and the results showed that H2 have similar impact as of H1 as shown in Fig. 4.15. It can be concluded that the performance of the slotted patch antennas can be enhanced and controlled by varying the slot parameters.

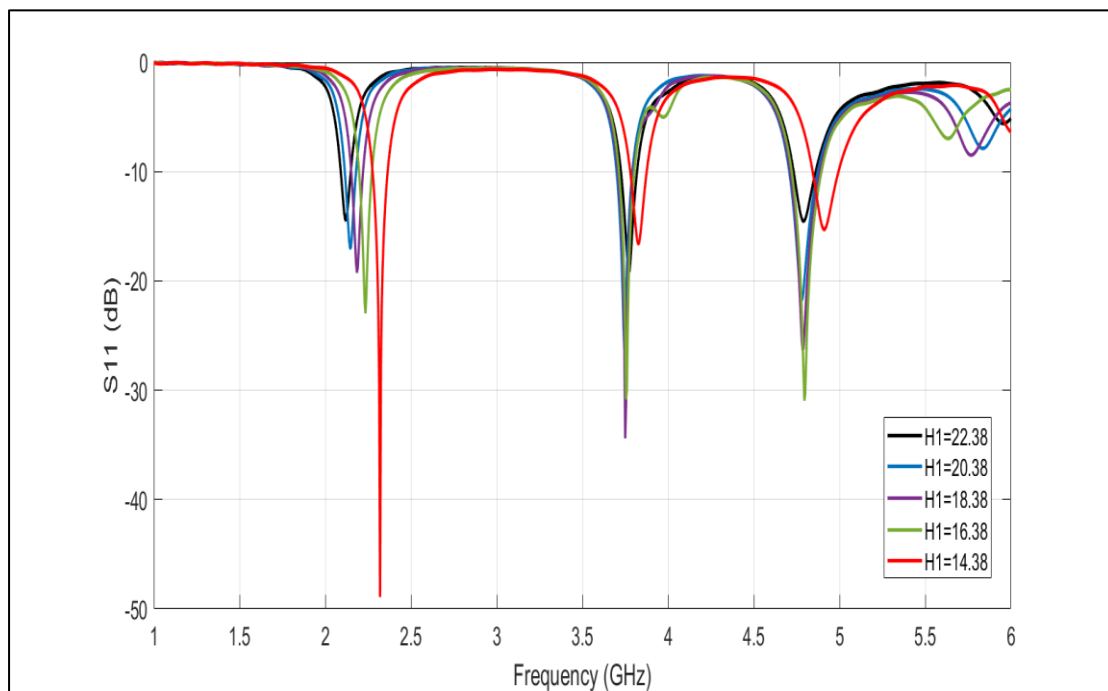


Fig.4.14: Simulated S11 for Antenna 2 by varying the Height the locate of front slot (H1).

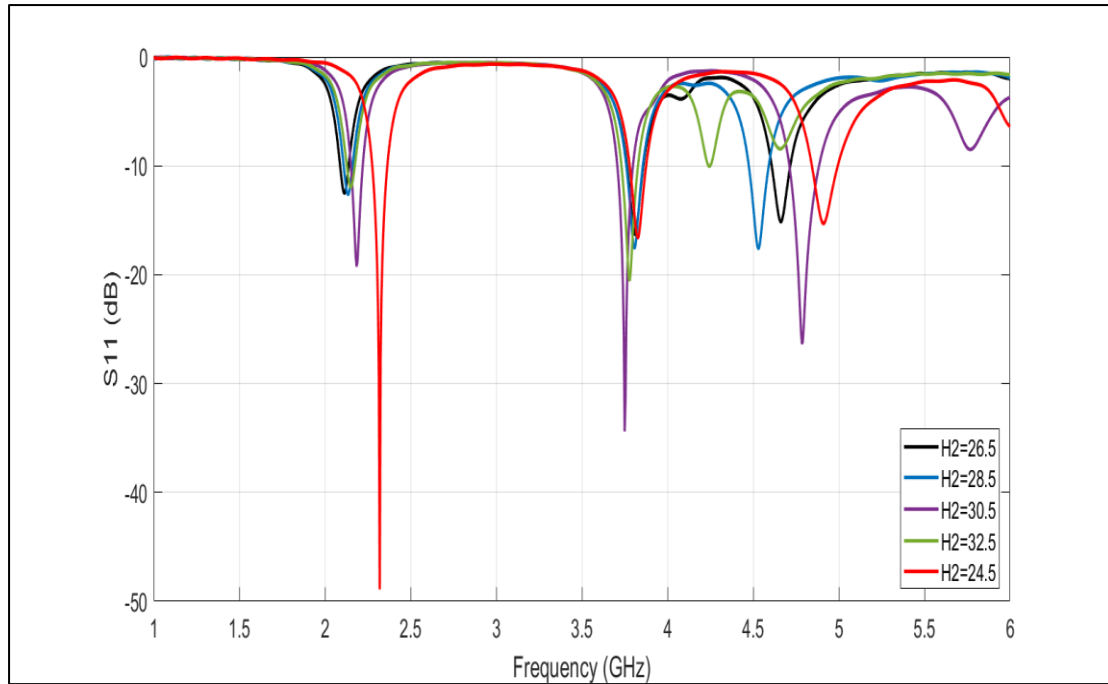


Fig.4.15: Simulated S11 for Antenna 2 by varying the Height the locate of back slot (H2).

4.2.3 Antenna 3 of rectangular patch with double slot

For the rectangular patch with double slot design, the impact of the distance between the two slots was also studied to observe the impact of moving the slots horizontally (shown in Fig.4.16). The reflection coefficient of the designed antenna for the case of decreasing the distance (d) at distances of 24 mm, 20 mm and 8 mm is illustrated in Fig.4.17. It is found that when the distance between the slots is reduced, the lower band frequency is increased while the upper band frequency decreases significantly with an increase in return loss (S11) value in both cases. Furthermore, for the middle frequency band around 4.5 GHz, the resonant frequency is kept almost unchanged with varying the distance between the slots and the Bandwidth (BW) = $f_H - f_L = 95.5, 74.6, 122$ MHz respectively.

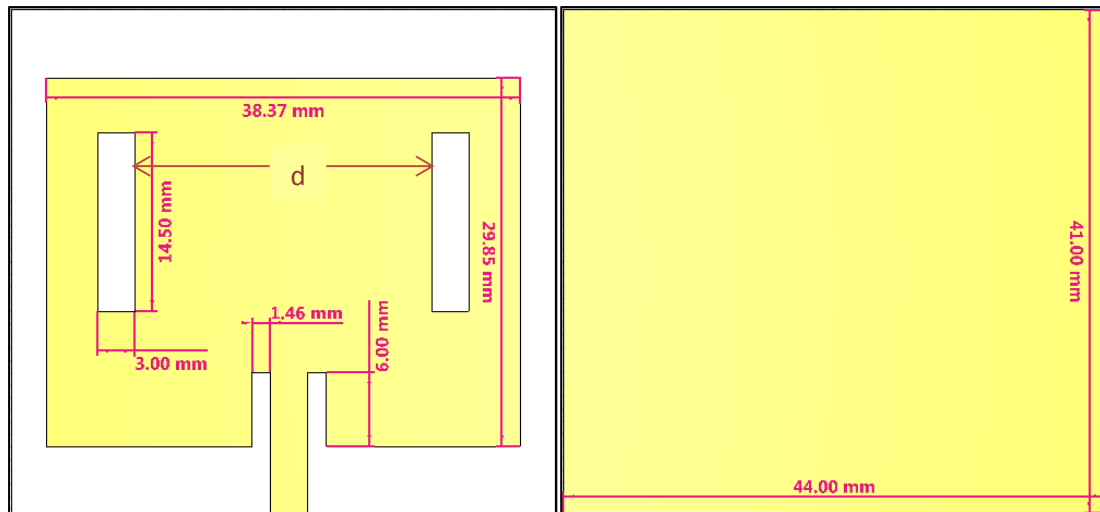


Fig.4.16: Antenna 3 (Rectangular patch with double slot) all dimension in mm.

Table 4.3: Geometrical details of Antenna 3.

Name	Value (mm)
Width of substrate (W_s)	44
Length of substrate (L_s)	41
Width of patch (W_p)	38.37
Length of patch (L_p)	29.85
Width of ground plane (W_g)	44
Length of ground plane (L_g)	41
Width of feeding line (W_f)	3
Length of feeding line (L_f)	12.10
Width of inset feeding line (W_s)	1.46
Length of inset feeding line (L_D)	6
Thickness of substrate (h_s)	1.645
Dielectric constant of substrate (ϵ_r)	4.3
Thickness of copper (h_t)	0.035
Width the locate of two slots (d)	24, 20 and 8

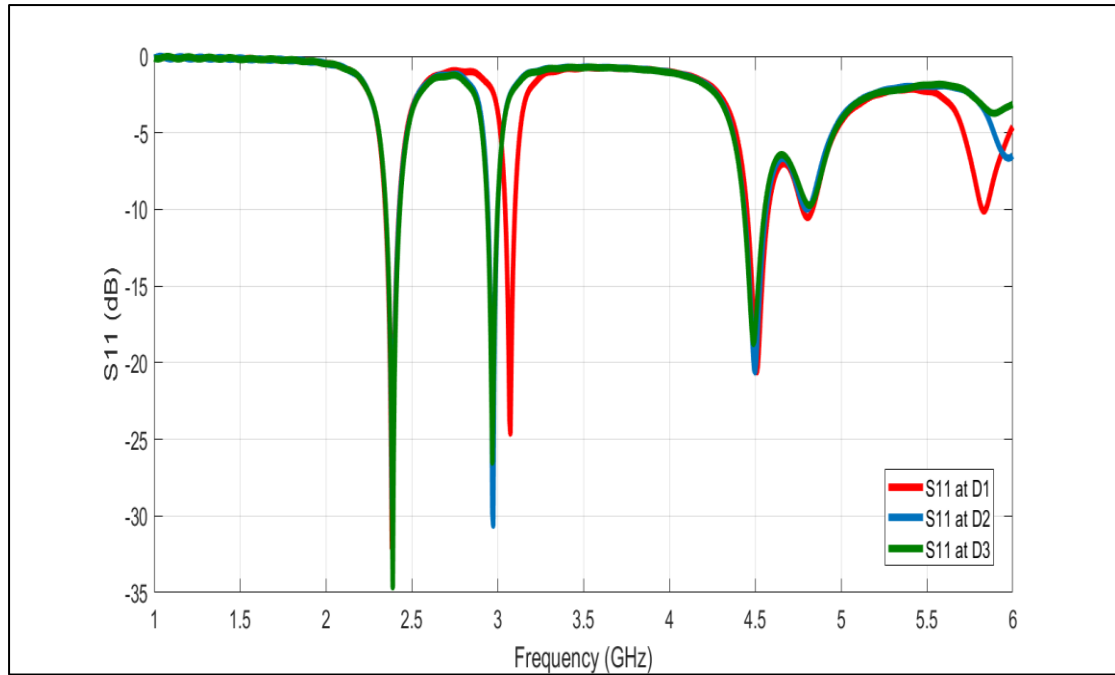


Fig.4.17: Simulated S11 for Antenna 3 (Rectangular patch with double slot).

4.2.4 Antenna 4 of rectangular patch with Sierpinski fractal slot

Rectangular patch triangle fractal slot antennas are a type of microstrip antenna that can operate at multiple frequency bands. The fractal geometry that is employed here is the Sierpinski gasket as shown in Fig.4.18. These antennas are composed of a rectangular patch with a triangular fractal slot, which is etched into the patch as illustrated in Fig.4.19. The fractal slot helps to increase the bandwidth of the antenna, allowing it to operate at multiple frequencies. This makes rectangular patch triangle fractal slot antennas a popular choice for applications that require wide frequency range of operation such as in wireless communication systems. In particular, these antennas are well-suited for the frequency bands at 2.3, 3.7, 4.4, 4.7 and 6.6 GHz and the Bandwidth (BW)= $f_H - f_L = 80.3, 86, 70.6, 183$ and 70 MHz respectively as demonstrated in Fig.4.20, which are commonly used in many wireless communication applications. In this context, the design and analysis of

these antennas have become an active area of research in the field of antenna engineering.

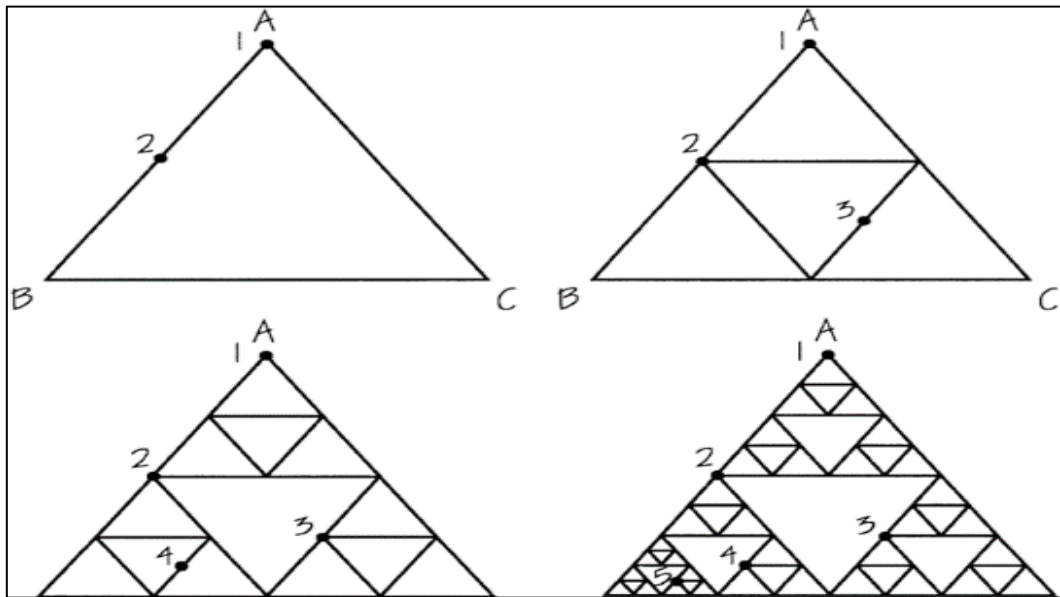


Fig.4.18: Triangle slot of Sierpinski.

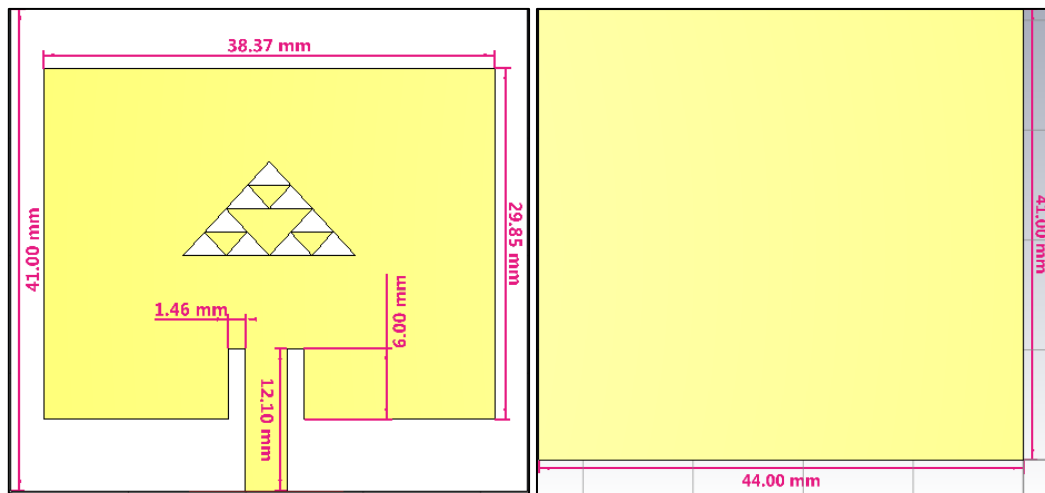


Fig.4.19: Antenna 4 (Rectangular patch triangle slot antenna) all dimensions in mm.

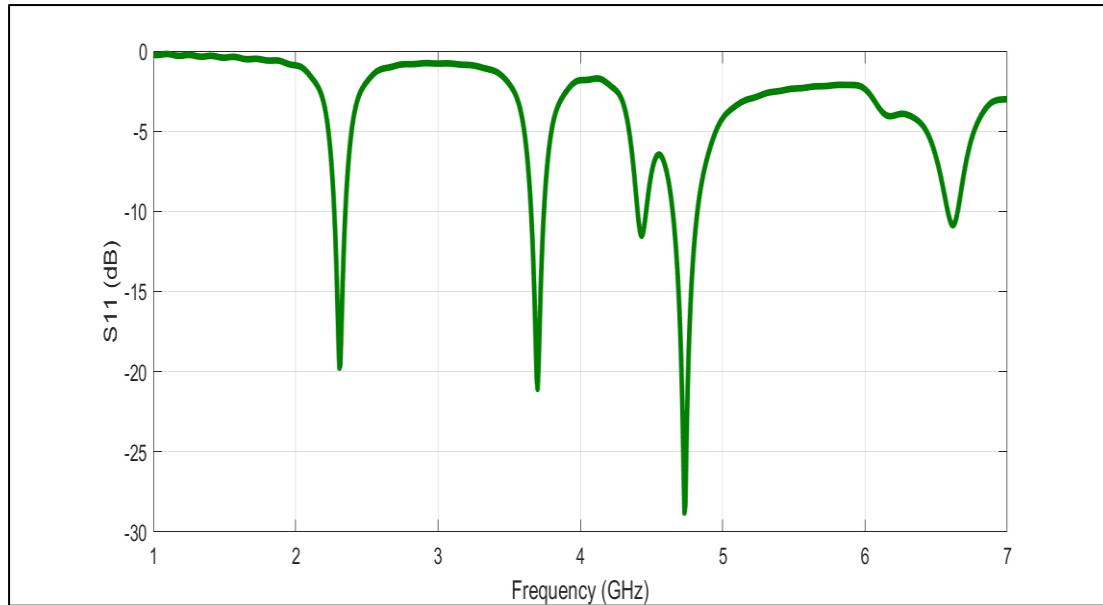


Fig.4.20: Simulated S11 for Antenna 4.

4.2.5 Antenna 5 of Slotted UWB Circular Patch Antenna

An Ultra-wide band (UWB) circular patch antenna is designed and simulated without slot at the beginning. Two slots are then added to the structure to study the impact of adding slots to the patch antenna structure as shown in Fig.4.21. The circular patch antenna without slot exhibits a wide frequency band of operation starts from 2.4 GHz to 5.6 GHz as depicted in Fig. 4.22. This frequency of operation is utilized in several communication systems. In addition, in slotted UWB circular patch, it was noticed that the slots add another frequency band centered around 6.2 GHz. The distance between the two slots are varied by 2mm, 4mm and 8mm and its impact was observed. The results showed that varying the distance between slots can only affect the center frequency of the newly added band and the Bandwidth (BW)= $f_H - f_L = 95.5, 74.6, 122$ and 110 MHz respectively as illustrated in Fig.4.23. This means that engineering the slots could adjust the frequency of operation around the frequency band of interest. The partial ground plane is located at front side of

substrate while the back side of substrate is left empty. Table 4.4 lists the geometrical details of Antenna 5.

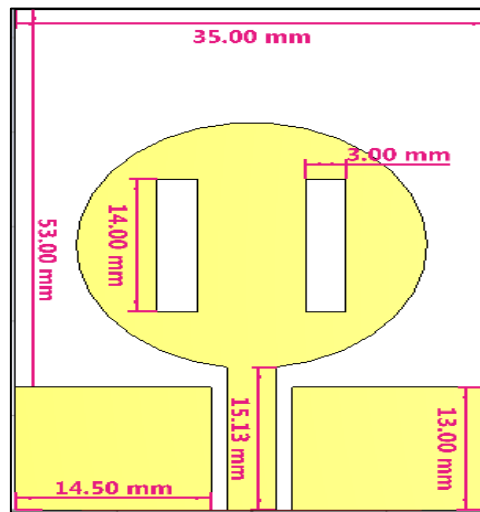


Fig.4.21: Antenna 5 (An Ultra-Wide Band (UWB) Circular patch antenna) all dimensions in mm.

Table 4.4: Geometrical details of Antenna 5.

Name	Value (mm)
Width of substrate (W_s)	35
Length of substrate (L_s)	53
Radius of patch (r)	13
Length of slot (L_1)	14
Width of slot (L_2)	3
Width of ground plane (W_g)	14.5
Length of ground plane (L_g)	13
Width of feeding line (W_f)	3
Length of feeding line (L_f)	15.13
Thickness of substrate (h_s)	1.645
Dielectric constant of substrate ϵ_r	4.3
Thickness of copper (h_t)	0.035

Width the locate of two slots (D)	2, 4 and 8
-----------------------------------	------------

Simulated S11 for Antenna 5 without slot as shown in Fig.4.22,

and the Bandwidth (BW)= $f_H - f_L = 3.4$ GHz.

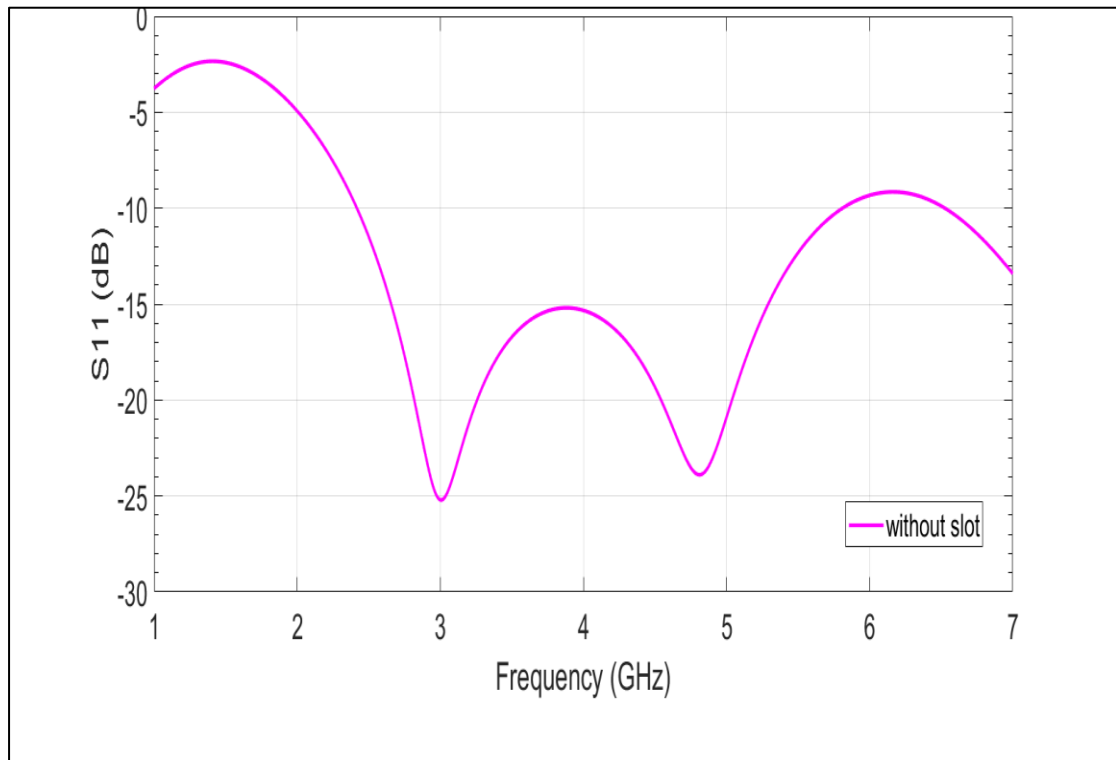


Fig.4.22: Simulated S11 for Antenna 5 without slot.

Simulated S11 for Antenna 5 by varying the distance between two slots (D) as shown in Fig.4.23, and the Bandwidth (BW)= $f_H - f_L = 3.2$ and 1.1 GHz respectively.

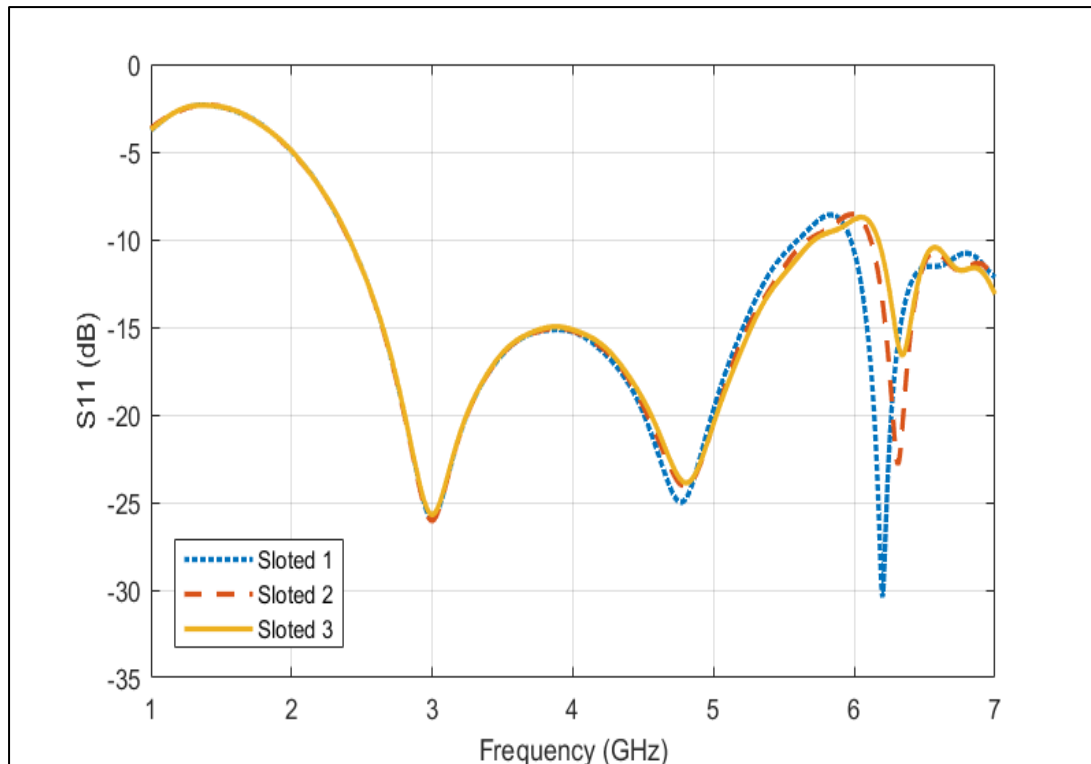


Fig.4.23: Simulated S11 for Antenna 5 by varying the distance between two slots (D).

4.2.6 Antenna 6 of Hexagonal ring fractal antenna with slot

CST software was used to design and simulate a hexagonal patch antenna. The antenna is constructed on a 1.6 mm thick FR-4 Printed Circuit Board (PCB) with a dielectric constant of 4.3. The antenna is designed to operate at wide range of frequencies. The substrate dimensions including antenna structure is (38×38) mm in total size. The prototype design of this antenna was in configuration hexagonal patch antenna as shown in Fig.4.24

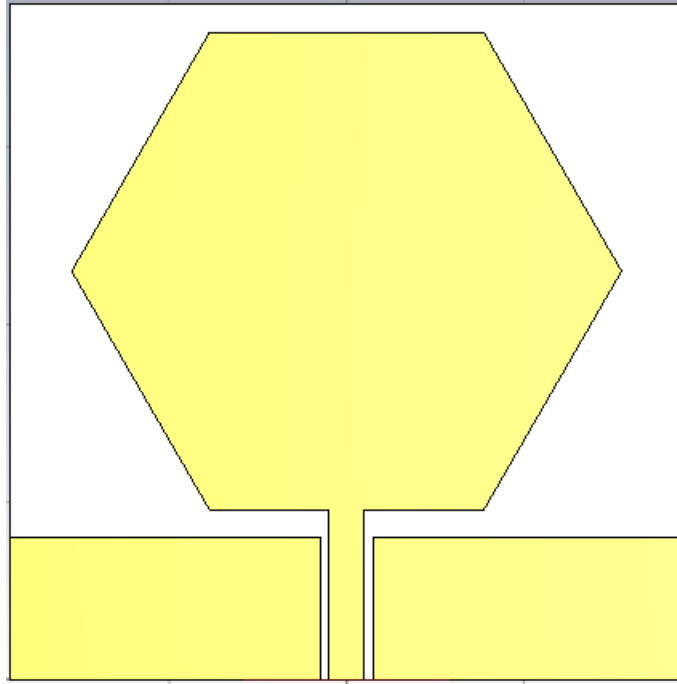


Fig.4.24: Hexagonal patch without slot antenna.

The radius of the hexagonal shape is varied from 12.49 to 15.49 mm and the S_{11} results are observed as illustrated in Fig.4.25. It can be seen that all the designed hexagonal antennas exhibit a wide frequency band of operation starts from 3 GHz to more than 6 GHz. It can also be seen that when radius is equal to 12.49 mm there is a good resonant frequency at 4.3 GHz with S_{11} is equal to -40 dB and also when changing the radius to 14.49 mm the antenna starts to operate slightly below 3GHz and an excellent resonant frequency appeared at 5.6 GHz with S_{11} is equal to -43 dB.

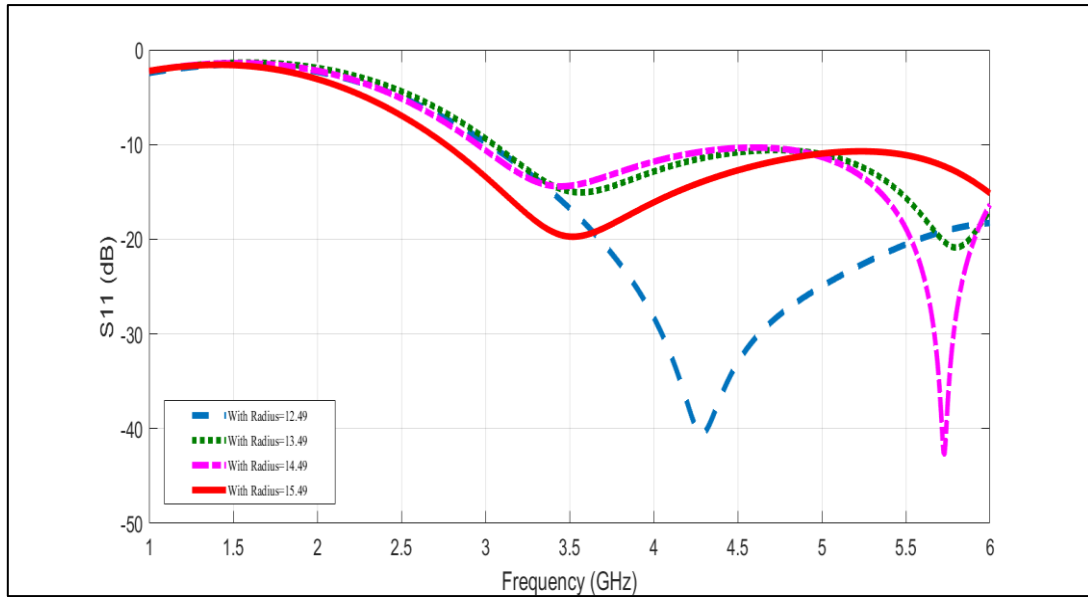


Fig.4.25: Simulated S11 versus frequency for Hexagonal patch antenna.

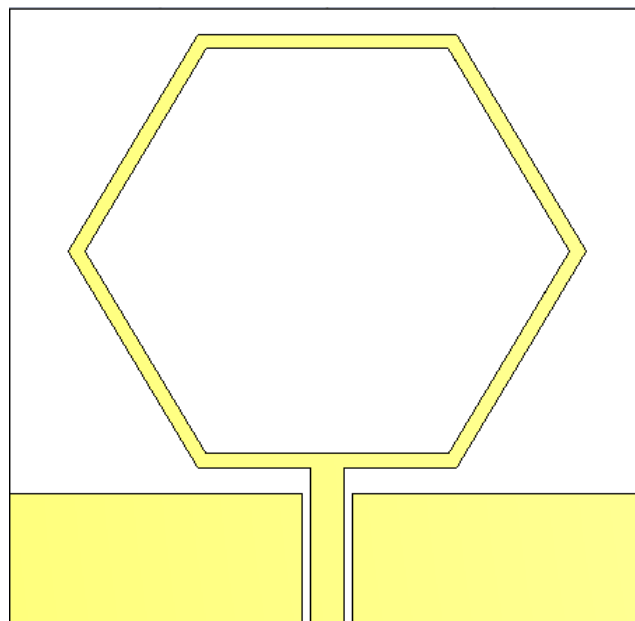


Fig.4.26: Hexagonal ring patch antenna.

A modification is made on the hexagonal patch to convert it into hexagonal ring antenna in order to improve the performance as depicted in Fig.4.27. However, the S11 results are poor and not promising. A resonant frequency band is appeared at 2.4 GHz with reflection coefficient around -10 dB as shown in Fig.4.27.

In order to improve the reflection characteristics and achieve multiband performance, a fractal geometry is built by replicating the hexagonal rings with a smaller scale (i.e self-similarity). Fig. 4.28 illustrates the newly proposed hexagonal fractal ring antenna.

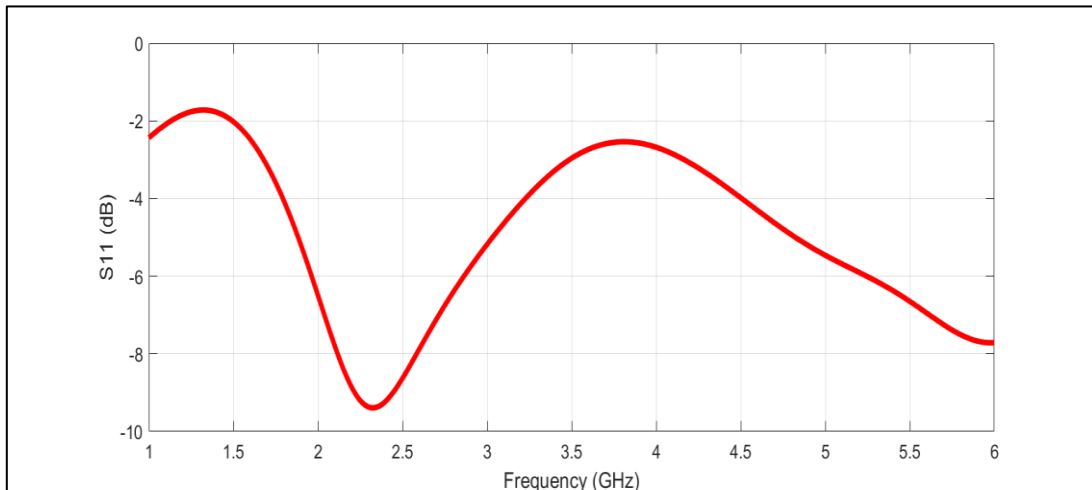


Fig.4.27: Simulated S11 versus frequency for Hexagonal ring patch antenna.

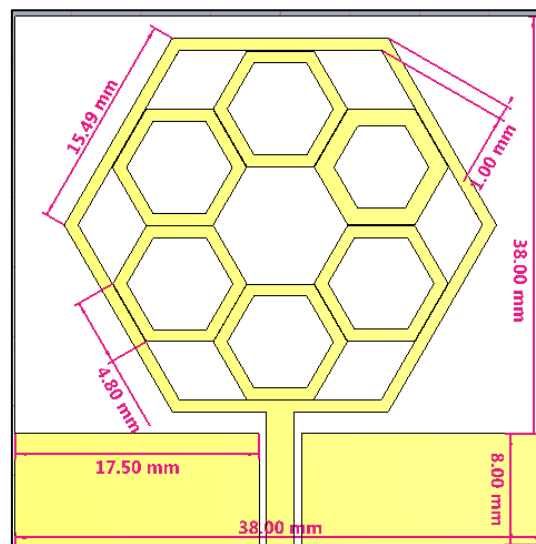


Fig.4.28: Hexagonal ring fractal antenna with slot with all dimensions in mm.

Table 4.5 displays the dimensions for Antenna 6 (Hexagonal ring fractal antenna).

Table 4.5: Geometrical details of Antenna 6.

Name	Value (mm)
Width of substrate (Ws)	38
Length of substrate (Ls)	38
Width of patch (Wp)	30.98
Length of patch (Lp)	26.83
Width of ground plane(Wg)	17.5
Length of ground plane (Lg)	8
Width of feeding line (Wf)	2
Thickness of substrate (hs)	1.645
Dielectric constant of substrate ϵ_r	4.3
Thickness of copper (ht)	0.035

The simulated S-parameters of the designed fractal antenna is illustrated in Fig.4.29, which typically gives a clear indication on the reflection and matching characteristics of the antenna. The S11 curve implies this antenna radiates very well at frequency bands at the range 1-6 GHz. It is worth mentioning that the fourth frequency band exhibits a very wide frequency range, which makes it perfect for sub-6 GHz 5G networks and above. And the Bandwidth (BW) = $f_H - f_L = 100$ and 93.3 MHz and 3.3 GHz respectively.

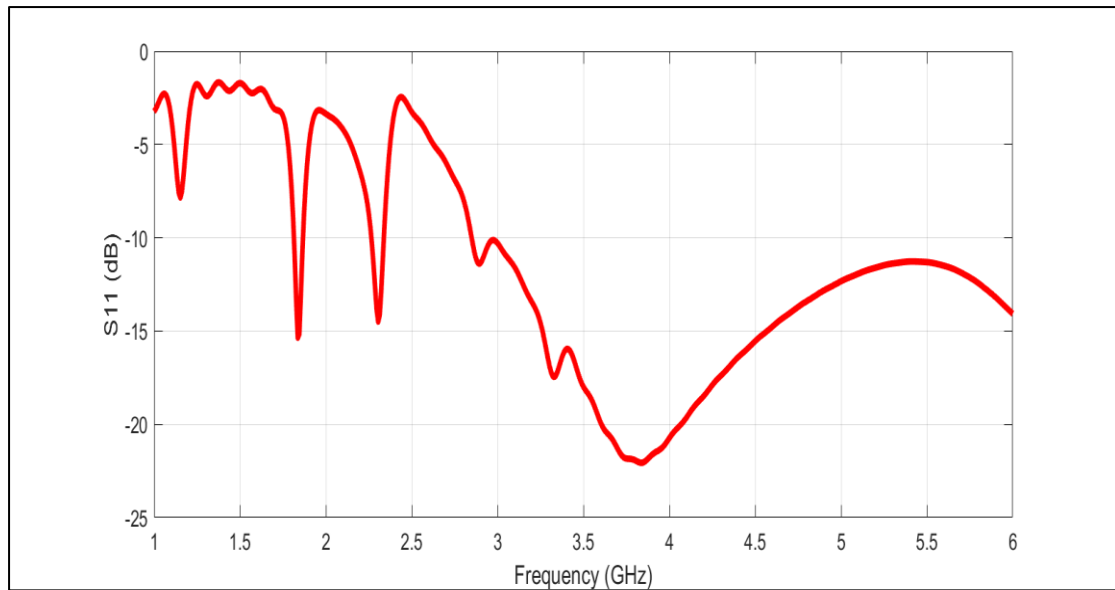


Fig.4.29: Simulated S11 for Antenna 6 (Hexagonal ring fractal antenna).

Fig.4.30 shows the antenna's 3D radiation pattern at 2.4 GHz. The antenna features have a directivity of 2.966 dBi. The ratio of the antenna radiation intensity in a given direction to radiation intensity that would be achieved if the power absorbed by the antenna were radiated isotropically is known as the antenna's IEEE gain.

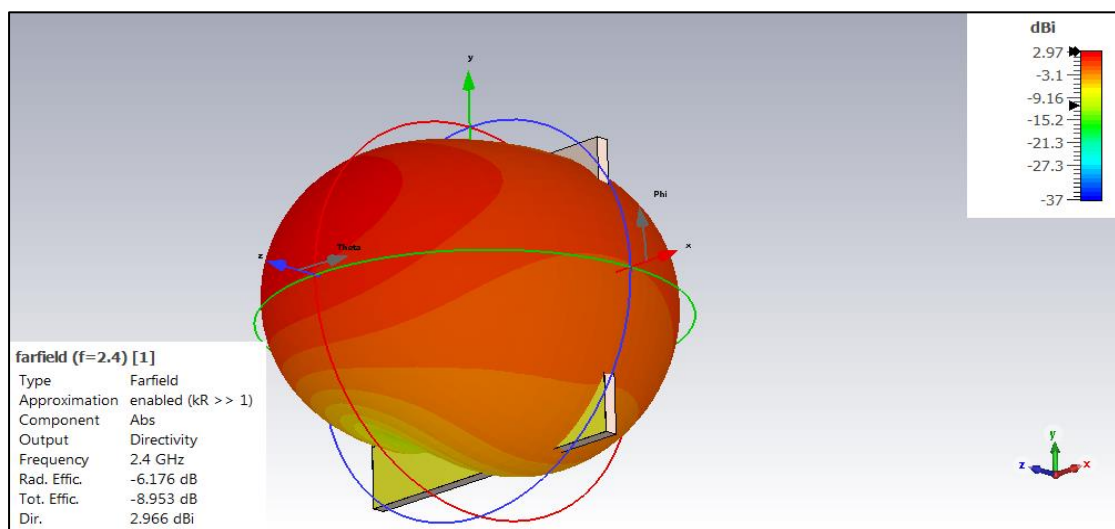


Fig.4.30: Simulated 3D radiation pattern at 2.4 GHz for Antenna 6.

Fig.4.31 depicts the 2D (polar) radiation pattern of antenna at 2.4 GHz. The main lobe magnitude has 2.6 dBi and the main lobe direction is 24.0

Fig.4.33 depicts the 2D (polar) radiation pattern of Antenna 6 at 3.6 GHz. the main lobe magnitude has of 2.8 dBi and the main lobe direction is 173.0 degrees. The side lobe level with angular width is 77.5 degrees. A polar map of the radiation pattern of the compact size antenna at 3.6 GHz reveals principal lob's magnitude to be 2.8 dBi at this frequency.

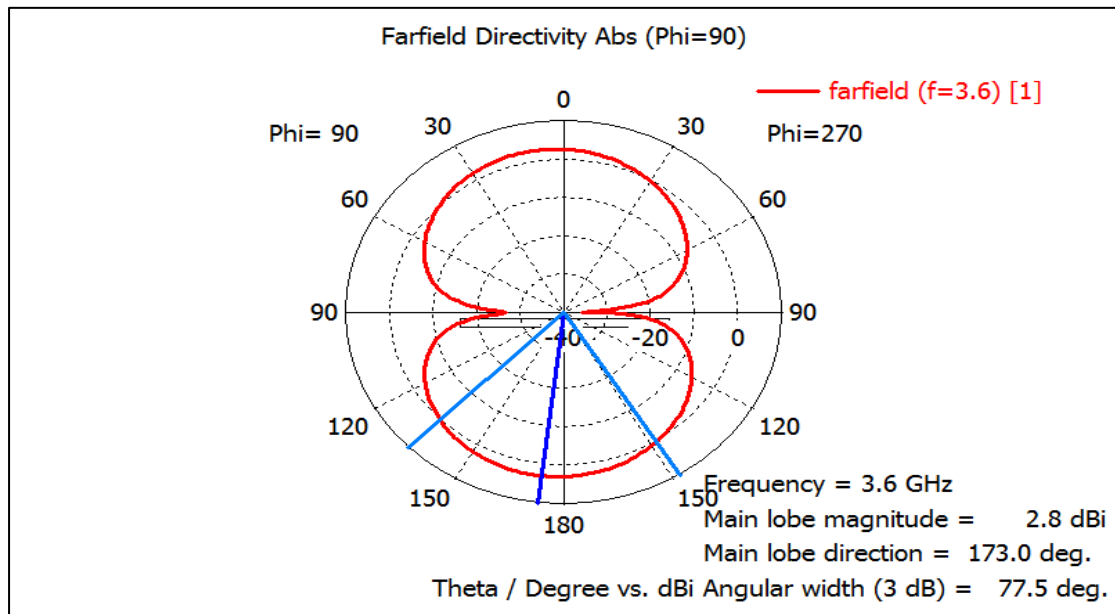


Fig.4.33: Simulated 2D radiation pattern at 3.6 GHz for Antenna 6.

Finally, the radiation pattern was plotted at 5 GHz. Fig.4.34 shows the antenna's 3D radiation pattern at 5 GHz where the recorded directivity was 4.343 dBi.

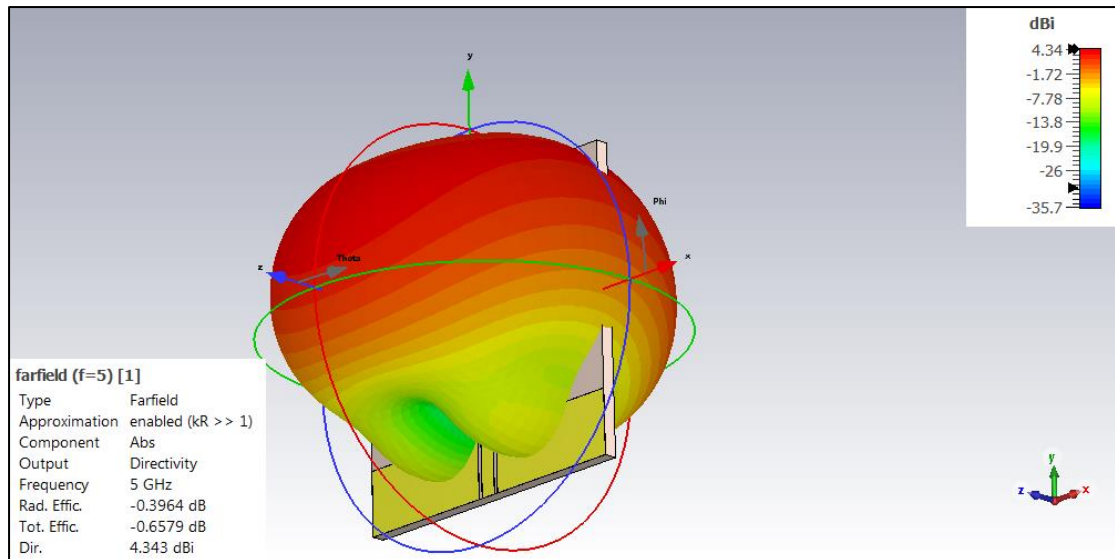


Fig.4.34: Simulated 3D radiation pattern at 5 GHz for Antenna 6.

Fig.4.35 depicts the 2D (polar) radiation pattern of antenna 6 at 5 GHz. the main lobe magnitude has 4.35 dBi and the main lobe direction is 156.0 degrees. The side lobe level with angular width is 62.3 degrees. A polar map of the radiation pattern of the compact size antenna at 5 GHz reveals principal lob's magnitude to be 4.35 dBi at this frequency.

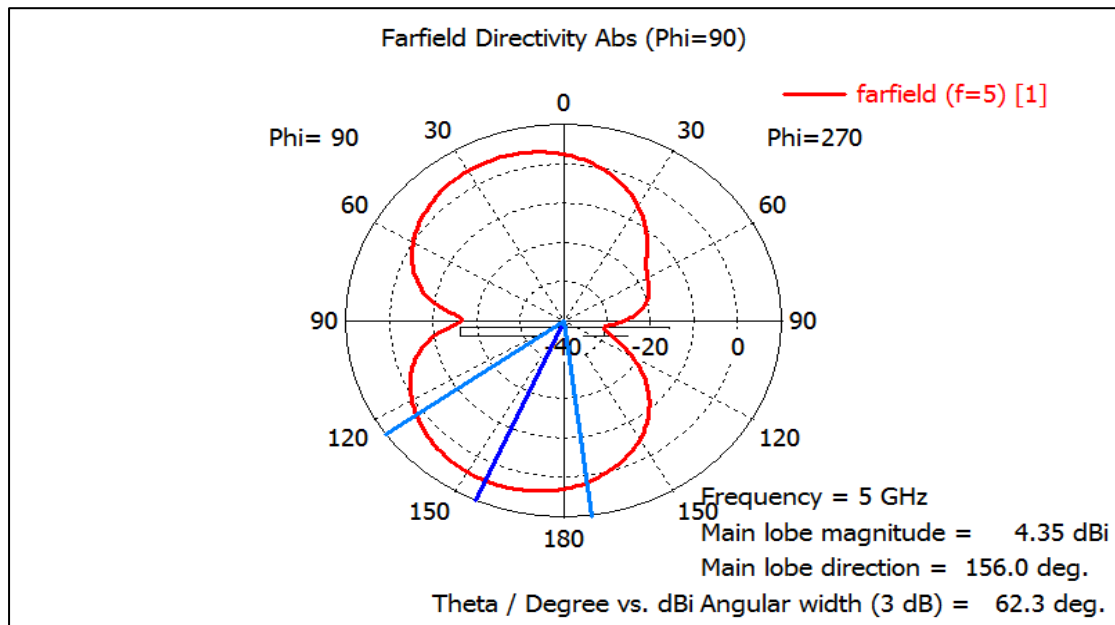


Fig.4.35: Simulated 2D radiation pattern at 5 GHz for Antenna 6.

4.2.7 Antenna 7 of circular ring patch fractal antenna

The design and simulation procedure of this antenna is similar to the hexagonal ring antenna. It starts with a circular patch antenna as shown in Fig.4.36. The radius of the circular patch was varied from 11.49 mm to 15.49 mm to study the impact of the patch size on the antenna performance. The simulation results of the S-parameters are depicted in Fig.4.37.

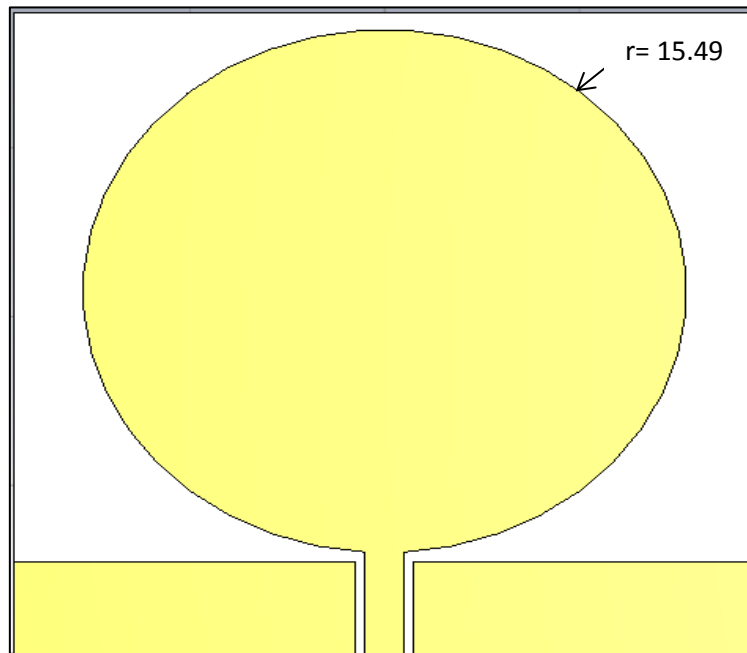


Fig.4.36: Circular patch without slot antenna

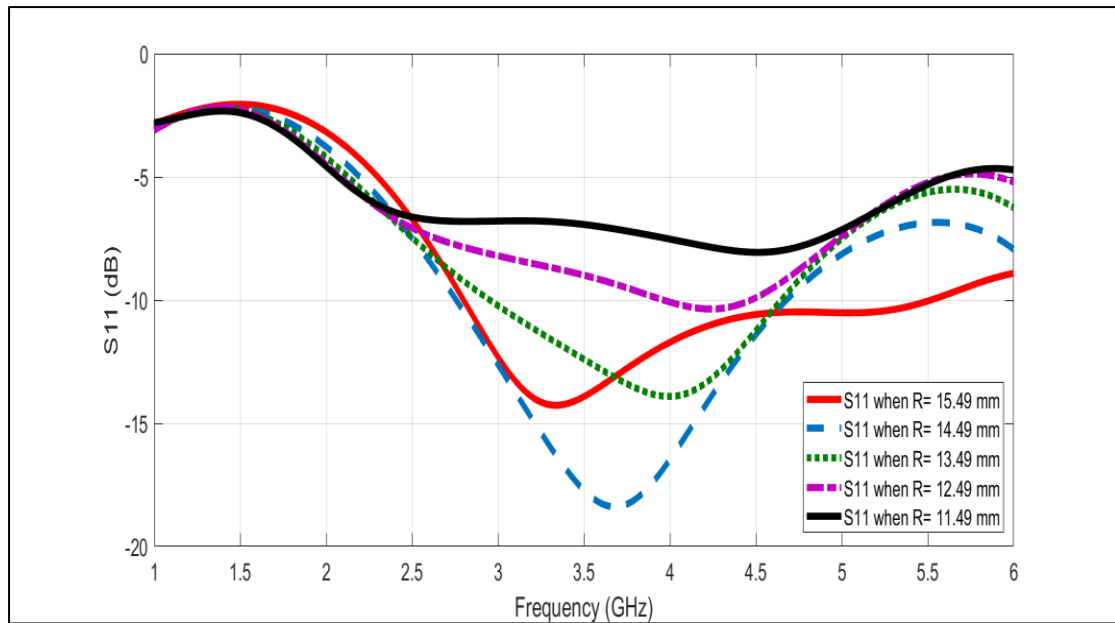


Fig.4.37: Simulated S11 versus frequency for Circular patch without slot antenna.

Fig.4.37 reveals that the best performance in terms of reflection characteristics was achieved at patch radius of 15.49 mm with S11 is equal to -18 at the resonant frequency of 3.6 GHz. The patch is now converted into ring antenna with same radius value (i.e. 15.49 mm) as illustrated in Fig. 4.38. The simulated S11 of the circular ring antenna is shown in Fig. 4.39.

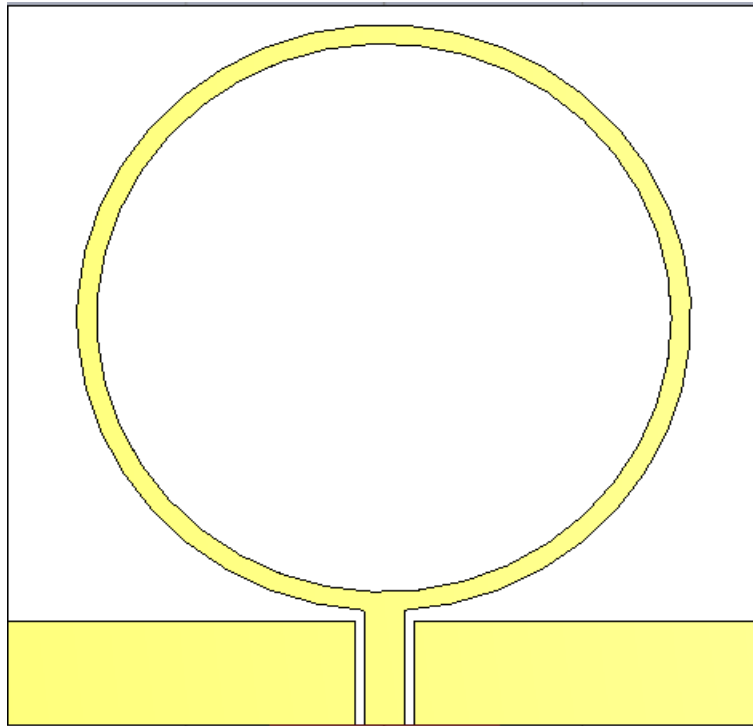


Fig.4.38: Circular ring patch.

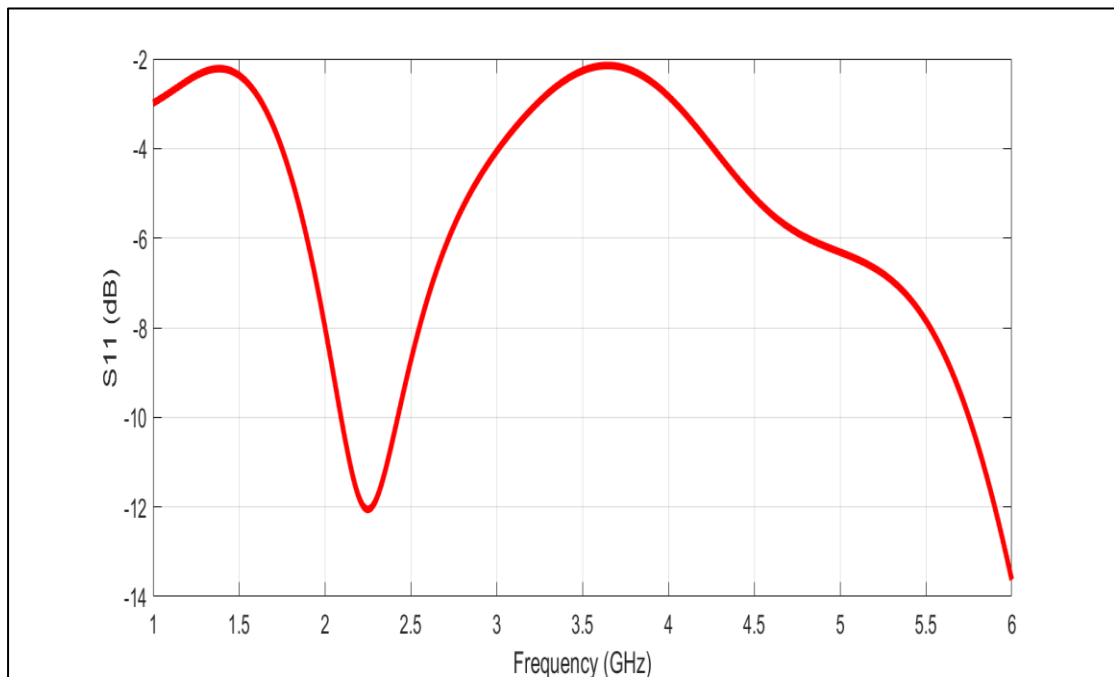


Fig.4.39: Simulated S11 versus frequency for circular ring patch.

Again, the structure of the circular ring antenna alone was not enough to improve the antenna performance. Thus, a new fractal geometry is proposed by replicating the circular ring many times but with smaller

radius as shown in Fig. 4.40. Table 4.6 displays the geometrical details of the proposed fractal antenna.

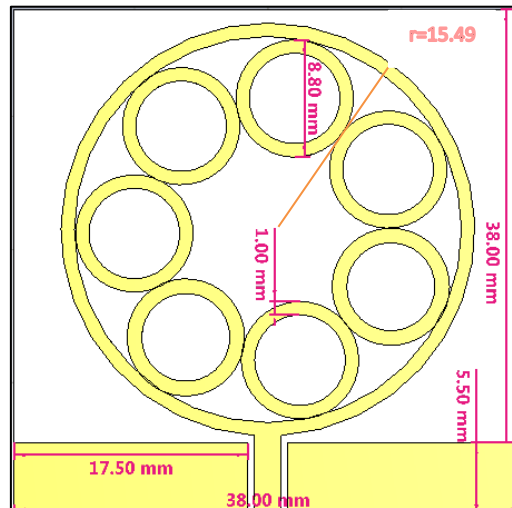


Fig.4.40: Circular ring fractal antenna with slot with all dimensions in mm.

Table 4.6: Geometrical details of Antenna 7.

Name	Value
Width of substrate (W_s)	38
Length of substrate (L_s)	38
Radius of circle (patch= r_1)	15.49
Radius of circle (patch= r_2)	4.4
Width of ground plane(W_g)	17.5
Length of ground plane(L_g)	5.5
Width of feeding line (W_f)	2
Thickness of substrate (h_s)	1.645
Dielectric constant of substrate ϵ_r	4.3
Thickness of copper (h_t)	0.035

The simulated S-parameters of the circular fractal ring antenna is shown in Fig.4.41. It is noticed that the designed antenna exhibits a dual band performance with two main bands at 2.5 and 4 GHz. It is also observed

that the second band is very wide so that it covers a wide range of communication systems, which makes this antenna preferable in energy harvesting applications. And the Bandwidth (BW)= $f_H - f_L = 300$ MHz and 1.8 GHz

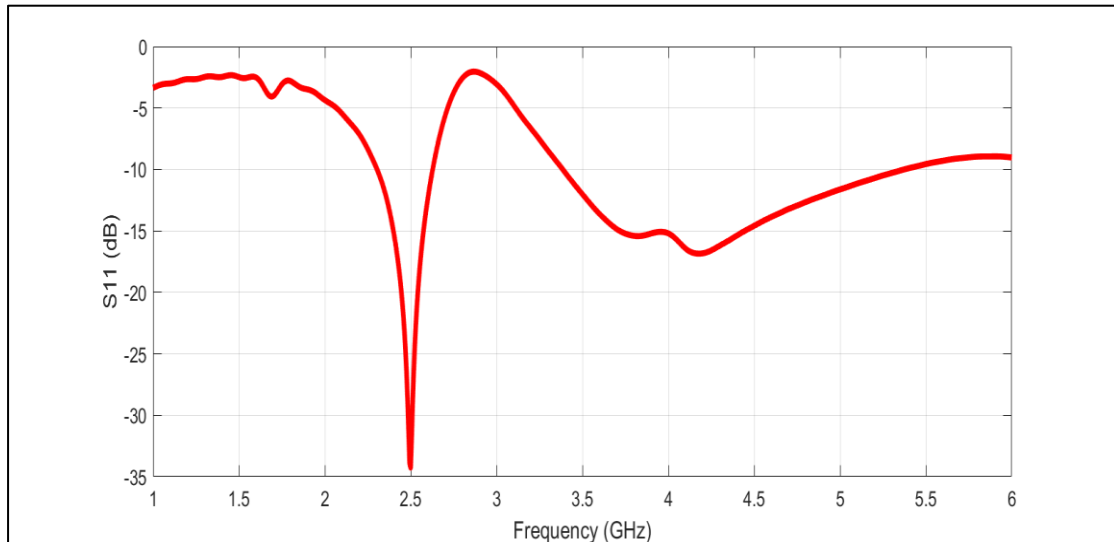


Fig.4.41: simulated S11 for Antenna 7 (Circular ring fractal antenna).

Fig.4.42 shows the antenna's 3D radiation pattern at 2.4 GHz. The antenna exhibits an omnidirectional radiation characteristics and has a directivity of 2.58 dBi.

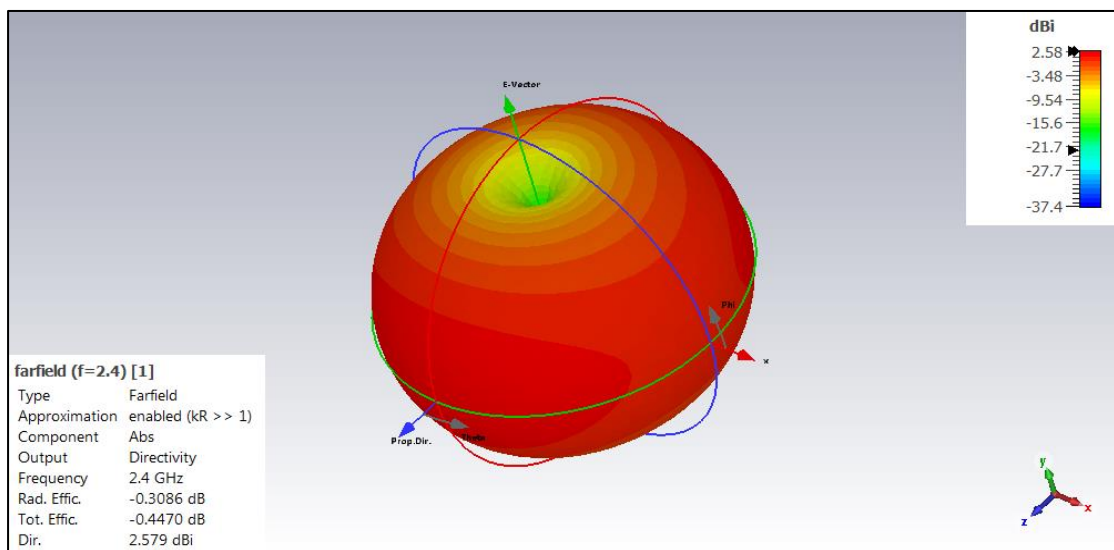


Fig.4.42: Simulated 3D radiation pattern at 2.4 GHz for Antenna 7.

The 2D (polar) radiation pattern of the designed circular fractal antenna at 2.4 GHz is depicted in Fig.4.43. The main lobe magnitude has 1.16 dBi and the main lobe direction is at 176.0 degrees. The side lobe level with angular width is 93.9 degrees.

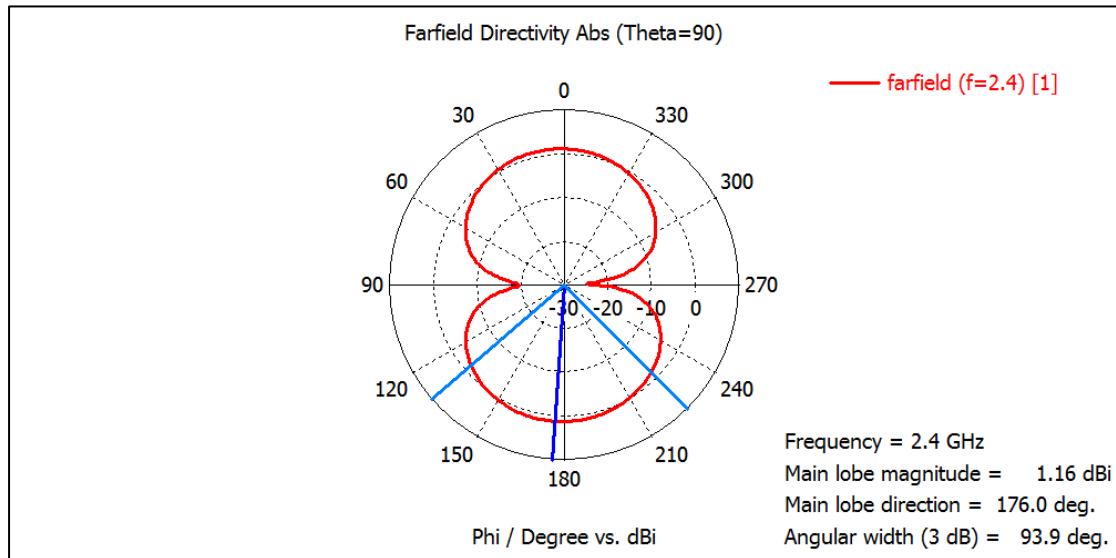


Fig.4.43: Simulated 2D radiation pattern at 2.4 GHz for Antenna 7.

The antenna's 3D radiation pattern at 3.6 GHz is shown in Fig.4.44, where the antenna has a directivity of 2.855 dBi at this frequency band.

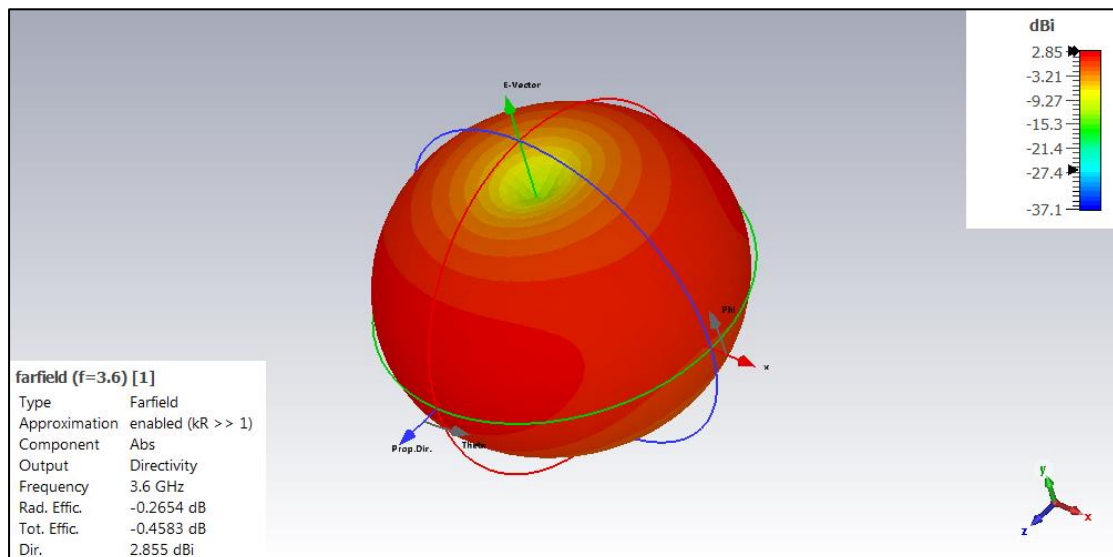


Fig.4.44: Simulated 3D radiation pattern at 3.6 GHz for Antenna 7.

Fig.4.45 below depicts the 2D radiation pattern of the designed circular fractal antenna at 3.6 GHz. The designed antenna has almost omnidirectional radiation pattern, which is highly preferable in this application.

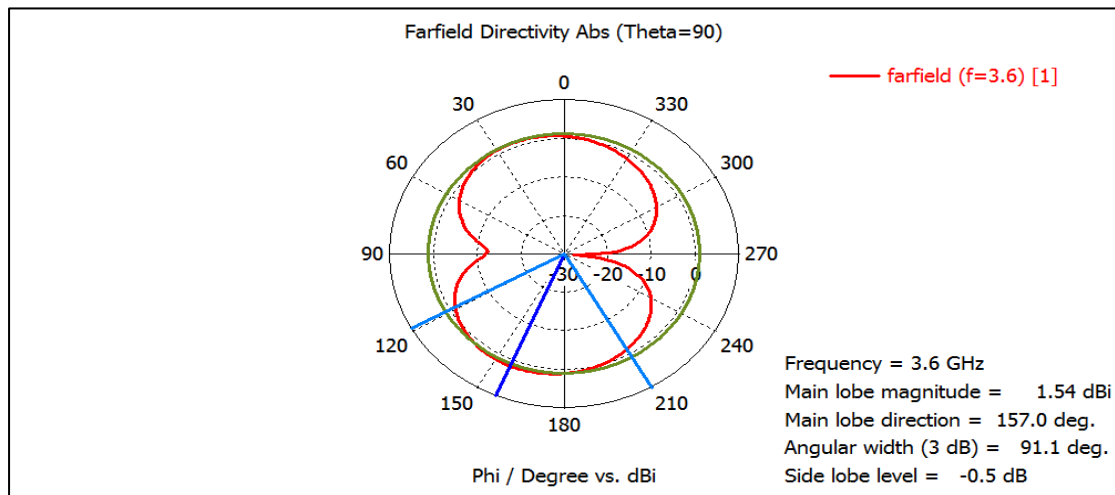


Fig.4.45: Simulated 2D radiation pattern at 3.6 GHz for Antenna 7.

Fig.4.46 shows the antenna's 3D radiation pattern at 5 GHz, where the antenna achieved higher directivity (4.707 dBi) compared with the lower frequency bands. The 2D radiation pattern of the designed circular fractal antenna at 5 GHz is illustrated in Fig. 4.47.

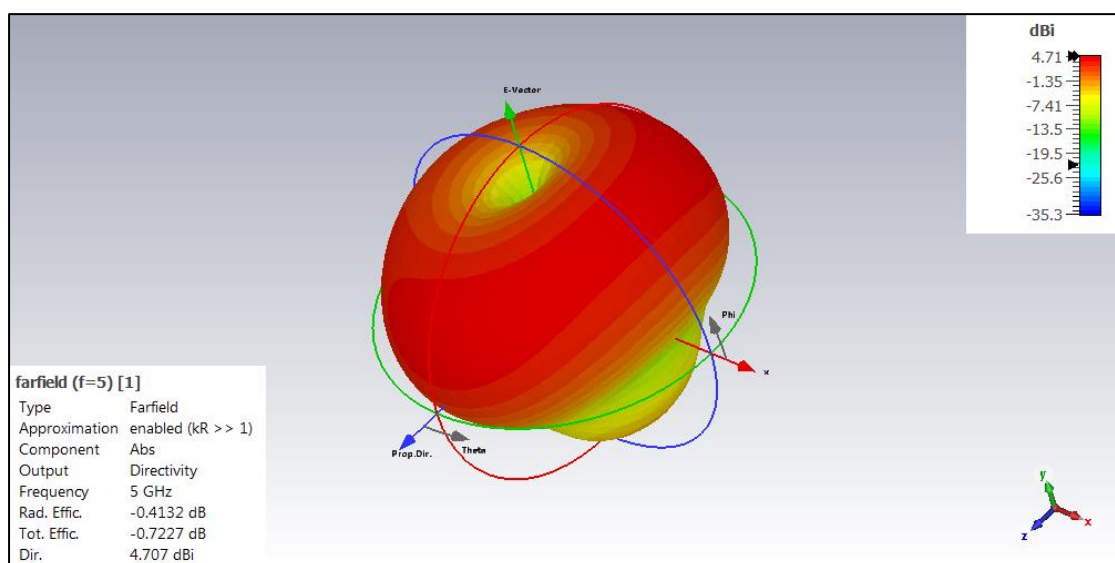


Fig.4.46: Simulated 3D radiation pattern at 5 GHz for Antenna 7.

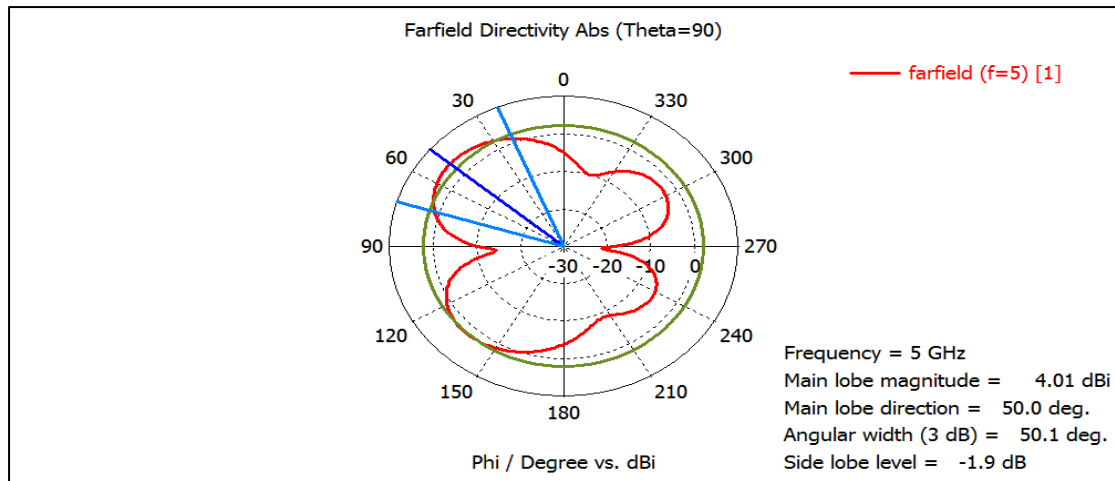


Fig.4.47: Simulated 2D radiation pattern at 5 GHz for Antenna 7.

4.3 Fabrication and Experimental Validation

The two fractal antennas (hexagonal and circular rings) are fabricated using PCB technology on a FR-4 substrate with dielectric constant of 4.3 and thickness of 1.6 mm. Fig.4.48 shows photographs of the manufactured hexagonal and circular ring fractal antennas. SMA connector is attached to each antenna for measurement purposes. Vector Network Analyzer is used to measure the S11 of the fabricated antennas. Fig.4.49 shows the experimental setup used to measure the S-parameters.

The comparison between the measured and simulated S11 for the hexagonal and circular fractal antennas are depicted in Figs. 4.50 and 4.51, respectively. It can be clearly seen from the S11 figures that there is a good agreement between the measured and simulated results for both antennas.

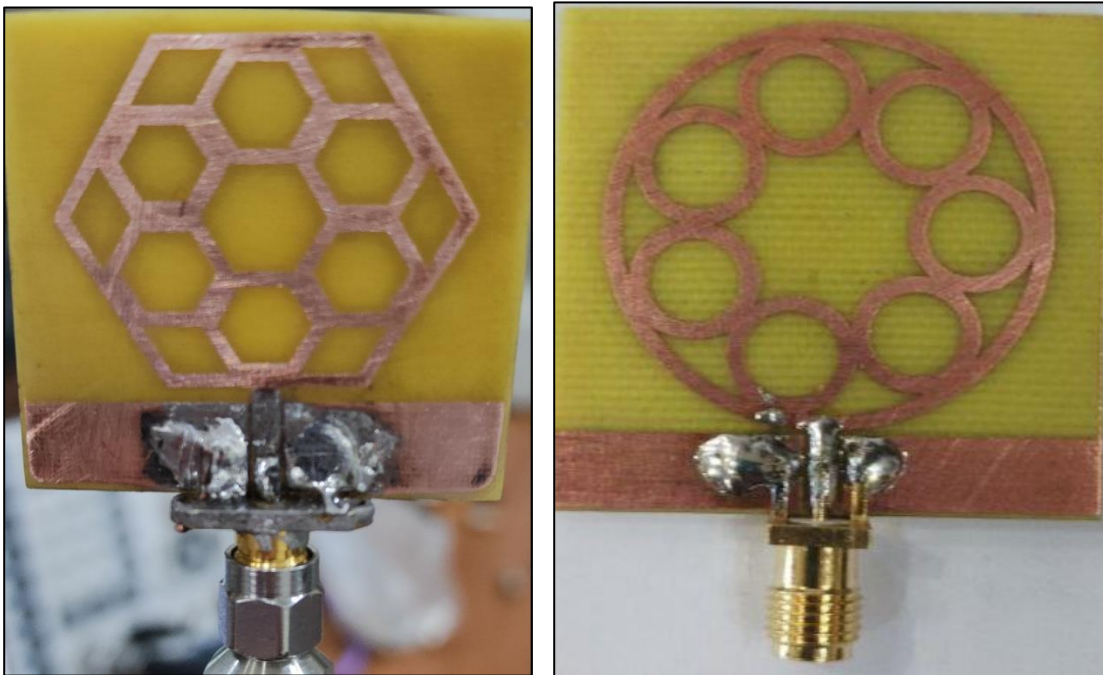


Fig.4.48: Photographs of the fabricated hexagonal and circular fractal antennas.

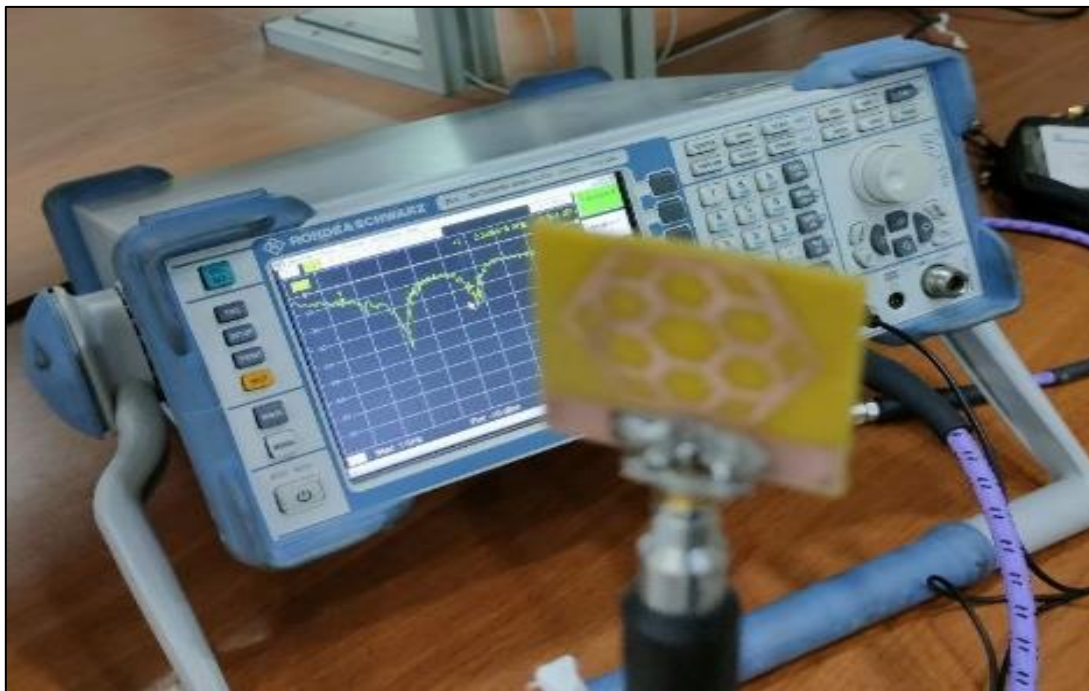


Fig.4.49: Shows the experimental setup used to measure the S-parameters for the fabricated antenna.

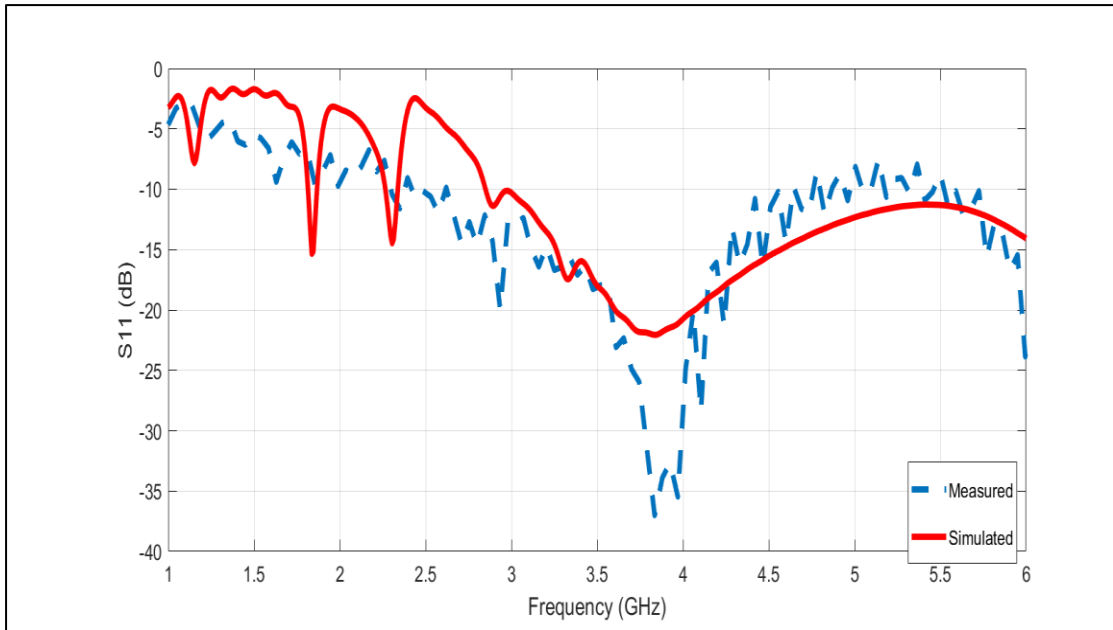


Fig.4.50: Measured and simulated S11 for the hexagonal ring fractal antenna.

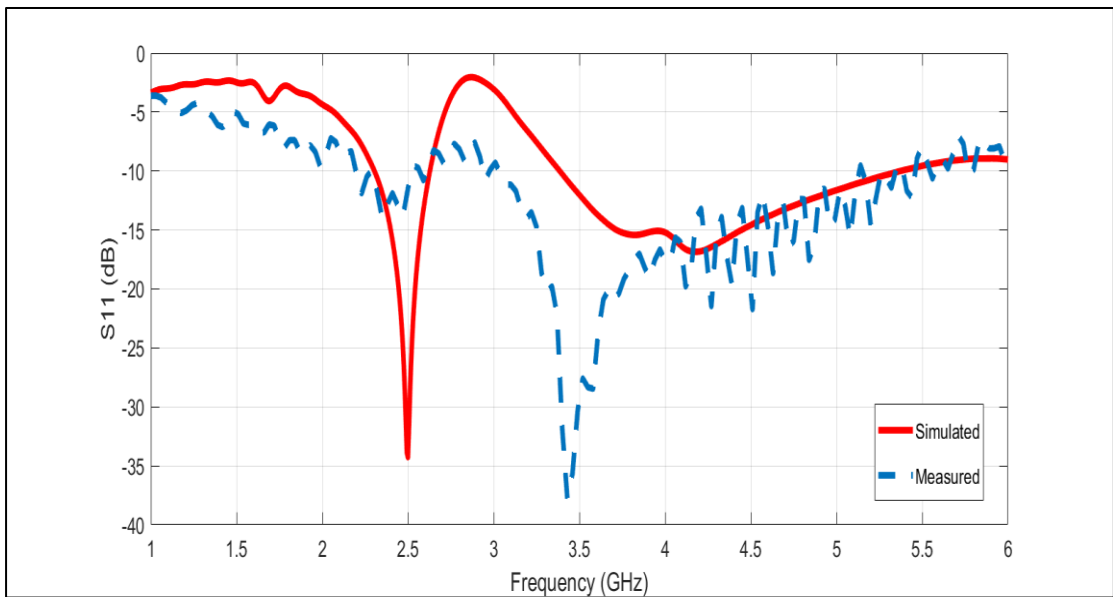


Fig.4.51: Measured and simulated S11 for the circular ring fractal antenna.

CHAPTER FIVE

CONCLUSIONS AND FUTURE WORKS

5.1 Conclusions

In this work, a voltage doubler rectifier circuit for energy harvesting applications was examined and simulated using Advanced Design System (ADS) software at the frequency bands of 2.4, 3.6, 5 GHz. The rectifier was designed and simulated using FR-4 substrate. In order to achieve maximum power transfer between the source (antenna) and the rectifier circuit, a proper matching network must be placed in between them. To this end, two types of matching networks were designed: LC-Circuit and the microstrip Transmission Lines (TL). The impact of input power on the output voltage and efficiency was investigated at different frequency band for the two types of the matching networks. The results showed that the total conversion efficiency of around 45% was achieved with an output DC voltage of 8 V at 2.4 GHz.

In the second part of this thesis, the role of the antenna in the rectifier systems was also investigated. Since the rectifier in this work is dedicated for energy harvesting systems, it is necessary to study the feasibility of designing tunable multiband antennas. Thus, slotted rectangular patch antennas is designed, simulated and the dimensions and location of slots were examined. The results showed that the multiband performance of the slotted antenna can be engineered by controlling the characteristics of the slot. Moreover, in this work, two fractal ring antennas (hexagonal and circular) were designed, simulated and implemented. Both antennas have been designed to operate at multiple frequencies including 2.4, 3.6, 5 GHz, covering important Wi-Fi and Bluetooth bands. They have advantages over traditional rectangular patch antennas as the fractal slot creates additional resonant frequencies in a compact size. Hexagonal

patch antennas generally offer better performance in terms of bandwidth, gain and efficiency compared to circular patch antennas, especially at higher frequencies. However, circular patch antennas are easier to design and fabricate.

In summary, for a multi-band antenna operating at sub-6 GHz systems, a hexagonal patch fractal ring antenna will likely provide the best performance in terms of bandwidth, gain and efficiency. However, a circular patch fractal slot antenna may be a good alternative if ease of design and fabrication are priorities. The choice of antenna geometry depends on the specific requirements and priorities of the given application. The multiband performance of these fractal slot antennas makes them suitable candidates for applications requiring operation in multiple Wi-Fi and Bluetooth bands, such as Internet of Things devices and wireless routers. In order to minimize the size of microstrip Transmission Lines (TL), the overall components have been modified. The aim is to achieve compact design with the highest conversion efficiency. The proposed rectifier in this work were designed to function with antennas and was optimized for a reference impedance of 50Ω . Finally, the designed rectifier circuit and fractal antennas were fabricated using PCB technology and there was a good and acceptable agreement between the simulated and measured results.

The following conclusions can be drawn out of the obtained results of this thesis:

- 1- Achieving high AC to DC conversion efficiency equal to 45% can be achieved using a voltage doubler rectifier.

2- Input power level less than 25 dBm and frequency range below 6 GHz are handled by Schottky diodes of the series HSMS-2820. For energy harvesting applications at 2.4, 3.6 and 5 GHz, this series is quite useful.

3- By combining all of components, including the LC-Circuit and Transmission Lines (TL) ideally, the rectifier circuit was reduced to a relatively small size. The developed rectifier circuit may be used successfully to charge batteries of industrial and medical applications.

4- Since there was a good agreement between the simulated and measured results, the design procedure for both rectifier and antenna using Advanced Design System (ADS) and Computer Simulation Technology (CST) is valid and suitable to other designs.

5. 2 Future works

Multiband rectennas have a lot of potential for future research and development. Here are some possible future works for this type of rectennas:

1. Optimization of the antenna and rectifier circuit design: The performance of the multiband rectenna can be improved by optimizing the design of the antenna and the rectifier circuit. This can involve using advanced simulation tools and optimization algorithms to find the best possible configuration of the rectenna.

2. Integration with energy storage devices: Multiband rectennas can be integrated with energy storage devices, such as batteries or supercapacitors, to store the harvested energy. This can improve the overall efficiency of the rectenna system and make it more practical for real-world applications.

3. Investigation of new materials and fabrication techniques: The use of new materials and fabrication techniques can enhance the performance and reliability of the multiband rectenna. For example, the use of metamaterials or nanomaterials can lead to improved efficiency and bandwidth.

4. Study of the rectenna's performance under different environmental conditions: The performance of the multiband rectenna can vary under different environmental conditions, such as temperature, humidity, and air pressure. Therefore, it is important to study how the rectenna performs under these conditions and how it can be optimized for different environments.

5. Development of new applications: Multiband rectennas can be used in a wide range of applications, such as wireless power transfer, energy harvesting from radio frequency sources, and sensor networks. Therefore, there is a need for research to explore new applications and to develop specialized rectenna designs for these applications.

References

- [1] W.C. Brown, "The history of power transmission by radio waves," IEEE Transactions on Microwave Theory and Techniques, vol. 32, no. 9, pp. 1230–1242, 1984.
- [2] S. Sudevalayam, P. Kulkarni, "Energy harvesting sensor nodes: survey and implications," IEEE Communications Surveys & Tutorials, vol. 13, no. 3, pp. 443–461, 2011.
- [3] C.R. Valenta, G.D. Durgin, "Harvesting wireless power: survey of energy-harvester conversion efficiency in far-field, wireless power transfer systems," IEEE Microwave Magazine, vol. 15, no. 4, pp. 108–120, 2014.
- [4] Derbal, M. C., Nedil, M. "A High Gain Dual Band Rectenna for RF Energy Harvesting Applications", Progress In Electromagnetics Research Letters,90,pp.29–36,2020.
- [5] Le, M. T., Tran, Q. C., Le, A. T., Minh, D. "A Multidirectional Triple-Band Rectenna for Outdoor RF Energy Harvesting from GSM900/GSM1800/UMTS2100 Toward Self-Powered IoT Devices", Progress in Electromagnetics Research M, 104, pp. 1–12, 2021.
- [6] Singh, N., Kanaujia, B. K., Beg, M. T., Khan, T., Kumar, S. "A dual polarized multiband rectenna for RF energy harvesting", AEU - International Journal of Electronics and Communications, 93, pp. 123–131, 2018.
- [7] Bakytbekov, A., Nguyen, T. Q., Huynh, C., Salama, K. N., Shamim, A. "Fully printed 3D cube-shaped multiband fractal rectenna for ambient RF energy harvesting", Nano Energy, 53, pp. 587–595, 2018.

- [8] Sabaawi, Ahmed MA, Qusai H. Sultan, and Tareq A. Najm. "Design and Implementation of Multi-Band Fractal Slot Antennas for Energy Harvesting Applications." *Periodica Polytechnica Electrical Engineering and Computer Science* 66, no. 3 (2022): 253-264.
- [9] Sabaawi, Ahmed MA, Qusai H. Sultan, and Mohammed S. Salim. "Design of Multiband Fractal Antenna for Energy Harvesting Applications." In *2021 12th International Renewable Energy Congress (IREC)*, pp. 1-4. IEEE, 2021.
- [10] H. Nishimoto, Y. Kawahara and T. Asami, "Prototype implementation of ambient RF energy harvesting wireless sensor networks," *2010 IEEE Sensors*, Kona, HI, 2010, pp. 1282-1287.
- [11] R. J. Vyas, B. B. Cook, Y. Kawahara and M. M. Tentzeris, "EWEHP: A Batteryless Embedded Sensor-Platform Wirelessly Powered From Ambient Digital-TV Signals," in *IEEE Transactions on Microwave Theory and Techniques*, vol. 61, no. 6, pp. 2491-2505, June 2013.
- [12] R. Shigeta et al., "Ambient RF Energy Harvesting Sensor Device With Capacitor-Leakage-Aware Duty Cycle Control," in *IEEE Sensors Journal*, vol. 13, no. 8, pp. 2973-2983, Aug. 2013.
- [13] A. N. Parks, A. P. Sample, Y. Zhao and J. R. Smith, "A wireless sensing platform utilizing ambient RF energy," *2013 IEEE Topical Conference on Power Amplifiers for Wireless and Radio Applications*, Santa Clara, CA, 2013, pp. 160-162.
- [14] M. Pinuela, P. D. Mitcheson and S. Lucyszyn, "Ambient RF Energy Harvesting in Urban and Semi-Urban Environments," in *IEEE Transactions on Microwave Theory and Techniques*, vol. 61, no. 7, pp. 2715-2726, July 2013.

- [15] S. Kim, "RF Energy Harvesting techniques for wirelessly Powered devices," School of Integrated Technology and Yonsei Institute of Convergence Technology, Yonsei University, Songdo, Incheon. 2017, 406-840, Korea.
- [16] Tran, L.-G.; Cha, H.-K.; Park, W.-T. RF power harvesting: A review on designing methodologies and applications. *Micro Nano Syst. Lett.* 2017, 5, 14
- [17] Heikkinen, j., Kivikoski, M. . Low-profile circularly polarized rectifying antenna for wireless power transmission at 5.8 GHz. *IEEE Microwave and Wireless Components Letters.* 2004, 14(4), 162–164.
- [18] Yo, T. C., Lee, C. M., Hsu, C. M., & Luo, C. H. Compact circularly polarized rectenna with unbalanced circular slots. *IEEE Transactions on Antennas and Propagation.* 2008, 56(3), 882–886.
- [19] Gao, Y. Y., Yang, X. X., Jiang, C., & Zhou, J. Y. A circularly polarized rectenna with low profile for wireless power transmission. *Progress In Electromagnetics Research Letters.* 2010, 13, 41–49.
- [20] Takhedmit, H., Cirio, L., Bellal, S., Delcroix, D., & Picon, O. Compact and efficient 2.45 GHz circularly polarised shorted ring-slot rectenna. *Electronics Letters.* 2012, 48(5), 253–254.
- [21] Masotti, D., Costanzo, A., Prete, M. D., & Rizzoli, V. Genetic-based design of a tetra-band high-efficiency radio-frequency energy system. *IET Microwaves, Antennas & Propagation.* 2013, 7(15), 1254–1263.
- [22] Valenta, C. R., & Durgin, G. D. Harvesting wireless power: survey of energyharvester conversion efficiency in far-field, wireless power transfer systems. *IEEE Microwave Magazine.* 2014, 15(4), 108–120.
- [23] Niotaki, K., Georgiadis, A., Collado, A., & Vardakas, J. S. Dual-band resistance compression networks for improved rectifier

performance. *IEEE Transactions on Microwave Theory and Techniques*. 2015, 62(12), 3512–3521.

[24] Song, C., Houg, Y., Zhou, J., Zhang, J., Yuan, S., & Carter, P. A high efficiency broadband rectenna for ambient wireless energy harvesting. *IEEE Transactions on Antennas and Propagation*. 2015, 63(8), 3486–3495.

[25] Chuma, E. L., Rodríguez, L. d. I. T., Iano, Y., Roger, L. L. B., & Sanchez-Soriano, M. A. Compact rectenna based on a fractal geometry with a high conversion energy efficiency per area. *IET Microwaves, Antennas & Propagation*. 2018, 12(2), 173–178.

[26] Singh, N., Kanaujia, B. K., Beg, M. T., Mainuddin, Khan, T., & Kumar, S. A dual polarized multiband rectenna for RF energy harvesting. *AEU - International Journal of Electronics and Communications*. 2018, 93, 123–131.

[27] Elwi, T. A. Novel UWB printed metamaterial microstrip antenna based organic substrates for RF-energy harvesting applications. *AEU - International Journal of Electronics and Communications*. 2019, 101, 44–53.

[28] Zheng, X., Song, Y., Li, J., Li, Y., & Wu, W. A multiband RF energy harvesting system for wireless sensor networks. *IEEE Transactions on Microwave Theory and Techniques*. 2019, 67(6), 2444–2455. doi: 10.1109/TMTT.2019.2906447.

[29] Zhao, S., Huang, Y., Wu, Z., & Zhang, Y. A multiband RF energy harvesting system with a broadband antenna and a reconfigurable matching network. *IEEE Transactions on Circuits and Systems II: Express Briefs*. 2019, 66(1), 26–30. doi: 10.1109/TCSII.2018.2846099.

[30] Zhang, S., Yang, X., Li, Z., & Li, Y. A multiband RF energy harvesting system with a broadband antenna and a reconfigurable

matching network for wireless sensor networks. *IEEE Access*. 2019, 7, 111388-111396. doi: 10.1109/ACCESS.2019.2938626.

[31] S. R. Khan, S. K. Pavuluri, G. Cummins, and M. P. Y. Desmulliez, "Wireless Power Transfer Techniques for Implantable Medical Devices: A Review," *Sensors*, vol. 20, no. 12, p. 3487, Jun. 2020, doi: 10.3390/s20123487.[Online].Available:<http://dx.doi.org/10.3390/s20123487>.

[32] Alshehri, S., Alshebeili, S., Almazyad, A., & Almazyad, S. A multiband RF energy harvesting system for wireless sensor networks. *IEEE Access*. 2020, 8, 152659-152667. doi: 10.1109/ACCESS.2020.3015455.

[33] Yang, J., Li, M., Zhang, H., Chen, Y., & Wu, Q. A multiband RF energy harvester with a broadband antenna and a reconfigurable matching network for wireless sensor networks. *Sensors*. 2021, 21(4), 1237. doi: 10.3390/s21041237.

[34] Pandey, R., A. K. Shankhwar, and A. Singh, "An improved conversion efficiency of 1.975 to 4.744 GHz rectenna for wireless sensor applications," *Progress In Electromagnetics Research C*, Vol. 109, 217{225, 2021.

[35] Lin, W. and R. W. Ziolkowski, "Wirelessly powered internet-of-things sensors facilitated by an electrically small Egyptian axe dipole rectenna," *Asia-Pacific Microwave Conference Proceedings, APMC*, 891{892, Dec. 2019, doi: 10.1109/APMC46564.2019.9038497.

[36] Okba, A., A. Takacs, and H. Aubert, "Compact at dipole rectenna for IoT applications," *Progress In Electromagnetics Research C*, Vol. 87, 39{49, 2018.

- [37] Carvalho, A., N. Carvalho, P. Pinho, and R. Goncalves, "Wireless power transmission and its applications for powering Drones," 8th Congress of the Portuguese Committee of URSI, 2014.
- [38] Takhedmit, H., L. Cirio, F. Costa, and O. Picon, "Transparent rectenna and rectenna array for RF energy harvesting at 2.45 GHz," 8th European Conference on Antennas and Propagation, *EuCAP 2014*, 2970{2972, 2014, doi: 10.1109/EuCAP.2014.6902451.
- [39] Takhedmit, H., Z. Saddi, and L. Cirio, "A high-performance circularly-polarized rectenna for wireless energy harvesting at 1.85 and 2.45 GHz frequency bands," *Progress In Electromagnetics Research C*, Vol. 79, 89{100, 2017.
- [40] Lu, P., X. S. Yang, J. L. Li, and B. Z. Wang, "A compact frequency reconfigurable rectenna for 5.2- and 5.8-GHz wireless power transmission," *IEEE Trans. Power Electron.*, Vol. 30, No. 11, 6006{6010, Nov. 2015, doi: 10.1109/TPEL.2014.2379588.
- [41] Li, X., L. Yang, and L. Huang, "Novel design of 2.45-GHz rectenna element and array for wireless power transmission," *IEEE Access*, Vol. 7, 28356{28362, 2019, doi: 10.1109/ACCESS.2019.2900329.
- [42] Palazzi, V., et al., "Design of a ultra-compact low-power rectenna in paper substrate for energy harvesting in the Wi-Fi band," 2016 IEEE Wireless Power Transfer Conference (WPTC), Aveiro, Portugal, Jun. 2016, doi: 10.1109/WPT.2016.7498823.
- [43] Sun, H., Y. X. Guo, M. He, and Z. Zhong, "Design of a high-efficiency 2.45-GHz rectenna for low-input-power energy harvesting," *IEEE Antennas Wirel. Propag. Lett.*, Vol. 11, 929{932, 2012, doi: 10.1109/LAWP.2012.2212232.
- [44] Olgun, U., C. Chen, and J. L. Volakis, "Investigation of rectenna array configurations for enhanced rf power harvesting," *IEEE Antennas*

Wirel. Propag. Lett., Vol. 10, 262{265, 2011, doi:10.1109/LAWP.2011.2136371.

[45] Niotaki, K., S. Kim, S. Jeong, A. Collado, A. Georgiadis, and M. M. Tentzeris, "A compact dual-band rectenna using slot-loaded dual band folded dipole antenna," IEEE Antennas Wirel. Propag. Lett., Vol. 12, 1634{1637, 2013, doi: 10.1109/LAWP.2013.2294200.

[46] Haboubi, W., H. Takhedmit, J.-D. Lan Sun Luk, S.-E. Adami, B. Allard, F. Costa, C. Vollaire, O. Picon, and L. Cirio, "An efficient dual-circularly polarized rectenna for RF energy harvesting in the 2.45 GHz ISM band," Progress In Electromagnetics Research, Vol. 148, 31{39, 2014.

[47] Bao, X., K. Yang, O. O'Conchubhair, and M. J. Ammann, "Differentially-fed omnidirectional circularly polarized patch antenna for RF energy harvesting," 2016 10th European Conference on Antennas and Propagation (EuCAP), Davos, Switzerland, May 2016, doi: 10.1109/EuCAP.2016.7481820.

[48] Cao, Y., W. Hong, L. Deng, S. Li, and L. Yin, "A 2.4 GHz circular polarization rectenna with harmonic suppression for microwave power transmission," Proceedings | 2016 IEEE International Conference on Internet of Things; IEEE Green Computing and Communications; IEEE Cyber, Physical, and Social Computing; IEEE Smart Data, iThings-GreenCom-CPSCoM-Smart Data 2016, 359{363, May 2017, doi: 10.1109/iThings-GreenCom-CPSCoM SmartData.2016.85.

[49] Huang, F. J., T. C. Yo, C. M. Lee, and C. H. Luo, "Design of circular polarization antenna with harmonic suppression for rectenna application," IEEE Antennas Wirel. Propag. Lett., Vol. 11, 592{595, 2012, doi: 10.1109/LAWP.2012.2201437.

[50] H. W. Cheng, T. C. Yu, and C. H. Luo, "Direct current driving impedance matching method for rectenna using medical implant

- communication service band for wireless battery charging," *IET Microwaves Antennas & Propagation*, vol. 7, pp. 277-282, Mar 19 2013.
- [51] Avago Technologies, "Schottky Diode Voltage Doubler," Application Note 956-4, 2010.
- [52] Avago Technologies, "HSMS-282x Surface Mount RF Schottky Barrier Diodes," Data Sheet, 2014.
- [53] P. Lipinski, "On charging the battery of an Implantable device," *Modern Problems of Radio Engineering, Telecommunications and Computer Science, Proceedings*, pp. 365-366, 2002.
- [54] C. R. Liu, Y. X. Guo, H. C. Sun, and S. Q. Xiao, "Design and Safety Considerations of an Implantable Rectenna for Far-Field Wireless Power Transfer," *IEEE Transactions on Antennas and Propagation*, vol. 62, pp. 5798-5806, Nov 2014.
- [55] R. Alrawashdeh, "Implantable antennas for biomedical applications," PhD thesis, University of Liverpool, 2015.
- [56] S. A. Kumar and T. Shanmuganatham, "Implantable CPW-fed Z-monopole antennas at 2.45 GHz ISM band for biomedical applications," *International Journal of Microwave and Wireless Technologies*, vol. 7, pp. 529-533, Oct 2015. 10.
- [57] S. A. Kumar, J. N. Sankar, D. Dileepan, and T. Shanmuganatham, "Design and Performances of Implantable CPW Fed Apollian Shaped Antenna at 2.45 GHz ISM Band for Biomedical Applications," *Transactions on Electrical and Electronic Materials*, vol. 16, pp. 250-253, Oct 25 2015.
- [58] H. Y. Lin, M. Takahashi, K. Saito, and K. Ito, "Design of Miniature Implantable Tag Antenna for Radio-Frequency Identification System at 2.45 GHz and Received Power Analysis," *IEICE Transactions on Communications*, vol. E97b, pp. 129-136, Jan 2014.

- [59] C. R. Liu, Y. X. Guo, and S. Q. Xiao, "Capacitively Loaded Circularly Polarized Implantable Patch Antenna for ISM Band Biomedical Applications," *IEEE Transactions on Antennas and Propagation*, vol. 62, pp. 2407-2417, May 2014.
- [60] H. Li, Y. X. Guo, and S. Q. Xiao, "Broadband circularly polarized implantable antenna for biomedical applications," *Electronics Letters*, vol. 52, pp. 504-505, April 2016.
- [61] R. Alrawashdeh, *Implantable Antennas for Biomedical Applications*, University of Liverpool, 2015.
- [62]. C.A. Balanis, *Antenna Theory*, 2nd edition. New York: John Wiley & Sons, Inc., 1997
- [63]. K.C Gupta, Ramesh Garg, Inder Bahl, Prakash Bhartia, *Microstrip lines and Slot lines*, Second Edition, Artech House INC, Boston: London, 1996, ISBN 0-89006-766-X
- [64] Mayborod DV (2012) Dualband circular disk microstrip antenna. In: *IEEE international on ultra-wideband and ultra-short impulse signals*, pp 161–163, Sep 2012
- [65] Balanis CA *Antenna theory and design*. 1992, 3 edn.

الملخص

تم تصميم المقومات في هذا العمل على أساس تقنية مضاعفة الجهد وتمت محاكاتها بواسطة برنامج نظام التصميم المتقدم (ADS). حصلت المقومات المصممة في هذا العمل على كفاءة تحويل من التردد اللاسلكي إلى تيار مستمر بمقدار حوالي ٤٥,٢٢% عند نطاق التردد ٢,٤ جيجا هرتز مع فولتية اخراج مستمرة تصل إلى ٢,٢ فولت. بالإضافة إلى ذلك، تبلغ الكفاءة المحققة حوالي ٢٩,٨٩% عند ٣,٦ جيجا هرتز مع فولتية اخراج مستمرة وصلت إلى ١ فولت وحوالي ٢٧% عند ٥ جيجا هرتز مع فولتية اخراج مستمرة تصل إلى ١,٧ فولت، وهو ما يكفي لتشغيل معظم الأجهزة و/أو شحن البطارية المزروعة. علاوة على ذلك، تم تصميم ومحاكاة وتنفيذ العديد من الهوائيات الكسورية Fractal متعددة النطاقات وعريضة الحزمة في هذا البحث باستخدام برنامج CST studio. تم تصميم هوائيين UWB لتغطي الترددات ٢,٤ جيجا هرتز و ٣,٦ جيجا هرتز و ٥ جيجا هرتز. تم تصميم الهوائيات بسطح أرضي جزئي في الجانب الأمامي من الهوائيات ويتم توصيل موصل SMA بمنفذ إدخال الهوائيات. ويسهل هذا التصميم دمج الهوائيات المقترحة مع المقومات لتشكيل هوائي تقويم لنظام WPT. هوائيات التقويم المصممة (مقوم + هوائي) تم تصنيعها باستخدام تقنية PCB. تم اختبار أداء النماذج الأولية المصنعة في المختبر و تمت مقارنة النتائج المقاسة مع نتائج المحاكاة وتبين أنه تم تحقيق توافق جيد ومقبول، مما يجعل تصميم المقوم والهوائي صالحا. وقد أكدت هذه التجارب بشكل كبير فائدة الهوائيات المقترحة في هذا العمل لإنتاج كمية كافية من الطاقة للعديد من الأجهزة والتطبيقات.

إقرار المشرف

نشهد بأن هذه الرسالة الموسومة (تصميم وتنفيذ هوائي تقويم متعدد النطاقات لحصد طاقة الترددات الراديوية المحيطة) تم اعدادها من قبل الطالب (عبد الله محمد عجيل حسين) تحت اشرافنا في قسم هندسة الالكترونيك / كلية هندسة الالكترونيات / جامعة نينوى، وهي جزء من متطلبات نيل شهادة الماجستير/علوم في اختصاص هندسة الالكترونيك.

التوقيع:

الاسم: أ. م. د احمد محمد احمد السبعاعي

التاريخ: ٢٠٢٣/١١/

إقرار المقوم اللغوي

اشهد بأنه قد تمت مراجعة هذه الرسالة من الناحية اللغوية وتصحيح ما ورد فيها من أخطاء لغوية وتعبيرية وبذلك أصبحت الرسالة مؤهلة للمناقشة بقدر تعلق الأمر بسلامة الأسلوب أو صحة التعبير.

التوقيع:

الاسم: م. د اوس عادل عبدالوهاب

التاريخ: ٢٠٢٣/١١/

إقرار رئيس لجنة الدراسات العليا

بناءً على التوصيات المقدمة من قبل المشرف والمقوم اللغوي أشرح هذه الرسالة للمناقشة.

التوقيع:

الاسم: أ. د قيس ذنون نجم

التاريخ: ٢٠٢٣/١١/

إقرار رئيس القسم

بناءً على التوصيات المقدمة من قبل المشرف والمقوم اللغوي ورئيس لجنة الدراسات العليا أشرح هذه الرسالة للمناقشة.

التوقيع:

الاسم: أ. د قيس ذنون نجم

التاريخ: ٢٠٢٣/١١/

إقرار لجنة المناقشة

نشهد بأننا أعضاء لجنة التقويم والمناقشة قد اطلعنا على هذه الرسالة الموسومة (تصميم وتنفيذ هوائي تقويم متعدد النطاقات لحصد طاقة الترددات الراديوية المحيطة) وناقشنا الطالب (عبد الله محمد عجيل حسين) في محتوياته وفيما له علاقة بها بتاريخ / ١١ / ٢٠٢٣ وقد وجدناه جدير بنيل شهادة الماجستير/علوم في اختصاص هندسة الالكترونك.

التوقيع:
عضو اللجنة: أ.م.د. محمد شويش احمد
التاريخ: ٢٠٢٣/١١/

التوقيع:
رئيس اللجنة: أ.د. قيس ذنون نجم
التاريخ: ٢٠٢٣/١١/

التوقيع:
عضو اللجنة (المشرف): أ.م.د. احمد محمد
احمد السبعاري
التاريخ: ٢٠٢٣/١١/

التوقيع:
عضو اللجنة: أ.م.د. محمد عبدالرحمن احمد
التاريخ: ٢٠٢٣/١١/

قرار مجلس الكلية

اجتمع مجلس كلية هندسة الالكترونيات بجلسته المنعقدة بتاريخ: / ١١ / ٢٠٢٣
وقرر المجلس منح الطالب شهادة الماجستير علوم في اختصاص هندسة الالكترونك

مقرر المجلس: أ.م. د بلال علاء الدين جبر
التاريخ: / ١١ / ٢٠٢٣
رئيس مجلس الكلية: أ. د خالد خليل محمد
التاريخ: / ١١ / ٢٠٢٣



جامعة نينوى
كلية هندسة الالكترونيات
قسم الالكترونك

تصميم وتنفيذ هوائي تقويم متعدد النطاقات لحصد طاقة الترددات
الراديوية المحيطة

عبد الله محمد عجيل حسين

رسالة في هندسة الالكترونك

بإشراف

الاستاذ المساعد الدكتور

احمد محمد احمد سلامة السبعاعي

2023م

1445هـ

تصميم وتنفيذ هوائي تقويم متعدد النطاقات لحصد طاقة الترددات
الراديوية المحيطة

رسالة تقدم بها

عبد الله محمد عجيل حسين

إلى

مجلس كلية هندسة الإلكترونيات - جامعة نينوى
وهي جزء من متطلبات نيل شهادة الماجستير
علوم في هندسة الإلكترونيك

بإشراف

الإستاذ المساعد الدكتور

احمد محمد احمد سلامة السبعاعي

٢٠٢٣ م

1445 هـ